Fatigue assessment of Orthotropic Steel Decks

Realization of a parameter sensitivity study by development of a parametric model

D.H. (Daan) Exterkate

Fatigue assessment of Orthotropic Steel Decks

Realization of a parameter sensitivity study by development of a parametric model

Thesis report

by

D.H. (Daan) Exterkate

to obtain the degree of Master of Science
at the Delft University of Technology
to be defended publicly on 1 October, 2024 at 15:45 PM.

Thesis committee:
Chair:	Dr. Ir. M. Pavlovic	TU Delft
Supervisors:	Dr. Ir. F.P. van der Meer	TU Delft
	Ir. H. El Bamby	TU Delft
	Ir. C.M. Stellinga	Antea Group
	Ir. T.S. Jaspers Focks	Antea Group
Place:	Faculty of Civil Engineering and Geosciences, Delft	
Project Duration:	November, 2023 - September, 2024	
Student number:	5169917	

An electronic version of this thesis is available at `http://repository.tudelft.nl/`.

Cover image: Illustration of an orthotropic steel bridge deck [1].

Preface

This thesis marks the final step in obtaining the Master's degree of Civil Engineering at the Delft University of Technology. During this master, I followed the Structural Engineering track and additionally worked as a TA for python programming. These interests led to the subject of this research, which is related to the complex fatigue verification of orthotropic steel decks. In this thesis a parametric model is developed, determining fatigue damage in orthotropic steel decks, and used to determine influences of important parameters on the bridge.

Firstly I would like to thank Antea Group, for the opportunity of performing my research there, but also for the use their equipment, knowledge and software. I would like to thank Coen Stellinga and Thijmen Jaspers Focks for their feedback and guidance during this project. I would like to extend special gratitude towards Coen Stellinga for his dedication to helping me. Providing me with feedback and knowledge numerous amount of times, whether it was the first thing on a Monday morning, on a Sunday afternoon or even once at night. Thanks Coen!

Furthermore, I would also like to express my gratitude towards my thesis committee for helping me throughout this period. During feedback session they provided helpful suggestions and feedback. I would like to thank Marko Pavlovic and Frans van der Meer for the guidance during this project and feedback during the meetings. Additionally, I would like to thank Hagar El Bamby, for her feedback and her ever-present positive mindset.

Lastly, I would like to thank my friends, family and girlfriend for their support, and for providing some needed distraction during this project.

Enjoy reading.

Daan Exterkate
Delft, September 2024

Abstract

Orthotropic steel decks (OSDs) are commonly used in bridge construction due to their material efficiency and strength. However, fatigue issues in welded joints remain a concern. Fatigue cracks often occur due to high stress concentrations, especially under heavy traffic loads. Current approaches of determining damage in a bridge are limited by the computational demands of Finite Element (FE) models to calculate stresses and the complexity of the fatigue verification. Consequently, there has been limited exploration of parametric optimization for OSDs. This research seeks to address this gap by developing a parametric model to assess the fatigue performance of OSDs according to the ROK version 2.0, the new Dutch Guideline, additionally focusing on identifying the influence of key design parameters through a parameter sensitivity analysis (PSA). This study aims to provide insights for optimizing OSDs to enhance fatigue resistance and design. Thereby aiming to increase material efficiency about OSDs and creating a parametric framework to determine damage in an OSD.

This resulted in the following research question: *How can a parametric model be developed to assess the fatigue performance of Orthotropic Steel Deck bridges and what insights can be gained from analyzing the influence of key design parameters?*

To answer this question, in part 1 a literature study is performed. This began by reviewing the theory of the OSD's and fatigue, identifying the critical fatigue parameters which were expected to influence the incorporated directly ridden details. Furthermore, the Dutch regulations and state-of-the-art about automatizing of fatigue verifications were explored, after which a parametric model is developed.

Part 2 began by developing this model. Simplifications in the mesh and loading scheme are tested and applied to ensure the model is fast and sufficiently accurate. Utilizing various mesh sizes in different regions helps to reduce computation time by almost 300% while maintaining accuracy. Additionally incorporating symmetry in the loading scheme further reduces the computational time by about 127%. With this model, the first part of the main research question is answered. The model is used to find the governing details in the bridge within the design domain of the ROK [2]. The governing details are: the crack initiating at the weld toe located at the intersection of the trough and the deckplate, and the crack initiating at the weld root located at the intersection between the deckplate, trough and crossbeam. Which are respectively detail 1A and 1C of the ROK[2]. After this, a benchmark model is found to start the PSA and a sensitivity analysis is conducted for these previously mentioned details by systematically altering one parameter at a time (OAT).

Results of the PSA are distinguished for the two aforementioned details. For detail 1C, the deckplate thickness and trough top width influence the damage of the detail primarily, represented by respectively an exponential function and second order polynomial. The crossbeam thickness influences the damage by maximally 30% of the damage number of the benchmark, while this parameter is not included in the analytical solution. Other included parameters show small or negligible influence on the damage of detail 1C. The governing load position within the design domain is the transversal load distribution exactly above the middle of a trough. Furthermore, a difference in stiffness exists between two trough legs of the same trough for detail 1C, significantly influencing the damage. The governing transversal location of detail 1C is at the trough leg closest to the main girder.

For detail 1A, by far the most influential parameter on the damage of this detail is the deckplate thickness, having a exponential influence. The trough center-to-center distance has the second greatest influence on the damage, this can be represented by a second order polynomial. The top trough width and crossbeam center-to-center account for a maximum influence of the damage number of 20% of the benchmark damage number. The influence of the other included parameters were small or negligible. The governing transversal location of detail 1A is, similarly to 1C, at the trough leg closest to the main girder.

The validation of the model shows a great difference in the difference in damage numbers obtained from version 2.0 of the ROK in comparison with version 1.4. Validation of the Goereese bridges therefore show damage numbers greater than 1 for the 2 aforementioned details. It is suggested to show extra attention to bridges designed with ROK version 1.4, or earlier versions, and to repair occurring cracks in a way that the local damage complies with the verification of ROK version 2.0. The parametric tool can play a useful part in this when expanded. Another future use case can be to support the goal of the Rijkswaterstaat of replacing the current labor-intensive fatigue calculation method with a table that outlines the dimensions of OSDs, by generating a large amount of data.

Contents

Nomenclature

List of Abbreviations

2D	Two dimensional
3D	Three dimensional
API	Application programming Interface
CAFL	Constant Amplitude Fatigue Limit
CTC	Center-to-center
DC	Detail Category
DOF	Degree of Freedom
FE	Finite Element
FEA	Finite Element Analysis
FEM	Finite Element Method
HSS	Hot Spot Stress
MPa	Megapascal
NRMSE	Normalized Root Mean Square Error
OAT	One-at-a-time
OSD	Orthotropic Steel Deck
PSA	Parameter Sensitivity Analysis
RMSE	Root Mean Square Error
ROK	Richtlijn Ontwerp Kunstwerken
SCF	Stress Concentration Factor
SLS	Serviceability Limit State
TS	Technical specification
TT	Traffic Type
U.C.	Unity Check

ULS	Ultimate Limit State

List of Symbols

$\Delta\sigma$	Stress range
$\Delta\sigma_c$	Characteristic value of stress range
ρ	Density
σ	Stress
σ_y	Yield stress
σ_{ENS}	Effective Notch Stress
σ_{HS}	Hot Spot Stress
ctc_{cb}	Crossbeam center-to-center distance
ctc_{tr}	Trough center-to-center distance
E	Elasticity modulus
G	Shear modulus
h	height
h_{tr}	Trough height
N	Number of cycles
t	Thickness
t_{cb}	Crossbeam thickness
t_d	Deckplate thickness
t_{tr}	Trough thickness
v	Poisson ratio
w	Deflection
$w_{tr,bot}$	Trough bottom width
$w_{tr,top}$	Trough top width

List of Figures

List of Tables

Introduction

1.1. Research context

Orthotropic steel decks (OSD's) play a crucial role in modern bridge construction. The OSD offers a strong and material efficient solution for a bridge, especially suiting for long span and movable bridges due to its low self-weight and efficient design [3]. The OSD system consists of a slender steel plate, which is stiffened by a set of longitudinal ribs. The system is transversely supported by floorbeams, and longitudinally supported by a set of main girders. These longitudinal ribs are the plate stiffeners and can have multiple designs and geometries, see Figure 1.1. Because of its layout, the system has different properties in the two perpendicular directions, or similarly; the system is ORTHOgonal and anisoTROPIC. Hence, an orthotropic deck [4].
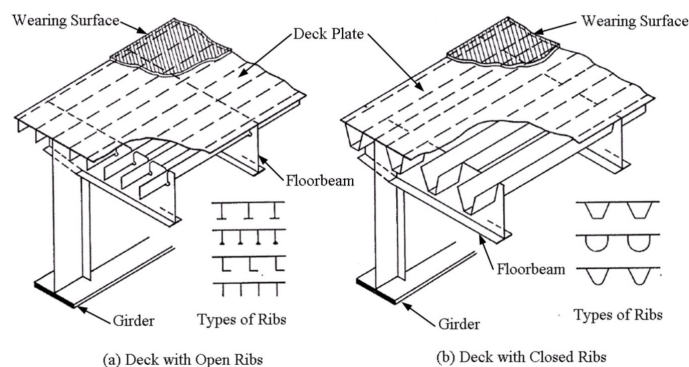
Figure 1.1: Components of the OSD bridge system [3].

The OSD involves a substantial number of welded connections. These welded connections introduce welding residual stresses [5], and geometrical stress concentrations. This, in combination with heavy traffic loads, cause the welded joints to become critical starting locations for fatigue cracks. These cracks are being observed increasingly more in operational Orthotropic Steel Deck structures [6]. In the Netherlands, fatigue cracks have been detected in numerous bridges [7], causing need for early replacement or repair. Fatigue is recognized to play a major role in the design and lifetime of an OSD.

1.2. Research problem

While the advantages are apparent, these structures are laborious to assess and have a history of occurring fatigue cracks. An adequate Finite Element (FE) model is needed to determine the occurring stress ranges, making such computationally expensive model is time-consuming. Consequently, the parametric optimization possibilities of an OSD are rarely explored. This is undesirable, as unlocking the potential for parametric OSD optimization could lead to more efficient solutions, and a substantial gain in knowledge on the influence of specific parameters on bridge design. When a parameter optimization is executed, for example by De Corte [8], Fettahoglu[9] or Xia et al. [10], the influence of only one or two parameters could be studied, due to the complexity and substantial time required of fatigue verifications and computational power required.

Few studies towards the optimization of an OSD regarding multiple parameters can be found in literature [11],[12] or [13]. A possible reason could be the difficulty in assessment, as multiple fatigue details of the OSD should be incorporated, and multiple locations in the deck could be governing. Additionally, considerable computational power is needed to execute multiple FEM models. Also, Stellinga's research [14] demonstrated that it is not possible to parameterize the location of the initial anticipated fatigue crack in the bridge. Nevertheless, as done by van der Laan [11] and Baandrup [13], a parameterized model can be developed based on assumptions about the anticipated location of the fatigue crack.

As traffic volume continues to rise and fatigue cracks are observed on Dutch bridges, there is an ever growing interest in optimizing OSD's and understanding the impact of various parameters. Further research on the optimization and the influence of parameters on OSD's is crucial for designing bridges that are more efficient, leading to economic and environmental benefits.

1.3. Aim and objective

This thesis aims to assess the potential for more efficient material use in an OSD by mapping the effects of various parameters on the bridge. To realize this aim a parametric model of an OSD regarding the fatigue verifications of the ROK [2], which are the Dutch regulations, will be developed. By a successful parametrical design, a sensitivity study of the OSD can be executed and valuable information can be obtained regarding influences of bridge parameters on the bridge design, and about the creation of a parametric model. Furthermore, the parametric framework could be used to calculate preliminary designs of an OSD, or this framework could be extended in future research to include additional details, parameters or locations in which the stress is returned.

To help reach the aim of the research, objectives can be specified:

1 Make well founded assumptions based on literature and knowledge of experienced structural engineers about the to be checked critical locations on the bridge.

2 Create a parametric FE model in-line with the Dutch regulations.

3 Pair the parametric FE model with a fatigue life verification tool.

4 Create data of numerous designs and select an initial bridge design to start a parameter sensitivity analysis.

5 Execute a parameter sensitivity analysis

6 Validate made assumptions in the model.

1.4. Research scope

To conduct a full-on study on the verification of an OSD bridge is practically not feasible due to the extensive checks required for this verification and time-restrictions imposed on this thesis. This section outlines the research scope of the thesis.

1.4.1. Design limits

First of all, while acknowledging the regulatory need of conducting checks for the Ultimate Limit State (ULS), the Serviceability Limit State (SLS), stability, detailed connections, and more, it is necessary to clarify that this research exclusively focuses on the fatigue limit state of the OSD bridge. The design space of the bridge is also limited in terms of the to be used parameters. Given the numerous parameters present in the bridge, it is not feasible to incorporate all of them into the parametric optimization process. Thus, as much key parameters as feasible will be used, regarding time-constraints on this research. This is similar for the incorporated fatigue details, as incorporating all recognized fatigue details is not feasible regarding time-constraints. Additionally, this research exclusively incorporates the design of the superstructure of the bridge, it is assumed that the substructure is correctly designed for the occurring loads.

1.4.2. Case study

This research bases itself on a case-study OSD bridge; the Goereese bridge. The Goereese bridge is an OSD bridge located in Stellendam, The Netherlands. Refer to chapter 6 for details regarding the bridge. In this research, the Goereese bridge is subjected to a generalization process to obtain a more friendly parameterizable model, as the parametrization of the model could take up a considerable amount of time of this thesis. Other notable advantages of simplifying the geometry are the ability to study the effects of several bridge parameters without the interference of complex geometry effects, and the ability to reduce the required computational power. This research, like the case study and currently the vast majority of OSD bridges in the road network, considers trapezoidal troughs as stiffeners, as prescibed by the ROK [2].

1.4.3. Dutch standards

Due to the location of this bridge (the Netherlands), and the adherence to Dutch practises of Antea Group NL, this research relates to the application of the Dutch regulations. This implies that wherever possible, the ROK [2] and Dutch annexes are used in combination with the Eurocode [15]. However, due to computational expensive models or time-restrictions some deviations of the Dutch regulations may be needed, these assumptions need to be appropriately justified and evaluated.

1.4.4. Fatigue details

The fatigue details correspondent with deck type B, a deck with continuous stiffeners and no cut-outs are considered. Furthermore, only directly ridden details are considered in the development of the parametric model. These details occur in or at the deckplate of the OSD, and this means that the details are vastly prone to local loads only. These are fatigue details 1A, 1C, 2A, 2B, 5, 6A and 6B of the ROK [2], see Annex A. These details are initially considered as the deck plate significantly influences the weight of the bridge, and the weight is important for observing the influences of parameters in this research. Moreover, incorporating only details influenced mostly by local loads could facilitate a faster FE model, presumed that more simplifications can be implemented when details have this feature.

1.4.5. Bridge parameters

Many possible bridge parameters can be identified. To keep the parametric model concise, informative and make-able, 8 variables are included in the model. These variables are based on which parameters are expected to have the most influence on the weight of the bridge and on the considered details. These parameters are briefly stated in this section but are further explained in Chapter 6. The considered 8 parameters are: the deckplate thickness t_d, trough thickness t_{tr}, crossbeam thickness t_{cb}, top width troughs w_{top}, bottom width troughs w_{bot}, center to center distance crossbeams ctc_{cb}, center to center distance troughs ctc_{tr} and the height of the troughs h_{tr}.

1.5. Research questions

To guide this thesis and reach its objectives as best as possible, the following main research question is formulated:

> **Research Question Main Research Question**
>
> How can a parametric model be developed to assess the fatigue performance of Orthotropic Steel Deck bridges and what insights can be gained from analyzing the influence of key design parameters?

To answer the research question this thesis tries to find a parametric OSD model automatically complying with fatigue verifications of the ROK [2] to the fullest extent, with possibilities of optimizing an initial design with this model. Developing such parametric model additionally allows to gain insight into influences of multiple bridge parameters on the bridge design and fatigue unity checks. To generate such parametric model and utilise it to the best of its abilities, and therewith be able to answer the main research question, supporting sub research questions are identified.

Part 1: Literature review

The literature review firstly introduces the fundamental topics of fatigue and the Orthotropic Steel Deck to gain understanding about the fatigue in welded joints and the fatigue verification in OSD's according to the dutch guidelines. Questions regarding the method of the ROK, general applicability of an OSD and the state-of-the-Art on parametric optimization will be answered:

RQ-1:   *How is the fatigue verification executed in conformity with the Dutch regulations?*

RQ-2:   *How precise are stresses determined with the method of the ROK (2D shell elements with mesh refinement and local thickenings) compared with stresses of a 3D solid element model?*

RQ-3:   *To what extent does a parametric model with automated fatigue verifications already exist and what assumptions do they incorporate?*

Part 2: Parametric model

This second part is about the making and explanation of the parametric model with automated fatigue verifications. The parameter sensitivity analysis and the model validation will additionally be executed. The following sub-questions will be answered:

RQ-4a: *What assumptions about the loading scheme are necessary or can be implemented to render the calculation of the parametric model within a tenfold of minutes?*

RQ-4b: *What other assumptions about the parametric model are necessary or can be implemented to render the calculation of the parametric model within a tenfold of minutes?*

RQ-5:   *Which conclusions can be drawn from the parameter sensitivity analysis?*

RQ-6:   *To what extent are the made assumptions in Part 2 about the loading scheme and parametric model correct for the governing model of each detail?*

Part 3: Research Outcome

Finally, in the last part, an answer is be given to the main research question. Additionally, the discussion and other conclusions are stated.

1.6. Methodology

This section outlines the approach used to be able to find answers to the previously stated research questions. This research utilizes a combination of parametric modeling alongside a comprehensive sensitivity analysis to contribute towards the aim of assessing the possibility for a more efficient material use of an OSD. Five different aspects are distinguished.

1.6.1. Literature review

The first part of this thesis discusses the literature review. It comprises of three chapters, respectively covering the theory of fatigue and its verifications, orthotropic steel decks, and the state-of-the-Art about the parametric modelling of an OSD.

1.6.2. Parametric model development

A parametric Finite element model is made with the use of Python, excel and an a SCIA Engineer Application Programming Interface (API). This model is based on input parameters as stated in section 1.4.5 , and contains a select amount of details (7), as explained in 1.4.4.

1.6.3. Initial data creation

The parametric model is used to calculate numerous different designs while changing parameters. This way a lot of data and information is gained about the damage numbers and stresses of the different designs. A manual grid search is used to analyse this data in the search for an optimized design to use as a benchmark for the parameter sensitivity analysis.

1.6.4. Parameter sensitivity analysis

A detailed parameter sensitivity can help to understand the influence of various design parameters on the design life and fatigue damage in the bridge. The analysis is performed with the data of the damage numbers of the various designs.

1.6.5. Model validation

The parametric model is validated in two ways. Firstly, the model assumptions which are needed to achieve a fast enough model are validated. Secondly, comparisons with existing other solutions and the original case study are performed.

1.7. Structure of the Report
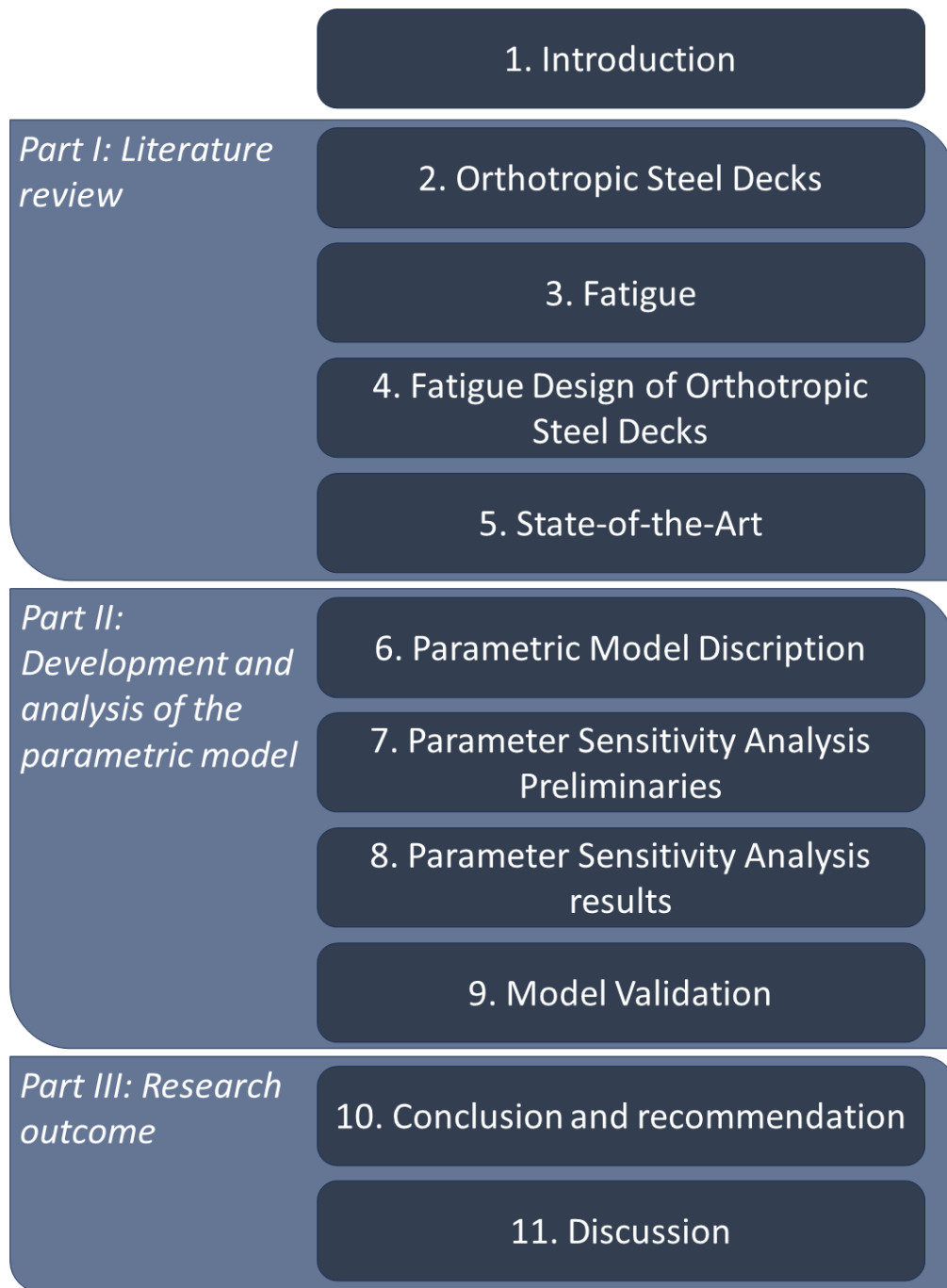
Figure 1.2: Thesis structure.

Part I

Literature Review

<div align="right">

2

</div>

Orthotropic Steel Decks

This chapter gives an introduction to the Orthotropic Steel Decks. After shortly discussing its origin, the application possibilities, fatigue problems and the components of the orthotropic steel deck shall be evaluated. Finally, the structural behaviour of the OSD will be illustrated to gain a better understanding of the mechanics of the system.

2.1. Origin

The idea of an OSD started in the 1930s in the form of longitudinal I-shaped ribs welded to a steel deck plate, and attached to an underlying crossbeam, named as the "Battledeck floors", See Figure 2.1. The Salt River Bridge in Michigan is one of the first applications, not much later the system was applied more frequently as a part of the German Autobahn network [16]. In the post-war depression it became essential to save material, the orthotropic systems were favoured and further improved. [3]
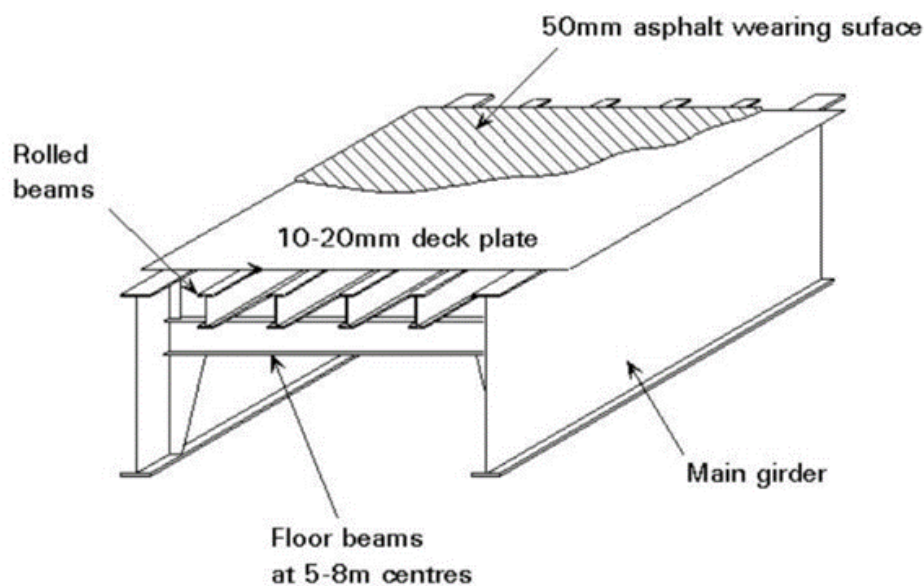
Figure 2.1: Battledeck floor [17].

The biggest difference of the battledeck floor with the modern OSD is the deck plate. Initially, the deck plate's sole function was to distribute the load across the overall structure. Consequently, stiffeners, crossbeams, and main girders still required their own top flange. In contrast, the modern OSD incorporates the deck plate as an integral component of the structural system, serving various functions in the process.

2.2. Application

Orthotropic steel deck bridges are used for their material efficient and strong design capabilities. The OSD system generates its efficiency from the the integral action between all the components; girders, crossbeams, stiffeners and the deck plate. Resulting in increased rigidity of the system. The loads acting on the structure's surface are transferred from the deck plate, through the crossbeams and stiffeners to the main load carrying system, the main girders.

For the largest spanning bridges in the world, the orthotropic steel bridge deck remains the most viable bridge deck system [18]. Because, as holds for all long span bridges, the minimization of self-weight is the primary focus as this load is by far the predominant factor. However, the applicability of the OSD system is not exclusively for long span bridges, the system's shallow height, rapid construction, low self-weight and cost efficiency allow it to be used in many cases; Movable bridges, bridges in seismic zones, bridges where rapid construction is required, bridges where extended service life is required and bridges where cast-in-place concrete is difficult due to cold weather conditions [3].

Another key aspect in the design and application of an OSD is the fabrication quality of the system. The manual for Design, Construction, and Maintenance of Orthoropic Steel Bridges [3] states: 'History has demonstrated that refined analysis and design can be rendered meaningless when the construction is not executed properly. Orthotropic decks are complex in terms of fabrication and must be treated with care. To be successful, they require detailed construction specifications and quality control measures in production'. The Dutch regulations [2] prescribe particularly strict fabrication of OSD fatigue details, which significantly increases the live span of an Orthotropic Steel Deck, illustrated in Appendix A.

2.3. Fatigue problems

After the introduction of the Orthotropic Steel Deck (OSD), its material efficiency and robust capabilities positioned it as the most cost-effective choice for highway bridges. However, during the 1970s, fatigue-related issues came to light in bridges constructed as early as the 1960s [19] [20] . Despite the already existing awareness of the fatigue phenomenon, unexpected cracks emerged in various weld details. Still to this day, fatigue problems in orthotropic steel decks are observed in spite of intensive design checks and research. Chapter 3 introduces to this topic.

2.4. Components

OSD's consists of multiple components, already visible in Figure 2.1. The different components are, in the same order of the load path; the asphalt- or wear-layer, deck plate, stiffeners, crossbeams and the main girders. This section describes the use of each component.

An OSD always contains an asphalt- or wear-layer. This layer is in direct contact with the wheel loads on the bridge and account for a load spread trough the layer on the deckplate. Additionally, an asphalt layer can provide extra stiffness of the bridge. However, in the case study bridge a composite wear layer is used of only 10 mm as this is a bascule bridge, where weight of the bridge is of great importance. In this research this effect should be neglected, as stated by the ROK [2], due to the low contribution of the wear layer to the stiffness and structural integrity of the OSD.

The deck plate is the integral component of the system, it compositely acts with the other components since these are welded to the deck plate. The steel deck plate is the element with the highest influence on the self-weight of the system due to its size. However, it is also the element which is able to significantly increase fatigue performance when its thickness is increased [21]. Optimizing the deck plate is therefore a balance between lowering the self-weight, and thereby costs and environmental impact, and conforming with fatigue verifications.

The stiffeners are also an important part of the bridge. Multiple different stiffener types can be distinguished when designing an OSD. In general there are two types; stiffeners with open and closed cross-section. see Figure 2.2.
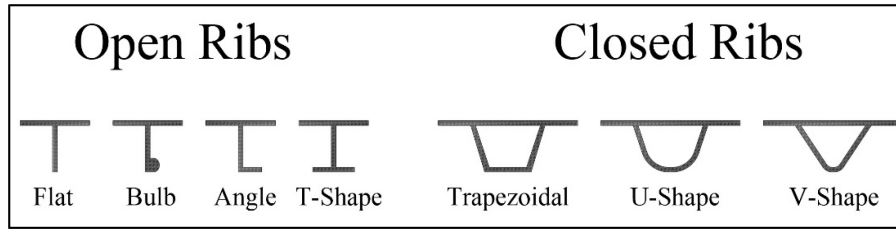
Figure 2.2: Common types of stiffeners [22].

The stiffeners with open cross-section are easier to be inspected, but have negligible torsional stiffness. These stiffeners are fabricated as inverted T-sections, flats, angles or bulb sections [23]. The closed cross-section have trapezoidal, rectangular of semicircular cross-sections [3]. These stiffeners have considerable torsional stiffness, are generally lighter than decks with open stiffeners, require fewer welds and have a smaller exposed steel surface, needing less paint [19]. However, the inside of the troughs cannot be inspected without damaging the bridge. Nevertheless, trapezoidal troughs are regarded as the most efficient type of stiffener by engineers and regulations, and therefore occur most frequently in OSD's.

The cross beams consist of composite profiles, having a similar shape with respect to an inverted T section, welded to the deck plate and the longitudinal stiffeners. The deck plate, stiffeners and cross beams as a whole is supported by the main girders. The crossbeams carry the load obtained trough the wear or asphalt layer, deckplate and stiffeners to the main girders, which carry it to the supports.

2.5. Structural behaviour

The OSD can be approximated by analytical behaviour of different subsystems. Distinction can be made between seven analytical subsystems in total, see Figure 2.1. The simultaneous and complex action makes that a detailed and accurate analysis of an OSD is destined to rely on the use of a Finite Element model. However, the analytical subsystems can gain understanding of the mechanical structure and deformation of an OSD. The working of the systems are listed in Figure 2.1 from really local to global behaviour.

These different subsystems formed the basis of the OSD analysis in early age. The behavioral systems which are indicated in Figure 2.1 are still valid to this day. In the recent decades, more local distortion mechanisms are uncovered that were previously unnoticed. [3]. For this thesis, the local phenomena are especially interesting due to the restriction to directly-ridden details. It is recognized that the deckplate stresses are primarily caused by a combination of the first two systems [3]. These two systems are discussed in the following paragraphs.

System 1 represents the local deformation of the deckplate and stiffeners. The illustrated load is the representation of one wheel of the axle of a truck. The response is affected by the spacing of the rib walls and the flexural stiffness of the deckplate and ribs [3]. The manual for design and construction of Orthotropic Steel Decks state that this system is one driving factor in the fatigue of the Rib-to-Deckplate weld, but is generally not a concern for strength based limit states. This system can be analysed simplistically by using a frame model of the transverse cross-section of the bridge, either flexible or rigid supports based on the rib flexural stiffness and span length [3].

System 2 represents the deckplate and trough deformation. The two-way load distributing behaviour of this 'panel' makes it a complex problem. Early solutions used orthogonal and torsional properties. The solution has been found in using the equation of Huber[3], see Formula 2.1.

$$D_x \frac{\delta^4 w}{\delta x^4} + 2H \frac{\delta^4 w}{\delta x^2 \delta y^2} + D_y \frac{\delta^4 w}{\delta y^4} = p(x,y) \tag{2.1}$$

In which D_x and D_y are the plate flexural rigidity in the x- and y-direction, H is the effective torsional rigidity of the plate and $p(x,y)$ is the loading at any point on the plate with coordinates of (x,y).

The solution of this equation can be only be found for trapezoidal troughs by averaging single closed troughs into a uniform property of idealized plate, of which the errors are not known. Some solutions

have been widely accepted, but have become outdated as in the present time this analysis is done by a Finite Element Analysis (FEA) [3]. Analysis show that system 2 is primarily influenced by the flexural and torsional stiffness of the ribs.

Table 2.1: Analytical subsystems [3]

System	Action	Figure	Result
1	Local Deck Plate Deformation		Transverse flexural stress in deck and rib plates and RD
2	Panel Deformation		Transverse deck stress from rib differential displacements
3	Rib Longitudinal Flexure		Longitudinal flexure and shear in rib acting as a continuous beam on flexible FB supports
4	Floorbeam In-plane Flexure		Flexure and shear in FB acting as beam spanning between rigid girders
5	Floorbeam Distortion		Out-of-plane flexure of FB web at rib due to rib rotation
6	Rib Distortion		Local flexure of rib wall due to FB cut-out
7	Global		Axial, flexural, and shear stresses from supporting girder deformations

3

Fatigue

Understanding the fatigue mechanism is important for this thesis. This chapter firstly introduces the subject to gain understanding of it. Secondly, it describes the method of fatigue resistance determination of the Dutch guidelines.

3.1. Fatigue process

Fatigue is the progressive degradation of a component due to cyclic loading over an extended duration [24] [25]. This process arises from repetitive stress cycles operating beneath the material's ultimate strength, and usually even far below the yield strength. The weakening of the material can be categorized into two distinct phases: the crack initiation/nucleation stage and the subsequent crack propagation stage.

3.1.1. Crack nucleation

The initiation period starts with slip occurring in the metal due to cyclic loading. Slip is a fundamental process in metallurgy involving the movement of one portion of a crystal relative to another along specific planes within the crystal lattice, known as slip planes. This movement is facilitated by the migration of dislocations along these slip planes. Dislocations, which are defects or irregularities in the arrangement of atoms within the crystal lattice, act as pathways for the movement of atoms during plastic deformation. As dislocations propagate through the crystal lattice, they enable the atoms to shift position, leading to the plastic deformation of the material [26].

Due to the cyclic shear stress in the material, a slip step occurs, and subsequently a reversed slip step in the same direction occurs, this leads to slip bands, See Figure 3.1. In the slip step some strain hardening occurs on the micro scale, which is not fully reversible. During the lifetime of an steel specimen, the crack initiation period is regarded as the main part of its fatigue life [25].
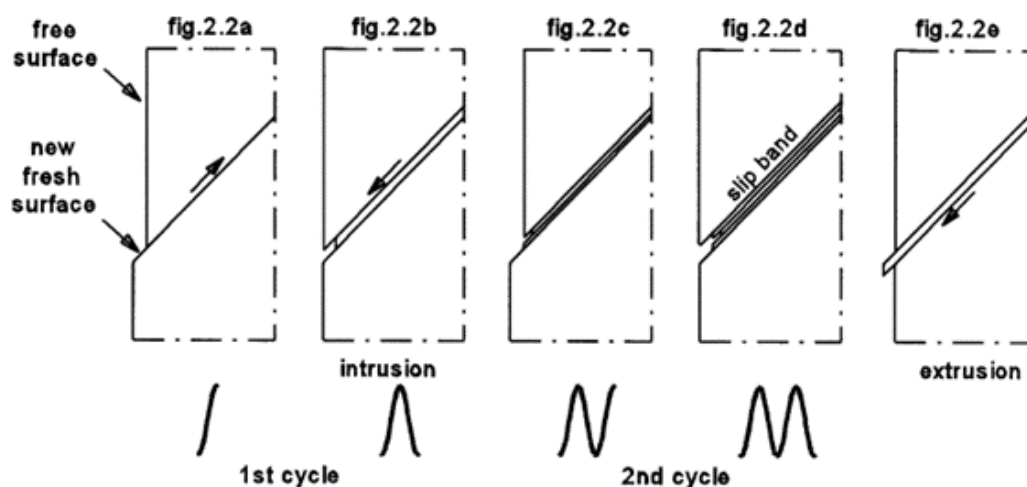
Figure 3.1: Slip band occurring in material which leads to crack nucleation [25].

12

Favourable places for cyclic slip to develop is in notches or other geometrical discontinuities, since these stress distributions cause a peak stress occurring at the surface [25]. This is illustrated in Figure 3.2, the geometrical discontinuity in the weld causes peak stresses, this is known as local stress raisers. Welds are such a place which display in-homogeneous stress distributions due to this phenomenon, because of their geometric discontinuities. Other local stress raisers which are also influential are the usage of different material, thermal expansion/contraction or welding defects Therefore, cracks in an OSD initiate at the welds.
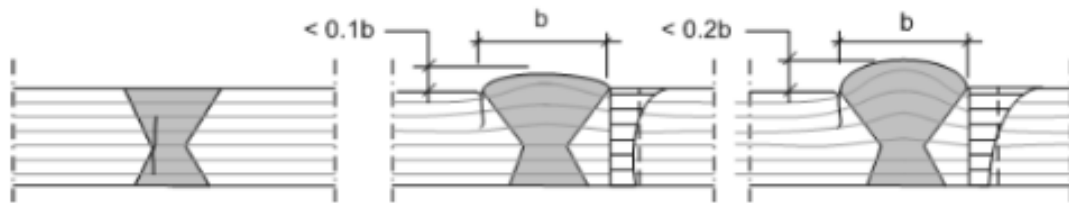
Figure 3.2: Stress peaks due to geometrical discontinuities [26].

3.1.2. Crack propagation and failure

The boundary between the crack propagation and the crack nucleation is reached once the micro crack growth rate does no longer depend on the material surface conditions [25]. After forming of the micro crack, the crack causes stress concentrations in the material, which also means that more slip bands occur. However, in time, the initial microscopic slip bands, which usually form at a 45-degree angle, do not form the crack direction anymore. Instead, the crack will grow in the direction perpendicular to the main principal stress direction [25]. The crack grows and eventually becomes a macro crack which is visible to the naked eye. The crack grows until failure, which is brittle failure in case of a single specimen. See Figure 4 and 5.
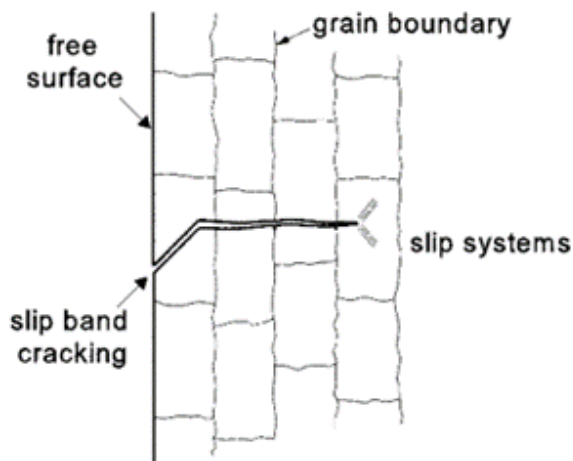
(a) Development of cracks in a material [25].
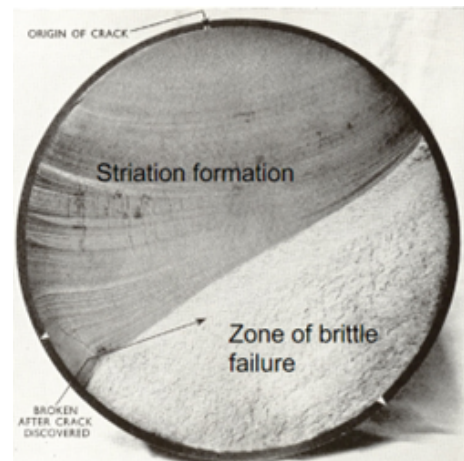
(b) Fatigue failure mechanism in a bolt [27].

Figure 3.3: Fatigue failure of a sample.

3.2. Fatigue resistance

The fatigue resistance of a single member is determined by laboratory testing. During testing, a specimen is subjected to alternating loading, usually constant in amplitude and below the yield limit of the tested steel. From the tests a number of load cycles until failure of the specimen is obtained associated with the magnitude of the constant alternating loading $\Delta\sigma$. When done properly for multiple different stress ranges, a curve can be obtained by fitting a smooth line trough these points in the stress range vs number of load cycles axis system, see Figure 3.4a.
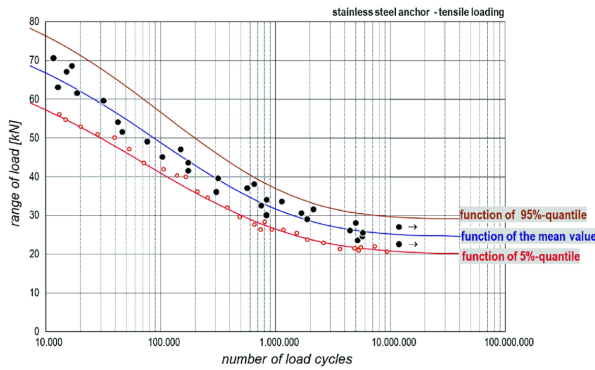
(a) Example of test results, x-axis with logarithmic scale [28].
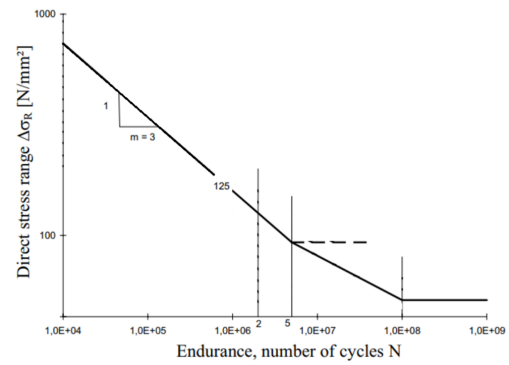
(b) Example of a S-N curve as in the Eurocode [15]

Figure 3.4: Test results and S-N curves.

From these tests the so-called S-N curves can be determined on log-log scale, which determine the resistance of a specimen or constructional detail and are represented by the following formula:

$$N = \frac{C}{(\Delta\sigma)^m} \tag{3.1}$$

See Figure 3.4b for an example of this curve. Such S-N curve is characterized by the characteristic value of the stress range $\Delta\sigma_c$, this is defined as the fatigue strength for $2 * 10^6$ constant loading ranges and a probability of survival of 97.7% [4]. In the example, Figure 3.4b, $\Delta\sigma_c = 125\ [N/mm^2]$.

3.3. Fatigue in welded joints

Orthotropic Steel Decks consist of many welds, which contributes to the systems susceptibility to fatigue. As stated in section 3.1.1, the crack initiation period is regarded as the main part of the fatigue life of a test specimen [25]. However, this is solely the case for an non-welded detail [29]. For welded details, the crack nucleation phase is significantly faster and the propagation phase is the main part of the fatigue life as the welds distort the stress flow in the material, See Figure 3.5.
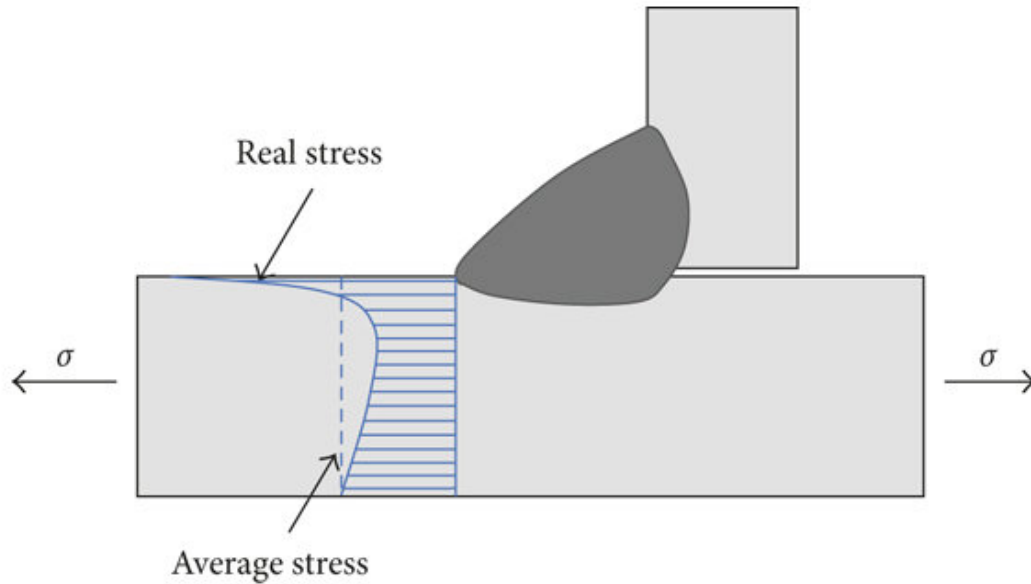
Figure 3.5: Stress flow in a welded joint [30].

The fatigue in welded joints is affected by the type of normal stress distribution which is employed. Three types of distribution can be distinguished: the nominal stress, the hot spot stress and the effective notch stress distribution, see Figure 3.6. The nominal stress refers to the stress computed in the cross-sectional area under consideration, disregarding any stress raising effects due to nearby welds or other macro-geometric discontinuities. The Hot Spot Stress is a linear approximation of the structural stress and will be further discussed in section 4.3.2. The effective notch stress is the distribution including the non linear stress effects.
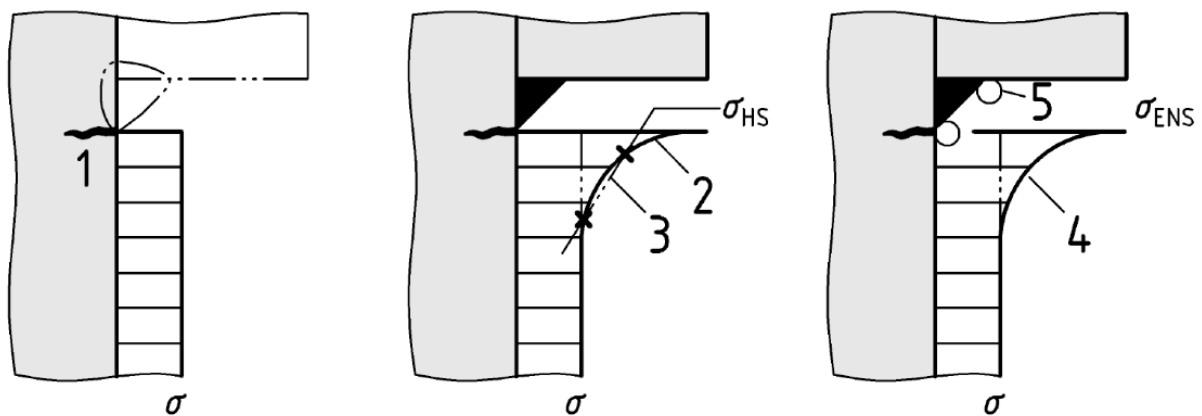
Figure 3.6: Different types of stress distributions in welded joints [31] .

Fatigue Design of Orthotropic Steel Decks

This chapter entails the method of performing a fatigue verification of an Orthotropic Steel Deck in agreement with the Eurocode [15] and the ROK [2]. The first section discusses the fatigue details of an OSD. After which the prescribed loading conditions and (FEA) modeling of an OSD are reviewed. The last section is about the cumulative damage method, and how to obtain damage numbers. These aspects are crucial for the understanding of fatigue verifications of orthotropic steel decks.

4.1. Fatigue details

Occurring fatigue cracks have been recognised by the regulations, and 27 different fatigue details have been distinguished [2]. These details have their own so-called detail category, which is the characteristic value of the stress range $\Delta\sigma_c$ for two million cycles, see section 3.2 . The different fatigue details additionally have requirements regarding the execution of the welding process and methods on how the stresses should be obtained in a FE model. The considered details in this research are displayed in Figure 4.1 and a detailed description (in Dutch) can be found in Annex A. In the figure below the detail categories for an OSD with a deckplate of 20 mm, automated and filled welds are additionally displayed.
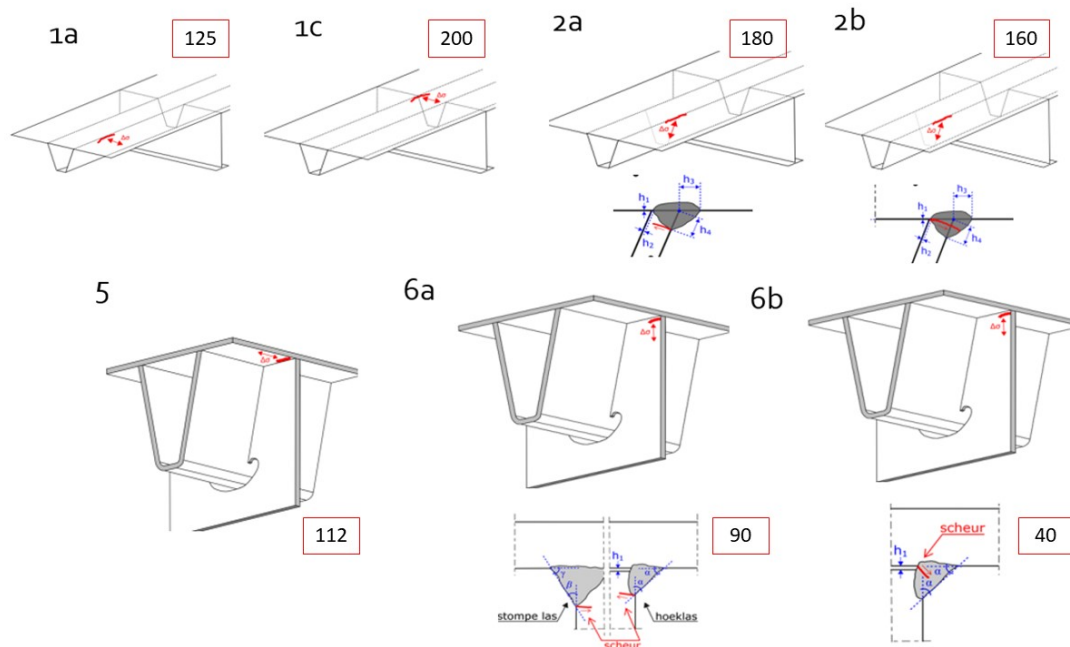
Figure 4.1: Visualisation of the considered details and their detail category [2].

When performing a fatigue design, every detail in the ROK which has a possibility of occurring should be verified. The details which should be incorporated can differ per type of OSD, depending on the stiffener types in the deck.

4.2. Load Model

Fatigue load model 4a from the Eurocode is prescribed by the ROK for an OSD bridge. This load model indicates all load cases which are to be considered in the design. Fatigue load model 4a can be found in the Dutch national annex of NEN1991-2 [32], See Table 4.1. The key aspects of this load case are the type of lorry, the amount of lorries, the axle load, the type of axles and the wheel track location and spreading.

Type voertuig		Verkeerstype				Wiel-type
Afbeelding van de vrachtwagen	Afstand tussen de assen m	Gelijkwaardige aslast kN	Lange afstand % [a]	Middellange afstand % [a]	Lokaal verkeer % [a]	
	4,5	70 130	20,0	50,0	80,0	A B
	4,20 1,30	70 120 120	5,0	5,0	5,0	A B B
	3,20 5,20 1,30 1,30	70 150 90 90 90	40,0	20,0	5,0	A B C C C
	3,40 6,00 1,80	70 140 90 90	25,0	15,0	5,0	A B C C
	4,80 3,60 4,40 1,30	70 130 90 80 80	10,0	10,0	5,0	A B C C C
[a] Percentage vrachtwagens.						

Table 4.1: Lorry types in Fatigue Load Model 4a [32].

Lorry types

Different types of trucks are distinguished in the load model, see Table 4.1. The 5 different types of vehicles are displayed in the first column, their information about the distance between the axles and the axle load are stated respectively in the second and third column.

Traffic type

The traffic types determine which trucks should be accounted for in which percentage of a certain total amount of trucks. The ROK prescribes for each new bridge of Rijkswaterstaat to assume the load conditions to be of 'long distance', which is column 'Lange afstand' in Table 4.1. This is incorporated in the ROK since Rijkswaterstaats' jurisdiction on bridges is almost exclusively the design and inspection on highway bridges. However, The Dutch national annex prescribes something different: The 'Long distance' traffic should be combined with traffic category 1 of Table 4.2 . The 'Medium distance', which is column 'Middellange afstand', should be combined with categories 2 and 3, and the 'Local traffic', which is column 'Lokaal verkeer', is valid for category 4. See Tables 4.1 and 4.2. The latter Table also states a certain amount of trucks passing per year for the corresponding traffic category. This research is based on a case study

which is part of a secondary road, and not a highway. Therefore, traffic category two is assumed in this study, meaning 500.000 trucks drive over the bridge each year.

Verkeerscategorie		$N_{obs,a,sl}$ per jaar en per rijstrook voor zwaar verkeer
1	Autosnelwegen (A-wegen) en wegen met twee of meer rijstroken per rijrichting en met intensief vrachtverkeer	$2,0 \times 10^6$
2	(Auto)wegen met gemiddeld vrachtverkeer (zoals N-wegen)	$0,5 \times 10^6$
3	Wegen met weinig vrachtverkeer	$0,125 \times 106$
4	Wegen met weinig vrachtverkeer en bovendien uitsluitend bestemmingsverkeer	$0,05 \times 10^6$
OPMERKING De aantallen zware voertuigen per jaar en per rijstrook voor zwaar verkeer $N_{obs,a,sl}$ zijn inclusief de trend.		

Table 4.2: Traffic categories [32].

Type of axles

The wheel type, accounted for in the last column in Table 4.1, determines the type of axles which are ought to be used. The different Letters; A, B and C correspond with Figure 4.3 . This configuration is similar to the one stated in the NEN 8701. However, the length of the wheels should be remodeled to 220 mm (instead of 320 mm), as prescribed by the ROK.

Table 4.3: Wheel types as found in NEN 8701 [33], guidelines of the ROK state to use a wheel length of 0.22 m instead of 0.32 m.

Transversal wheel track locations

The final consideration to be made about the position of the loads is the transversal wheel spread. A so-called multi-path model is proposed by the ROK [2]. The mid-position of the load spread should be placed on the most unfavourable transversal position dependent on the considered detail. The amount of positions to be regarded is limited to 3 in case of troughs [2], see Figure 4.2. Zou et al. [34] illustrates that taking this load spread from the Eurocode can lead to slight non-conservative results in few instances, and more complex distributions might give higher stresses. However, the new Technical Specification [35] states that the limitation to the defined distribution and these three positions can estimate the maximum damage in a bridge with a reasonable accuracy.
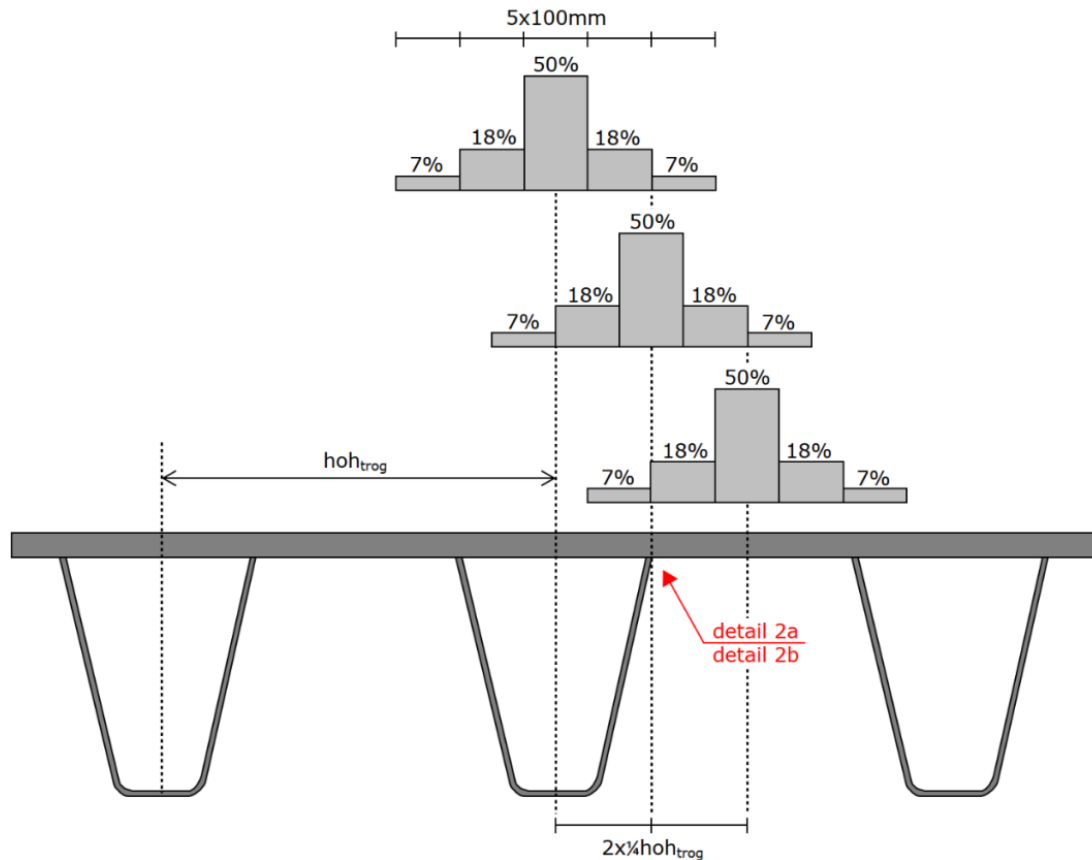
Figure 4.2: To be considered transversal positions of the wheel distributions [2].

4.3. FEM OSD Design

Analytical models are unable to determine the stress state around the weld accurately due to the presence of numerous complex and diverse weld configurations. Additionally, often these analytical solutions do not exist. In order to calculate the stresses in the vicinity of the weld, FEM analysis should be used. Although, this is not an easy task either, determining nominal stresses in certain details might not even be possible due to incomplete definition of it, and determining the hot spot stresses requires multiple criteria to be met. As stated, in this research the latter method is used, therefore these criteria and recommendations regarding the modeling choices of an OSD are reviewed.

4.3.1. Weld modelling

The nominal stress method currently incorporated in the NEN1993-1-9 [15] does not include all fatigue details and there is no clearly defined nominal stress as a result of the complex geometries of an OSD [36] [37]. As an alternative, the ROK incorporates the hot spot stress method. However, studies [38][39][40] show that hot-spot stresses in welded connections of OSD's are not well captured with conventional shell element FE models. Predominantly caused by stiffness increase due to the weld, which is not considered in the conventional models [36].

Research into the modelling of welds concluded that a method of local thickening of the connecting elements at welds yields significantly better stress results than a conventional shell element model without thickening when compared with a 3D model [36], combined with using the hot spot stress method. The ROK has therefore included this method, see Figure 4.3 for an example. Benefits of this 2D model are mainly the needed computational power, which is significantly less compared to a 3D element model.

(a) Considered weld.   **(b)** Modeling the local thickening.
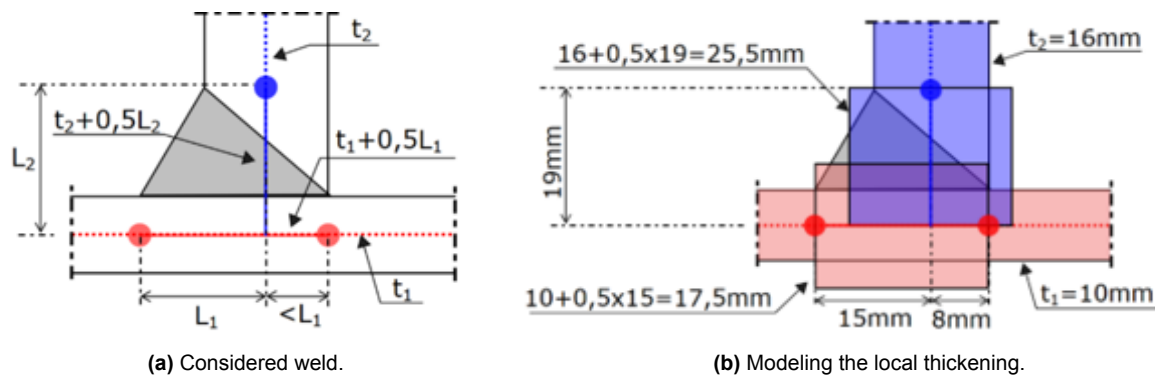
Figure 4.3: Example local thickening of a eccentric single weld according to the ROK [2].

Results of this method are compared to conventional shell element models and 3D element models. An example is given for detail C4C of the ROK [2], see Figure 4.4 . These details show rather similar hot spot stresses between the 3D model and the shell element model. The conventional shell element model, which is the 2D model without the local thickenings, shows significant differences in stresses and stress gradients. Although the detail in Figure 4.4 is not considered in this research, it shows the applicability of the local thickening method. Additionally, the study of [36] indicates that these methods are also tested and valid for eleven further details, including considered details. The study of this method is background to the new technical specification prTS1993-1-901 [35], the ROK adopted this method.
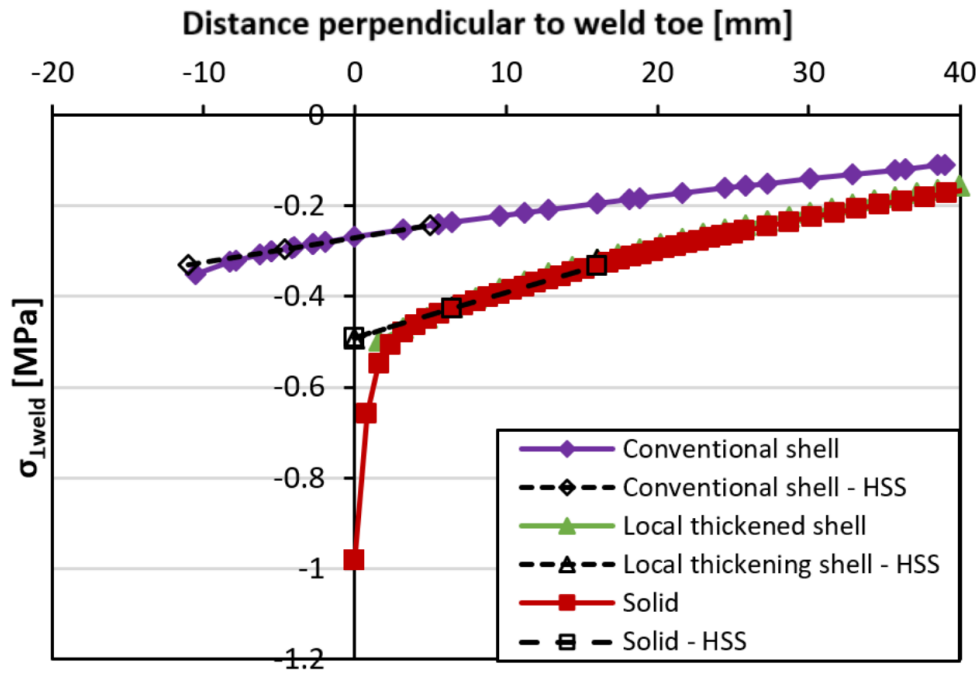
Figure 4.4: 3D element model vs 2D element models for detail C4c in the ROK [36].

4.3.2. Hot Spot Stress

Stresses in a weld of an OSD are determined with FE models. However, the computed total stress at the place of the weld are significantly influenced by non-linear peak stresses, while engineers are interested in the structural stress. It is known that at a distance of around 0.4 or 0.5 times the thickness of the plate, depending of the mesh (relatively fine 0.4 and course 0.5), the non-linear peak stresses are practically vanished [41], see Figure 4.5a. To obtain the structural stress, an approximation is made to make a linear extrapolation between reference points, towards the hot spot, see Figure 4.5b. These reference points are for the method in the ROK at a position of 1.5 and 0.5 times the thickness of the plate away from the hot spot.

(a) Graphical representation of the non-linear peak stresses and structural stress [41].

(b) Determination of the hot spot stress [42].
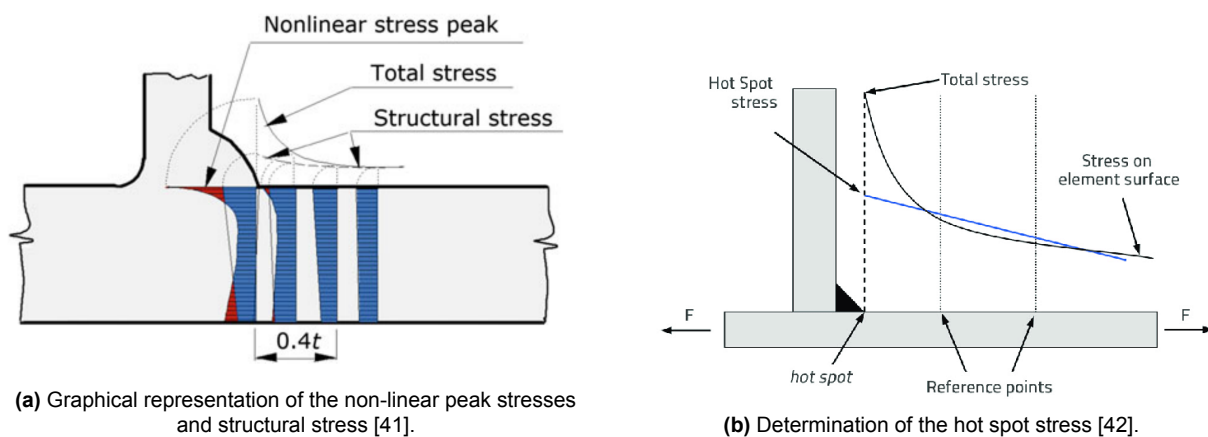
Figure 4.5: Visualization and determination of hot spot stresses.

4.3.3. Meshing

For the determination of the the structural stress at the hot spot, an appropriate mesh should be chosen. The balance between accuracy and calculation runtime is extra important for this study as the parametric sensitivity study requires many runs of the parametric model and thus has serious runtime constraints.

In literature, two meshing guidelines are proposed; one for relatively fine meshing and one for relatively course meshing [41]. The relatively course meshing is illustrated in Figure 4.6.
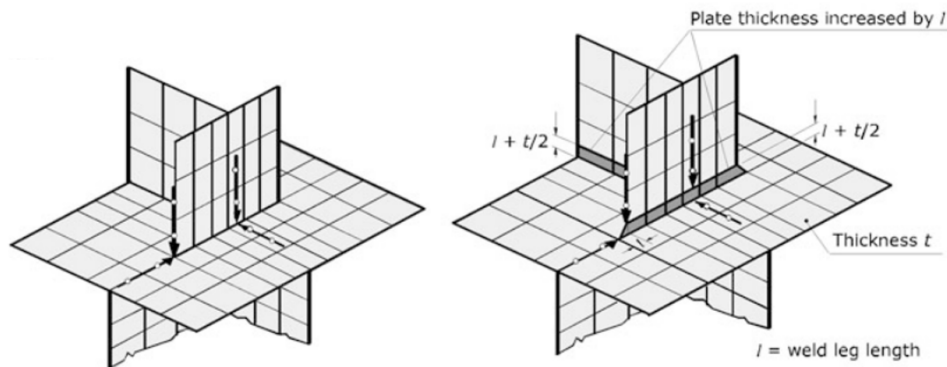
Figure 4.6: Example of relatively course meshing at the welds before the new rules of the ROK became practise. Left: without effect of welds. Right: welds included. [41]

The use of a relatively coarse mesh is sufficient when the structural hot-spot stress may be determined by extrapolating surface stresses to the hot spot [41]. This relatively course mesh should have an element size equal to the corresponding member thickness, and the stresses should be read-out at the center of an element, at a distance of 0.5 and 1.5 times the member thickness [41]. However, this used to be the practise, but it should be noted that the new rules provide different mesh sizes. The method of the ROK [2] is based on a finer local mesh. The variation in this requirement depends on the specific detail, but in most cases, it should not exceed 25% of the member thickness [2]. The stress extraction positions remain at a distance of 0.5 and 1.5 times the member thickness.

It should be noted that the only prescribed meshing is in the vicinity of the weld. As using these mesh sizes for the whole bridge is impossible due to excessive runtimes and huge computational memory required. In example studies in literature [11] [43], the global mesh size could be increased in order to ensure work-ability with the FEM model. The three troughs closest to the detail, and the area of the deckplate above these troughs should still be modeled relatively fine according to these studies. It should be noted that this modelling approach can be used for directly ridden details close by or in the deckplate itself, like the details included in this research.

4.3.4. Asphalt and wear layer stiffness
Asphalt on top of the Orthotropic Steel Deck provides an increase in stiffness of the total bridge. This accounts for a decrease in fatigue stresses when modeled correctly. The Eurocode [15] prescribes additionally to spread the wheel loads for the fatigue detail checks over an angle of 45 degrees. Furthermore, the ROK [2] prescribes to explicitly use the influence of temperature on the computational stiffness of the asphalt, and use 3D elements to model the influence of asphalt. However, the case study bridge does not possess an asphalt layer, but an epoxy wear surface of 10 mm. In contrary to an asphalt layer, the stiffness of this 10 mm wear surface layer is considered low enough that the influence is negligible regarding the fatigue verification, as indicated by the ROK [2].

4.4. Determination of stress ranges and damage

The regulations work with a stress interval spectrum per detail. These are occurring stress ranges over the lifetime of the bridge per detail. To obtain this, several factors should be taken into consideration, like the stress histories of the bridge, a dynamic amplification factor, the stress interval spectrum and cycle counting methods. These are explained in this section.

Stress histories

When all load cases are known, the stresses on the OSD bridge can be calculated by applying all loads in a FE model, and consequently using the hot spot stress method to determine the structural stresses at the constructional detail. This obtains a stress history, which is defined as 'A presentation of the expected fatigue action effect by arranging the stress cycles in chronological sequence' [15], as illustration an example from the Eurocode is given, see Figure 4.7. Such stress histories should be made for each constructional detail considered.
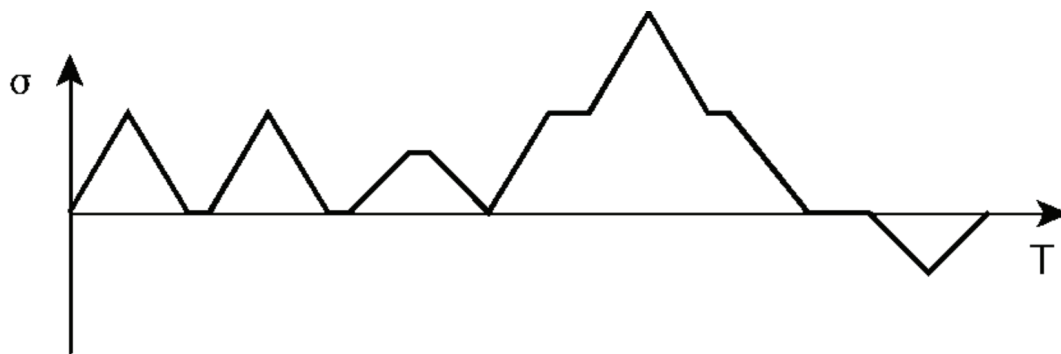
Figure 4.7: Example of a stress history graph [15].

Stress reversals

The Dutch guidelines defines three transversal load distribution, each having 5 lateral weaves, as stated in Section 4.2. The ROK [2] and Zou et al. [34] conclude that the effect of stress reversals from these lateral weaves cannot be ignored as this may result in overestimated fatigue life. This is due to the fact that the effect of a truck at the middle of the trough can be opposing to the effect of a truck in the middle of two troughs. And therefore the cumulative fatigue damage exceeds the fatigue damage of sum of the two trucks individually. This means that in terms of fatigue, not the effect of individual fatigue trucks should be considered, but the effect of a representative number of trucks, in random order, in different transverse positions [2], like indicated in Section 4.2.

Dynamic amplification factor

Before obtaining the stress ranges from this stress history, a dynamic amplification factor should be applied to stresses in the static model. This factor relates to the dynamic behaviour on the bridge when a truck passes an expansion joint. The ROK [2] uses a factor of 1.15 for all stresses of fatigue details within six meter from an expansion joint. Considering the case-study based bridge, with a length of only 10.7 meter and an expansion joint on each side of the bridge, a factor 1.15 must be applied to all stresses.

Stress interval spectrum

The determination of fatigue life is dependent on stress ranges. Which can be determined and illustrated in a stress interval spectrum. It contains values of the stress ranges occurring in the stress histories and the amount in which they occur in the lifetime. It basically consists of two steps; counting the stress ranges and drawing the stress interval spectrum, see Figure 4.8.

(a) Counting the stress ranges.

(b) Stress interval spectrum.
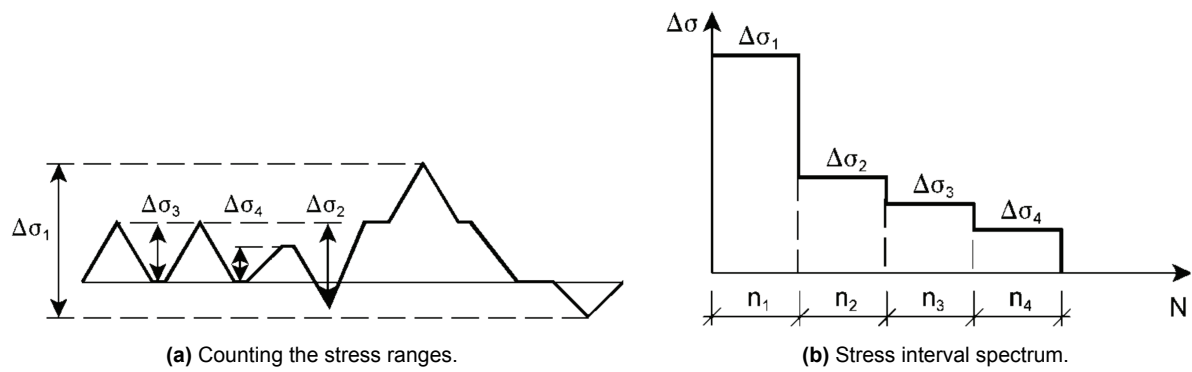
Figure 4.8: Obtaining the stress interval spectrum [15].

Two main methods to extract these stress ranges from the stress history exist; the reservoir method and the rainflow method. Before any of these methods can be carried out, the stress history needs to be reduced to a series of peaks and valleys. See Figure 4.9.

a) Original signal

b) Peaks/valleys

c) Reduced signal
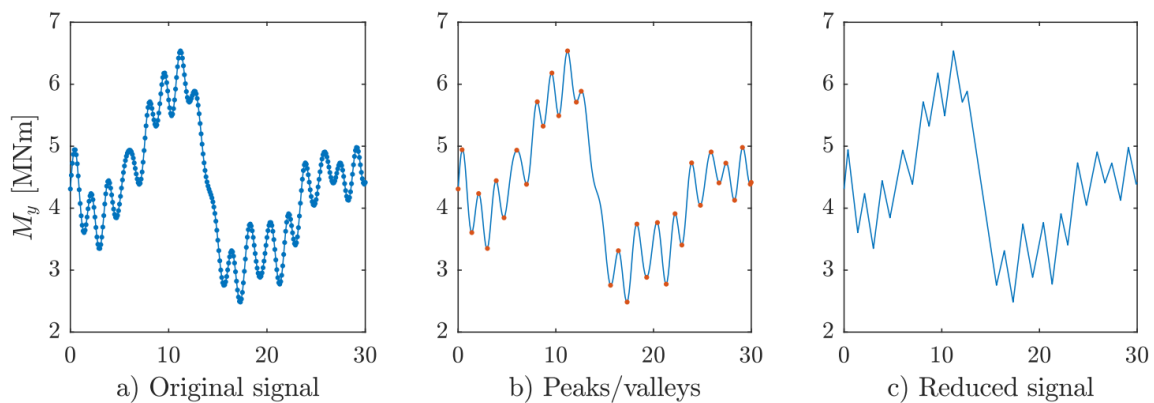
Figure 4.9: Preparing the stress history signal [44].

After preparing this signal, the reservoir or rainflow cycle counting method can be applied, both giving the similar stresses [45]. In this study the reservoir method is incorporated. To apply this method, the stress-time history is reorganized to commence with the highest peak. After which the stress-time history is conceptually filled with water and progressively drained from the lowest point. The height of the reservoir then corresponds to the stress range, see Figure 4.10.
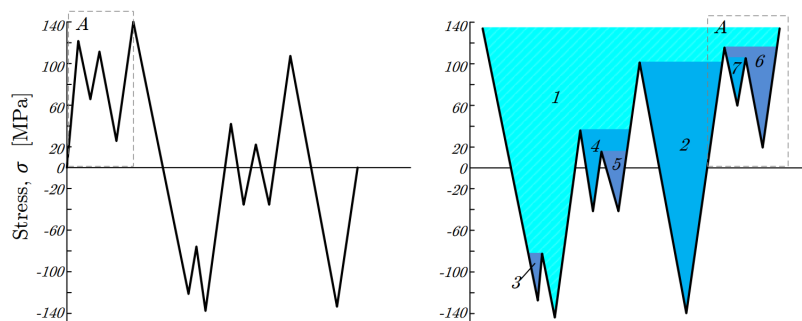
Figure 4.10: Executing the reservoir method, by M. Pedersen [44].

4.4.1. Fatigue resistance

As all stress ranges over the lifetime of the bridge can be determined. Now these occurring stress ranges in the different constructional details should be compared with the resistance of these details. The resistance is expressed as the amount of times a certain stress range may happen until failure, illustrated in S-N curves, as explained in Section 3.2.
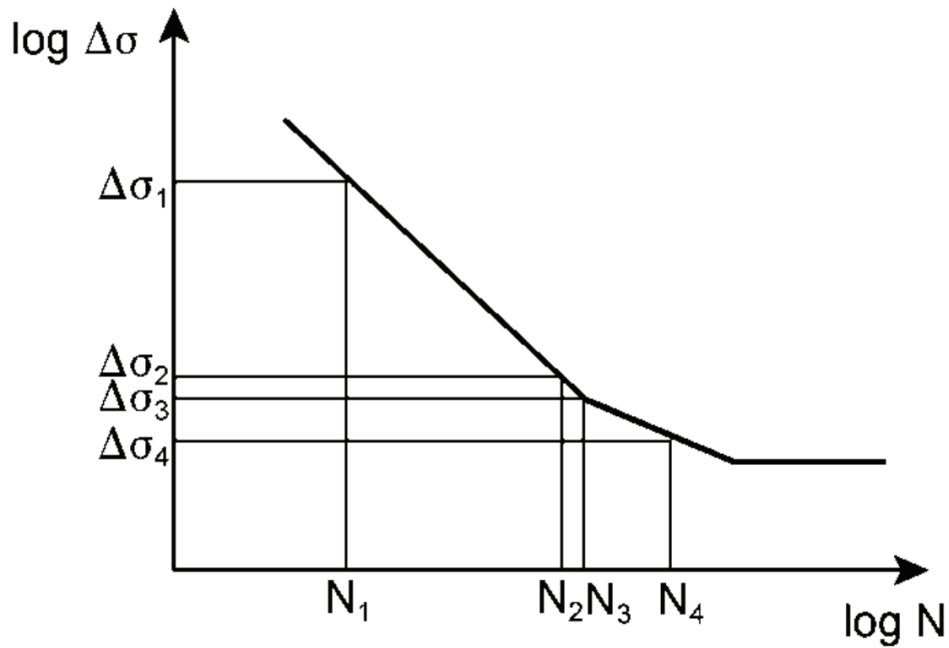
Figure 4.11: Number of cycles until failure for multiple stress ranges (for one detail) [15].

4.4.2. Fatigue damage
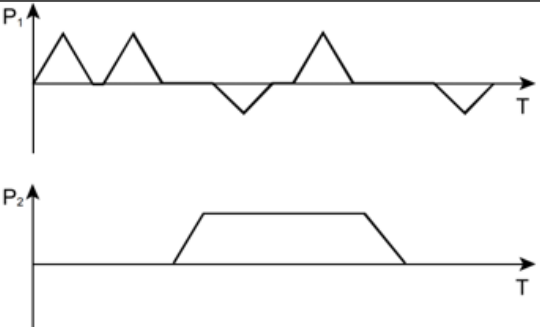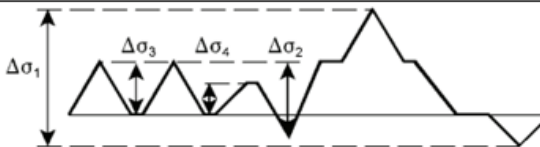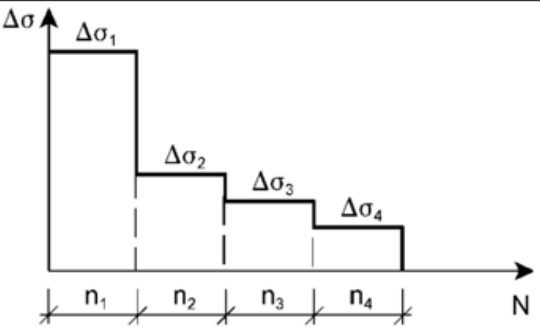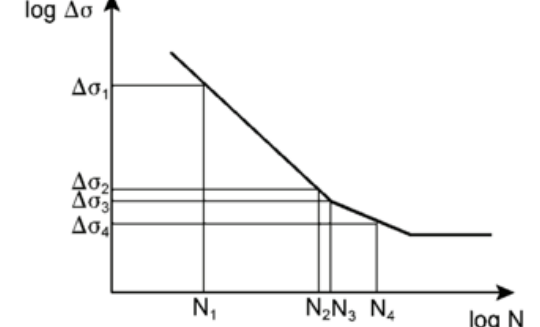
Fatigue damage is calculated with the determined stress ranges and resistance of a constructional detail. All different stress ranges occurring in an OSD above the cut-off limit contribute to the damage of the bridge, and the total damage should be calculated. Which is done with the Palmgren-Miner rule [15]:

$$\sum \frac{n_i}{N_i} = \frac{n_1}{N_1} + \frac{n_2}{N_2} + \frac{n_3}{N_3} + ... + \frac{n_n}{N_n} \leq D_L \tag{4.1}$$

In equation 4.1, the fatigue accumulation D_L is set as 1. Satisfying this equation means that the total damage is smaller than the fatigue accumulation. This rule is considered the Unity Check (U.C) for a single constructional detail.

4.4.3. Summary cumulative damage method

The process of obtaining stresses from the stress histories and calculating the damage number with is is called the cumulative damage method. For an overview a summary is given in Table 4.4.

a)	Loads P_i acting on the structure during its lifetime	
b)	Stress histories at the location of each detail	
c)	Counting the stress ranges	
d)	Stress range spectrum	
e)	Number of cycles till failure	
f)	Damage accumulation	$$\sum \frac{n_i}{N_i} = \frac{n_1}{N_1} + \frac{n_2}{N_2} + \frac{n_3}{N_3} + \frac{n_4}{N_4} \leq D_L$$

Table 4.4: Fatigue damage overview, obtained and translated from the Eurocode [15].

5

State-of-the-Art

Studies about optimizations in Orthotropic Steel Deck structures rarely exploit the use of a parametric model, and parameter sensitivity studies in OSD's which use a parametric model could not be found in Literature. This illustrates that the topic is still in its early stages of development. In this chapter the newest research papers with the topics of 1) parametric model optimization of an OSD and 2) parameter sensitivity in an OSD are evaluated to illustrate the current state-of-the-art.

5.1. Parametric optimization

Studies of Baandrup [13] and van der Laan [11] are one of the few that researched possibilities of exploiting parametric FE models to comply to fatigue verifications. The studies found significant optimizations in weight of the initial considered case-study bridge, around fifteen percent. Wei Huang et al. [12] also researched the possibility of optimizing the OSD, but no parametric model was used as this research utilized a response surface method. All named research exclusively focused on the optimization of the OSD, and no parameter sensitivity analysis is carried out. This is unfortunate as significant knowledge about relations could have been obtained with the made parametric model. The studies are difficult to compare as different parameters, details and even different design codes are employed in the studies. Therefore, the studies including parametric models are discussed separately.

Baandrup [13] used a parametric model with three structural details, which were regarded as governing. This research included ten design parameters and calculated designs with the cumulative damage method. The fatigue loading scheme was simplified to reduce the required computational power. The research calculated stresses with the hot spot method without the use of local thickenings, as is prescribed in the ROK [2]. The research showed an optimization of 16.7 percent for the case study; the Osman Gazi Bridge. This bridge had a deck with cut-outs around the stiffeners. This resulting bridge does not comply with the regulations. When complying with the Eurocode regulations at the time the weight savings were 5.8 percent. Very limited validation is executed regarding the model and the made assumptions. Question could be asked whether the used 2D model is accurate enough as the Literature review pointed out that conventional shell element models without local thickenings do not represent the stresses in the vicinity of the weld accurately. Additionally, just one loading truck has been used.

Van der Laan [11] used a parametric model as well, including local thickenings as prescribed by the ROK. Four structural details were included and seven parameters. The method to calculate damage was the cumulative damage method. A simplified loading scheme was used. The research included local thickenings to model the additional stiffness of the weld, in correspondence with the ROK. The research showed a 17.4 percent lighter deck regarding the case-study van Brienenoord bridge, which has a deck type with continuous troughs without cut-out. Unfortunately, the design does not comply to the regulations of the ROK. Additionally, disregarding the multi-path model of the transversal load distribution could lead to underestimated stress ranges. Furthermore, no validation of the location of details has been executed.

5.2. Parameter sensitivity

Multiple studies have been executed to research parameter sensitivities on Orthotropic Steel Decks, like Xia et al [10], Fettahoglu [9] or Fang et al. [46]. Many different structural details have been investigated. And parameter relations regarding these structural details have been found by manual calculations. No study has been found to include a parametric model to execute the parametric study. Therefore, each study considers the relation between only a small amount of details and parameters.

Ye Xia et al. [10] executed a parametric sensitivity analysis on a case study of the Bronx-Whitestone Bridge in the United States. The study incorporated four details for two different deck types: one with and without cut-outs, both with continuous troughs. The study researched the effect of the thickness of the deck plate, crossbeam web and rib wall thickness on the details at the intersection of the crossbeam and troughs. Concluded was that the critical location and detail varied when the parameters were changed, and that increasing the deck plate improved the fatigue life of the OSD system significantly for all considered deck details, see Figure 5.1. Also, using cutouts at the intersection of the crossbeams and the stiffeners did not influence the service life of the design drastically.
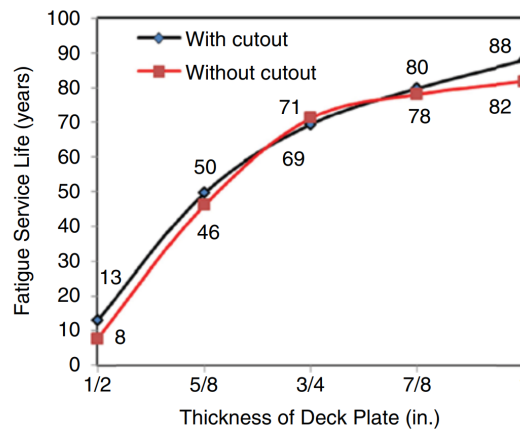
Figure 5.1: Influence of deck thickness on the fatigue life [10].

Additionally, the thickness of the crossbeam and the thickness of the ribs have been researched. The thickness of the crossbeam had a limited effect on fatigue resistance of the deck plate details and the weight of the bridge. In contrary, the influence of the rib both had significant influence on the maximum occurring stress in the OSD and on the weight of the bridge, see Figure 5.2.
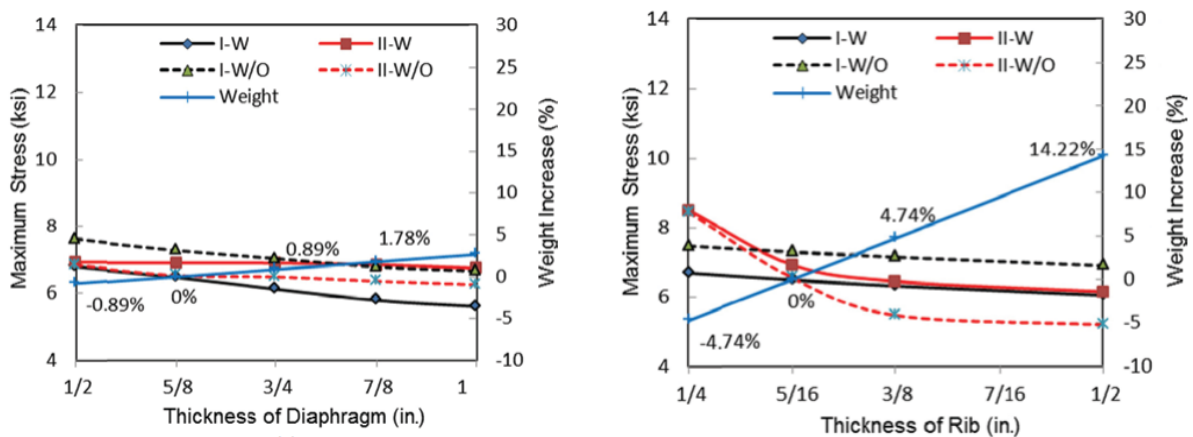
Figure 5.2: Influence of crossbeam web thickness and rib thickness on the maximum stress in the bridge and the weigth.

Fettahoglu's research [47] prescribes recommended ratios of parameters, specifically the ratios between the trough width to trough height and trough spacing to deck plate thickness. The author used the von Mises stress to compare the results of the FE analyses and to determine governing places with high stresses. This research did not include different loading schemes, which can also be influential for these governing places. The research concluded that ratios prescribed in the Eurocode, like a deck plate thickness greater than 10 or the ratio of rib spacing to deck plate thickness between 25 and 300 millimeters, are valid. Another significant conclusion is made that the height of a trapezoidal rib should be equal to its width. However,it must be noted that this is based on only one loading condition without implementation of transversal weaves. Conclusions can be made about this constraint with the obtained parametric model of this study. The study of Fettahoglu saw a significant reduction in von Mises stresses in the deck plate as it became more thick, and saw a reduction in von Mises stresses when using smaller rib spacing, see Figure 5.3. Another remarkable finding is the local minimum of the maximum displacement in the bridge when using a rib spacing of 300mm.
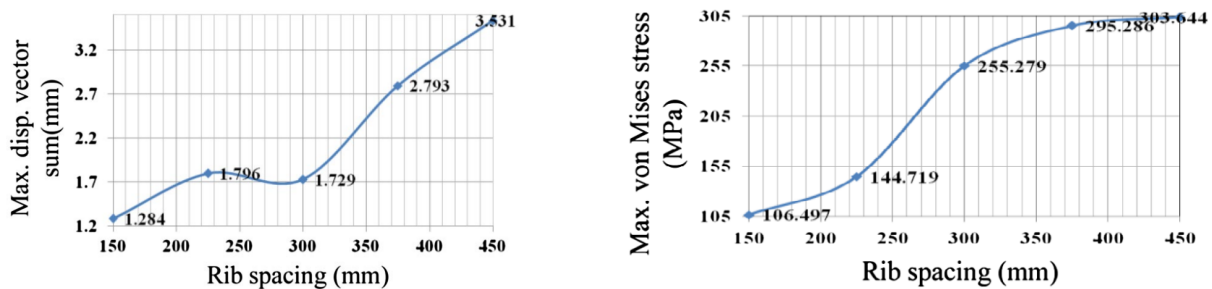
Figure 5.3: Influence of rib spacing on the maximum displacement and von mises stress in a case study bridge [47].

5.3. Conclusion

Section 5.1 included research towards OSD's which showed that the automatisation and parameterization of the fatigue calculation and a FE-model can be very powerful and can unlock the possibility of fast optimizations, like illustrated in [11] and [13]. Noted should be that the parametric model can only be used for fatigue verification with a simplification of the analysis so far due to the required computational power of the fatigue verifications according to the Dutch guidelines. Additionally, in both studies questions arise whether the simplifications made or modeling techniques used do not influence the stresses significantly. These parametric models are still in the early stage of development and include only limited validation in the existing studies.

In Section 5.2 studies towards the parameter sensitivity in OSD's are discussed. These kinds of studies relate different parameters to the fatigue life of the bridge, optimizing ratios between parameters and giving recommendations to future OSD designers. Although many studies have been executed, none used a parametric model with multiple details. Therefore, all studies usually only could research the influence of a few parameters, usually one or two, on a single detail. This section furthermore showed the importance of the deck plate. As this is the most significant cost factor when reduced, yet also a factor which can improve fatigue life greatly when enlarged.

The state-of-the-art illustrates that a parameter sensitivity analysis has never been executed with a para-metric model with automated fatigue verifications. Due to needed simplifications and limited validations questions arise if these stresses are correct. When performing an parameter sensitivity analysis simplifica-tions can be taken but the loading scheme should incorporate multi-path models, as literature points out that disregarding these transversal distributions stresses do not agree with reality. Executing a parameter sensitivity study with a parametric model could provide a lot of knowledge about the considered parameters on different fatigue details and the weight of the bridge. The parametric model should however, comply with reality. Furthermore, the model will also be a framework for automated and accurate fatigue verification. Additionally, other value can be identified. Possibly obtaining insight into governing fatigue locations on the bridge per detail. Additionally, the validation of the model provides information about the use-ability and possibly the precision of the model.

Part II

Development and analysis of the parametric model

<div align="right">

6

</div>

Parametric Model Description

This chapter entails the detailed description of the parametric model. First, a small case study introduction is given. The section thereafter describes workflow of the model and the parameters used in the parametric model and their ranges. Section 6.4. describes the general model properties like dimensions, material properties and support conditions. Subsequently, the considered details are evaluated and the local thickening approach is visualized. Additionally, The stress extraction of the model is envisioned. Section 6.7. entails the general mesh description and the mesh convergence study which is executed. The final section describes the loading used in the parametric model.

6.1. Case study introduction

The original model of the Case-study bridge is the Goereese bridge. The bridge is located in Stellendam, The Netherlands, see Figure 6.1a. The bridge is part of the N57 and spans the lock next to the Haringvliet river. The bridge consists of four identical bascule bridges, visible in Figure 6.1b. Two identical bridges besides each other with each two bascule parts. Due to this symmetry, the fatigue verification of only one part has to be studied.

(a) Location [48]

(b) Side view [49]

Figure 6.1: Goereese bridge, location and side view.

The bascule bridge includes complex aspects which are not modelled linearly. Additionally, it involves a large counterweight, see Figure 6.2a. This initial model is generalized for ease of parametrical design and a wider applicability in general. Other benefits are that the relations between the parameters do not include effects from from the non-linear geometry and that possibilities emerge to exploit symmetry conditions to reduce calculation time of the model. The initial model is showed alongside the generalized model to indicate the changes made, see Figure 6.2. The models contain 4 crossbeams, 2 main girders, a deckplate and troughs which are continuous throughout the length of the bridge. The models consist of 2D plate elements, including deformations from normal, shear, bending and warping forces.

(a) Original design   **(b)** Parametric design
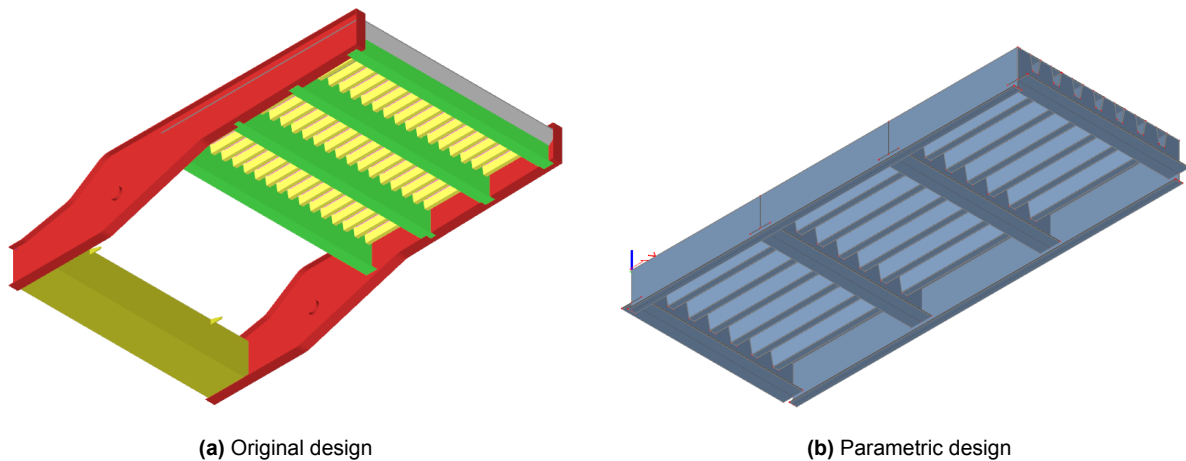
Figure 6.2: Original vs parametric model design.

6.2. Parameters

In the parametric model eight parameters are considered, see Table 6.1. The choice for these parameters is based on their influence on the weight of the bridge and on the considered details. In the Literature study the choice for all trough parameters and the deck plate thickness were already motivated. All parameters are additionally included in multiple figures of section 6.4.1.

Other included parameters beside the deckplate thickness and the trough dimensions are the center to center distance and the thickness of the crossbeams. The center to center distance of the crossbeam is expected to influence the fatigue life of the bridge as this parameter significantly affects the influence lines of the bridge and determines the trough span. Additionally, studies have shown that this parameter influences the fatigue life of the bridge [12][13]. It should be noted that within the parametric model, a constant bridge length is taken with four crossbeams in total. This means that the crossbeam center to center distance can vary, but the three spans should always total the length of the bridge. Therefore the varied parameter is the center to center distance of the middle crossbeams. Varying this parameter could help to draw possible conclusions about governing details on the bridge.

The thickness of the crossbeams is also incorporated as a design variable in the parametric model. This parameter has a significant influence on the deflection of the the crossbeam and deckplate, and thereby also effects the stresses at the details at the crossbeam, as shown by [43].

The table additionally includes a step-size, which is utilized in the parameter sensitivity study. These step-sizes are determined based on a combination of feasible designs and the need to limit the number of variants required for the sensitivity study.

Table 6.1: Parameters and their domain of the parametric model

Parameter	Symbol	Min [mm]	Max [mm]	Step size [mm]
Deck thickness	t_{dp}	10	30	1
Trough thickness	t_{tr}	6	8	1
Crossbeam thickness	$t_{cb,web}$	12	20	2
Top width troughs	$w_{tr,top}$	150	300	50
Bottom width troughs	$w_{tr,bot}$	100	200	25
Center to center troughs	ctc_{tr}	$w_{tr,top}$	$2\,w_{tr,top}$	25
Height troughs	h_{tr}	325	400	25
Center to center of middle crossbeams	$ctc_{cb,mid}$	3000	4000	100

6.3. Workflow

Before a detailed description is given for all parts of the model, an overview is created to illustrate the general framework and working of the parametric model. The parametric model is build in combination with different programs and tools, all executing different commands, See Figure 6.3
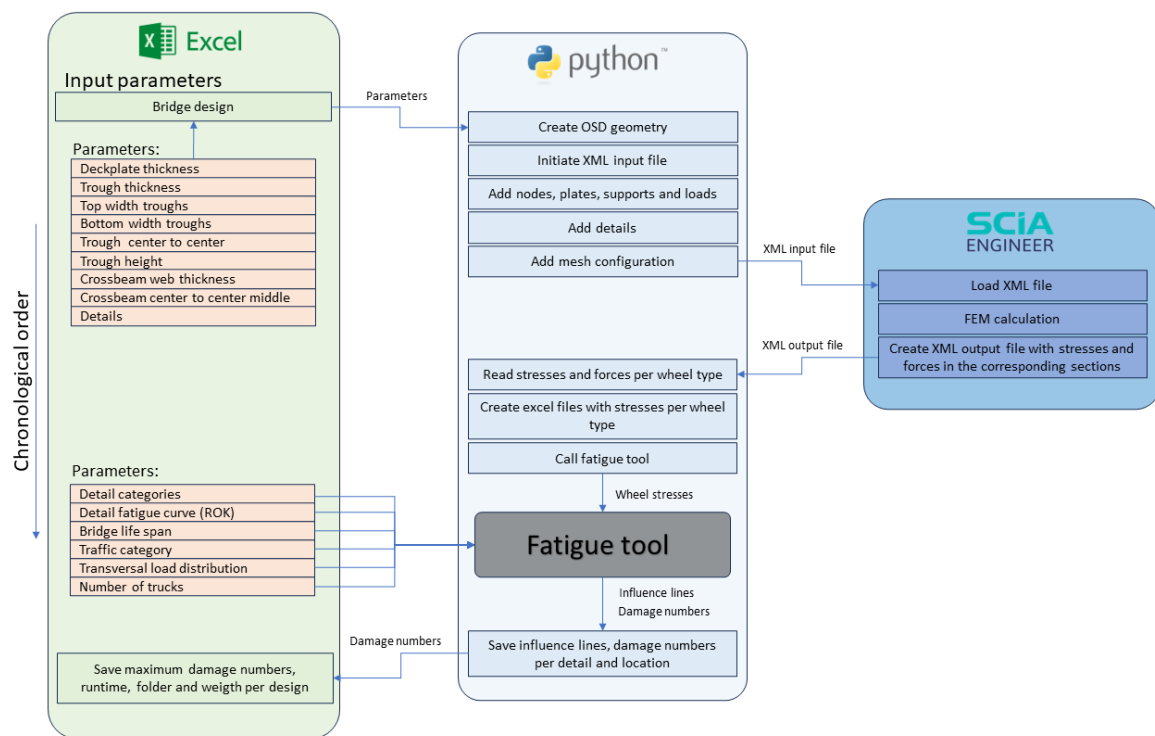
Figure 6.3: Workflow of the full parametric model including fatigue calculations.

6.4. General model properties

This section outlines the general properties of the model, including the bridge dimensions, the material properties of the steel used, the support conditions of the bridge and additional FE properties incorporated in the model.

6.4.1. Dimensions

Both the initial and generalized bridge consists of four main parts; the deckplate, main girders, crossbeams and stiffeners. The dimensions are shown for each part, including the model parameters described in section 6.2.

Deckplate

The length of the parametric design is rounded up to 11 meters relative to the original design, which is 10.8 meters. The deckplate thickness is 20 mm in the original design, in the parametric model the deckplate is variable. For the dimensions, see Figure 6.4.

(a) Original model dimensions   **(b)** Parametric model dimensions
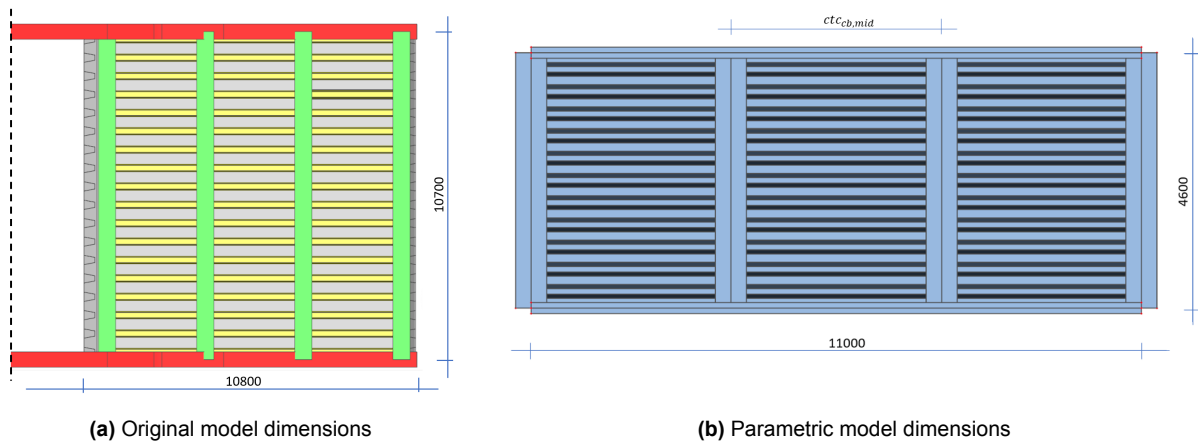
Figure 6.4: Original vs parametric model design, dimensions in mm.

The width of the parametric bridge is generalized to possess one driving lane. As the Dutch guidelines, in contrary to the Eurocode, state to take into account concurrency of traffic when considering more than one driving lane, this particular choice of one lane reduces the number of load combinations to be considered by at least half of of the total number of load combinations. Consequently, this provides a considerable faster calculation time of the FE model as the original bridge is designed to include two driving lanes. Additionally, it is anticipated that this reduction to one driving lane will minimally impact the fatigue verification of the deckplate details, as these details are highly influenced by the local geometry, and global influence is expected to be limited.

The carriageway of the bridge then depends on the width of one driving lane and the width of the remaining area. In the Netherlands, for one driving lane (100 km/h), generally a paved width of 4.6 meter is constructed as stated in the design guide [50]. This common design is adopted to the parametric model, which means the design width includes one driving lane of 3 meter in the center, and two remaining areas at the sides of 0.8 m. The assumption is made that the theoretical lane is the only lane where the traffic rides.

Main Girders

The main girders of the generalized design are simplified relative to the original design. The original design involved non-uniform main girders over the length of the bridge, which is not desirable for this parametric design. In the parametric design, the main girders are designed uniform over the length of the bridge. The dimensions of the main girder have been reduced in the generalization process to better align with the reduced width of the parametric model. The main girders are not changed in the parameter study. The dimensions are shown in Figure 6.5a

(a) Main girder   (b) Crossbeam   (c) Crossbeam 3D view
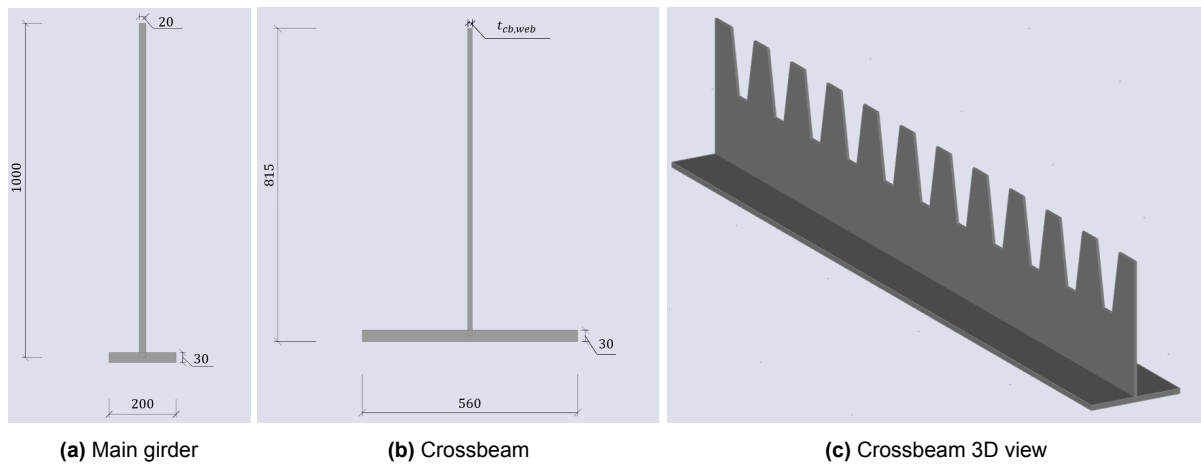
Figure 6.5: View and dimensions in mm of main girders and crossbeams

Crossbeams

The original model contains crossbeams varying in size and thickness. In the parametric model the four crossbeams are identical in shape. Their dimensions are visible in Figure 6.5b. The web thickness of the crossbeams is parameterizable. The dimensions of the crossbeam are decreased as the parametric model also received a significant reduction in width. The dimensions are derived from large H profiles. The crossbeam flanges are expected to not influence the details in the deck plate much and are taken as a constant.

Stiffeners

The parametric model contains trapezoidal stiffeners. All aspects of these troughs are selected to be design variables as these parameters are expected to significantly influence the bridge design and details in the deck plate. See Figure 6.6 for the different variables of the troughs.
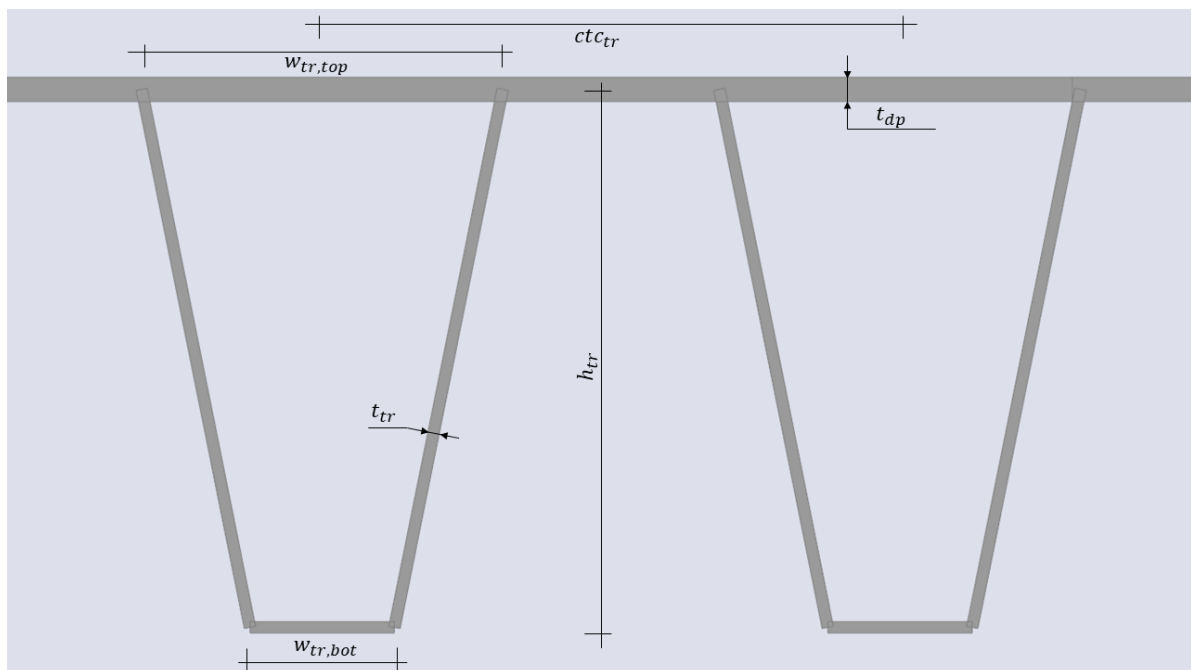
Figure 6.6: Parameters of the troughs and deckplate

6.4.2. Material properties

The material used is steel S355. As this material is used throughout the bridge, the Poisson ratio, E-modulus, density and shear modulus remain constant over the full design. In this research only elastic material properties are considered as the fatigue loads result in stresses in the structure far below the yield limit, when the OSD is adequately designed. See the Table 6.2.

Property	Symbol	Value	Unit
Yield stress	σ_y	355	N/mm^2
Elasticity modulus	E	210000	N/mm^2
Shear modulus	G	80769	N/mm^2
Poission ratio	v	0.3	$-$
Density	ρ	7850	kg/m^3

Table 6.2: Material properties of the used steel, in correspondence with EN1993-1-1. [51]

6.4.3. Support conditions

Where the original bascule bridge model is supported by a connecting bar, the parametric model has fully clamped line supports at the web and bottom flange of the main girders, see Figure 6.7.
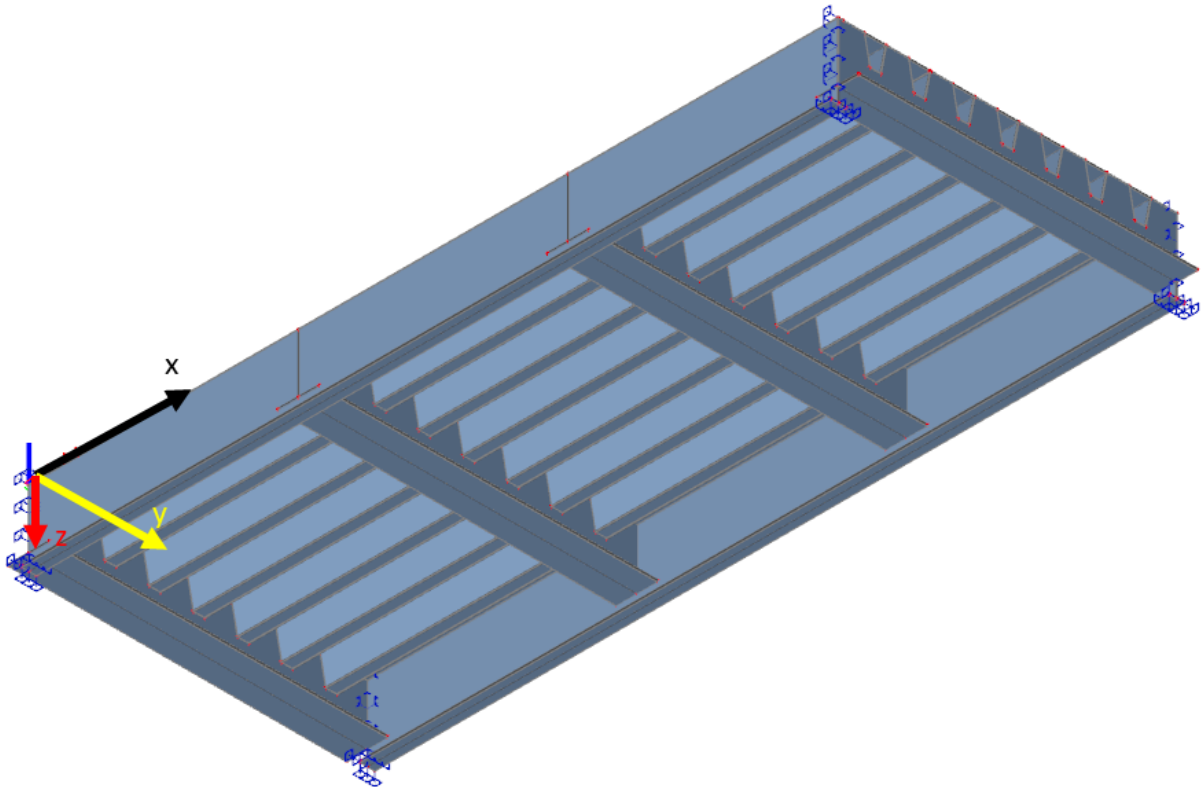
Figure 6.7: Boundary conditions (blue) of the parametric model.

6.4.4. FE model properties

The full model is made of 2D shell elements and only uses first order (linear) shape functions. The 2D elements consist of either three or four nodes [52], having either a triangular or quadrilateral shape. The triangular shape is used by the meshing algorithm highly sporadic, and the quadrilaterals are predominantly used. In correspondence with the ROK [2], which prescribes to use 4-node elements in the stress extraction zones.

6.5. Details

The ROK distinguishes 27 different details, of which eighteen should be checked when incorporating continuous stiffeners without a cut-out hole, like in this research. However, only the directly ridden details, the details in the deckplate, are included in the scope. The comprehensive description of these details by the ROK [2] are given in Annex A, Figure 6.8 illustrates the place of these details in an orthotropic deck.

These details are all included in the parametric model with the use of local thickenings, as described in Section 4.3.1 and by the Dutch regulations [2]. Details 1A, 1C, 2A and 2B use the same local thickening of the weld connecting the deckplate and the trough. Details 5, 6A and 6B also use the same local thickening; the deckplate to crossbeam weld. See Figure 6.8. Furthermore, the assumption is made that automated welds are included in the design for details 2A and 2B, which enhances their detail categories.
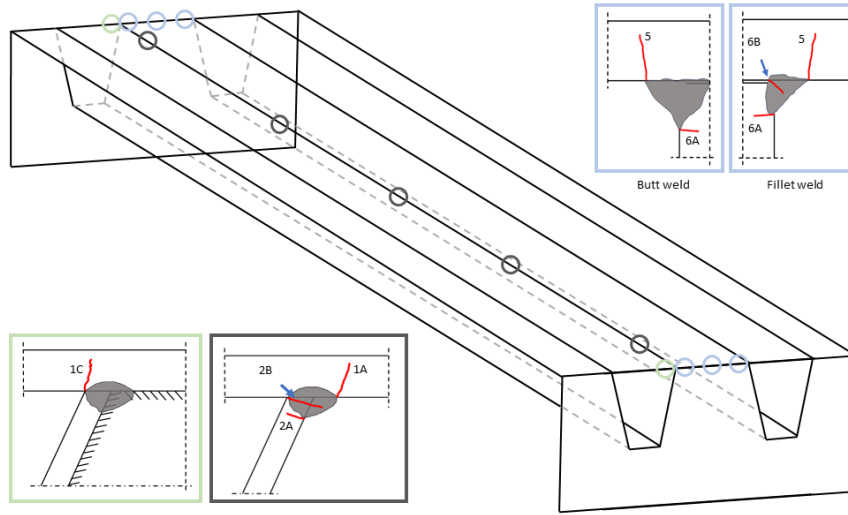
Figure 6.8: Details and their possible position.

The effects of the welds are factored in by modelling a thickened region. This region is defined inbetween the weld toes, the thickness of these elements are calculated trough the determined formulas incorporated in Figure 6.9.

$$h_3 = h_4 = t_2$$
$$L_1 = h_3 + 0.5 * \left(\frac{t_2}{\cos \theta} - t_1 * \tan \theta \right)$$
$$L_1^* = 0.5 * \left(\frac{t_2}{\cos \theta} + t_1 * \tan \theta \right)$$
$$L_2 = h_4 + \frac{t_1}{2 \cos \theta} - 0.5 t_2 \sin \theta$$

$$t_{1,mod} = t_1 + 0.5 L_1$$
$$t_{2,mod} = t_2 + 0.5 L_2$$

$$\gamma = 90° - \beta$$
$$L_1 = t_2$$
$$L_2 = 0.5 * t_1 + 0.5 t_2 \tan \gamma$$

$$t_{1,mod} = t_1 + 0.5 L_1$$
$$t_{2,mod} = t_2 + L_2$$
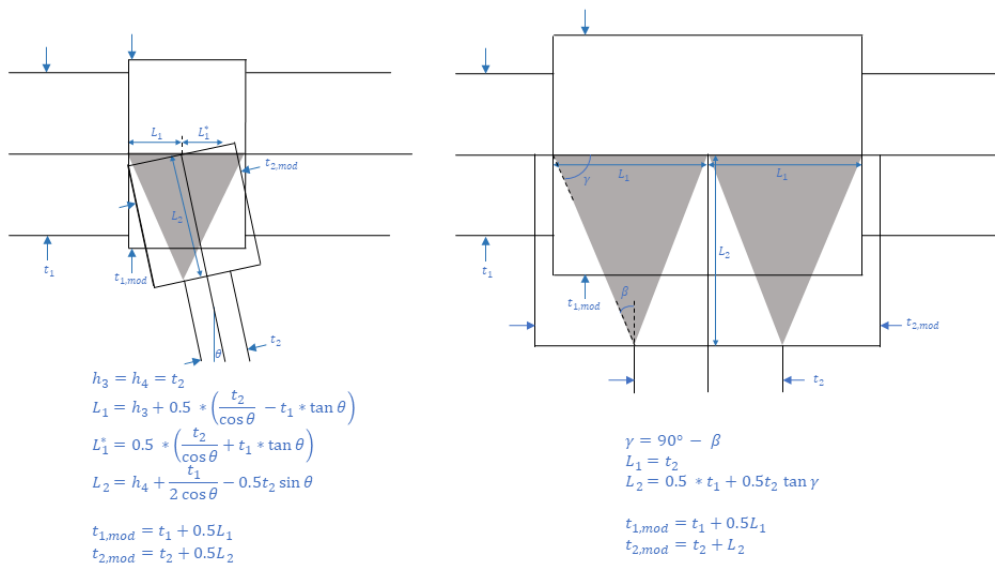
Figure 6.9: Local thickenings of welds occurring in the model. Left: thickenings trough-to-deckplate weld. Right: Deckplate-Crossbeam weld.

6.6. Stress extraction

The stress determined with the parametric model is extracted using the hot spot stress, as prescribed by the ROK [2] and illustrated in section 4.3 of the Literature review. An example is shown for detail 1A for the extraction of the stresses in the parametric model, see Figure 6.10. The stresses are extracted at point A and point B, to calculate the hot spot stress at the weld toe, which is point C, using linear extrapolation. In Figure 6.10, detail 1A is read out at midspan.
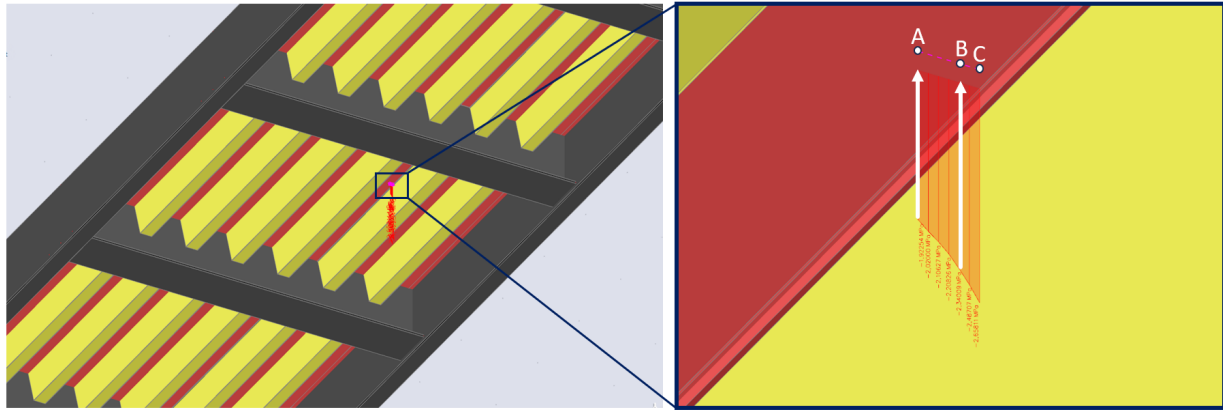
Figure 6.10: Stress extraction of detail 1A at the middle of the span.
.

6.7. Mesh description and convergence study

In section 4.3.3 of the literature review recommendations have been done about the to be used 'relatively course' mesh. To be certain that the chosen mesh is appropriate in both accuracy as in time, a mesh convergence study is done. This mesh convergence study incorporates two details, as optimising the mesh based on only one detail could lead to accurate results for the studied detail, but inaccurate results for other details. It should be noted that all eight details should be incorporated to know about the mesh accuracy of all eight details. Due to time restrictions, this is not applied. However, it is expected that all directly ridden details share similarities in the required mesh sizes. Furthermore, the two incorporated details are the most significant, as concluded in chapter 7. For all details, a local mesh refinement at the stress extraction position is incorporated, for detail 1A and 1C this value is 0.25 times the deckplate, as described by the ROK [2]. See the illustration in Figure 6.11.
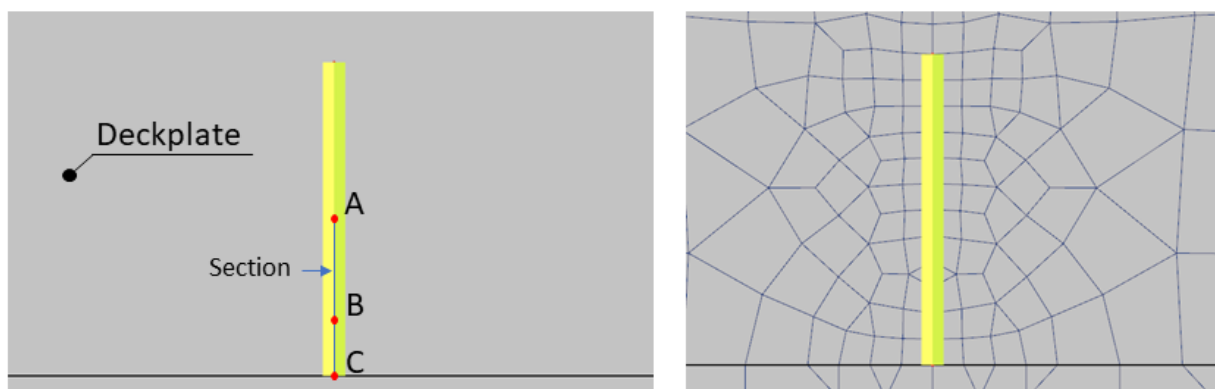
Figure 6.11: Local line mesh refinements used at the weld toe for detail 1A and at the weld root for detail 1C.

6.7.1. Initial mesh comparison

The used model for this mesh convergence study is a model with parameters that are displayed in Table 6.3. Initially, five different mesh configurations have been run for the model with one wheel type A running directly on the trough leg along the length of the bridge, which are 111 loads. These mesh element sizes are 200x200, 100x100, 50x50, 10x10 and 5x5, all in mm, see Figure 6.12. It should be noted that for element meshes of 10x10 and 5x5 not the full bridge could be modeled with these mesh sizes due to exponentially increasing runtimes and memory storage issues. In these models, the labeled mesh sizes for the three troughs closest to the detail and the deckplate area above them are maintained as the literature [41][43] indicates that this specific area nearly exclusively impacts the stresses in the detail. For the broader global part of the bridge, a uniform mesh size of 50x50 mm is used. Additionally, the configuration of the local thickenings and line mesh refinements as stated in section 6.5 are used throughout all models.

Table 6.3: Parameters OSD for mesh convergence study.

t_{dp}	t_{tr}	$w_{tr,top}$	$w_{tr,bot}$	ctc_{tr}	h_{tr}	$t_{cb,web}$	$ctc_{cb,mid}$
17	8	250	100	400	375	12	3800

(a) Detail 1A
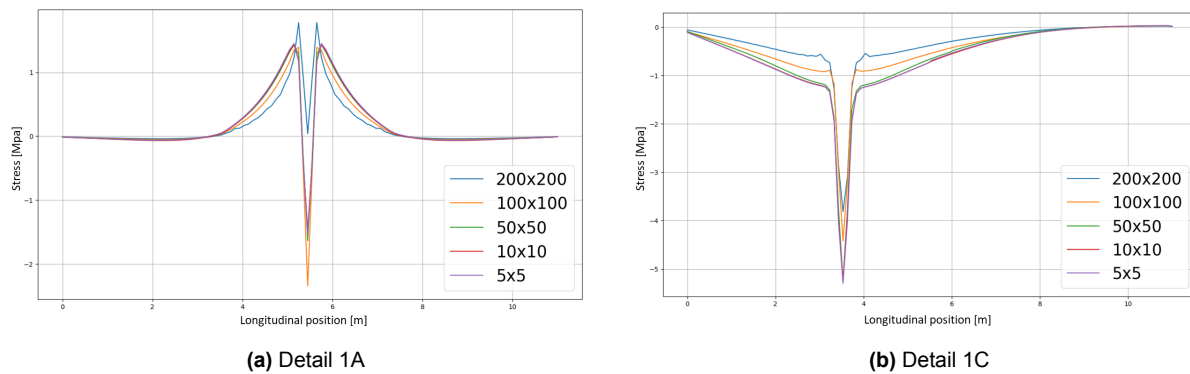
(b) Detail 1C

Figure 6.12: Influence line results with different meshes for detail 1A and 1C.

For detail 1A, see Figure 6.12a, the influence lines converge when applying a mesh size of 50x50mm or smaller. It is clearly visible that the lines of mesh sizes 50x50, 10x10 and 5x5 seem almost identical. In fact, the mesh with 50x50 has the most negative peak of the three similar meshes, and is thus faintly conservative. Additionally, for mesh sizes 100x100mm and bigger it is observed that these mesh generate much different stress ranges.

Detail 1C, see Figure 6.12b, behaves similar to detail 1A, the results converge to the lines with mesh size 10x10 and 5x5 mm. It is observed that the peak of the 50x50mm mesh is exactly the same as the value as the convergence values. However, about 0.3 meters away from the crossbeam the 50x50 line does approximate the influence line of two converging lines, however it is off by a small margin. This margin is at most approximately 0.03, which is about 0.5% of the total stress peak of the detail, which is considered accurate enough.

The accuracy appears satisfactory for a mesh size of 50x50 mm or smaller. However, the runtime of the models should also be compared as this element is crucial in this study due to the many runs of the parametric model required. The runtime of these models are determined and shown in Figure 6.13.
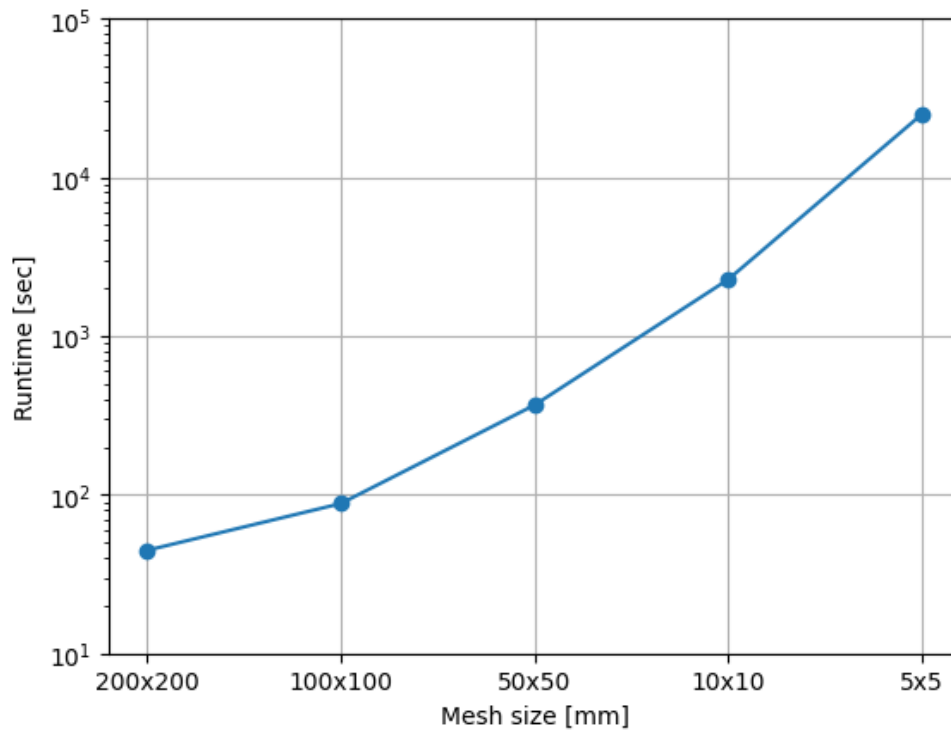
Figure 6.13: Run times of the different tested models.

The runtime is plotted on logarithmic scale, this represents the issue of the computational time becoming exponentially larger by using smaller mesh sizes. While these small meshes are accurate, the runtimes become too large. It is observed that an element mesh size of 50x50 mm is the largest mesh size where the stresses are still determined accurately. However, the computational time should also be sufficiently small. As seen in Figure 6.13, it takes 735.35 seconds to calculate one wheel running over the bridge. For one full analysis of a transversal distribution, all three wheels and all five transversal positions should be considered. Therefore the calculation time will be around 3 hours. Meshes with size 10x10 or 5x5 millimeter will have computation times around respectively 25 and 270 hours for one transversal distribution, assuming there is enough computational power to execute a model with these fine meshes. These meshes are therefore not applicable.

6.7.2. Local mesh refinement
The option to refine mesh locally is added, as previously illustrated with the 5x5 and 10x10 mesh in section 6.7.1, to distinguish certain areas in the bridge. As stated in the Literature study in section 4.3.3, it is not compulsory to mesh the whole bridge with the same meshing. In fact, studies have used a mesh refinement only for the 3 closest troughs and this area on the deckplate closest to the considered detail [11] [43]. The effects of this method are researched by comparing the full 50x50 mm mesh size with multiple other combined mesh sizes. In the parametric model 3 different mesh areas are determined. Firstly, the area of the three troughs and deckplate area closest to the detail, the rest of the deckplate and the crossbeams and the main girders, see Figures 6.14 and 6.15 and Table 6.4. It is worth noting that a fourth region is present at the position of the detail. The mesh size at this position does not vary per design but consistently aligns with the specifications of the ROK, having a usual mesh size of 0.25 times the deckplate thickness.

(a) 3D view
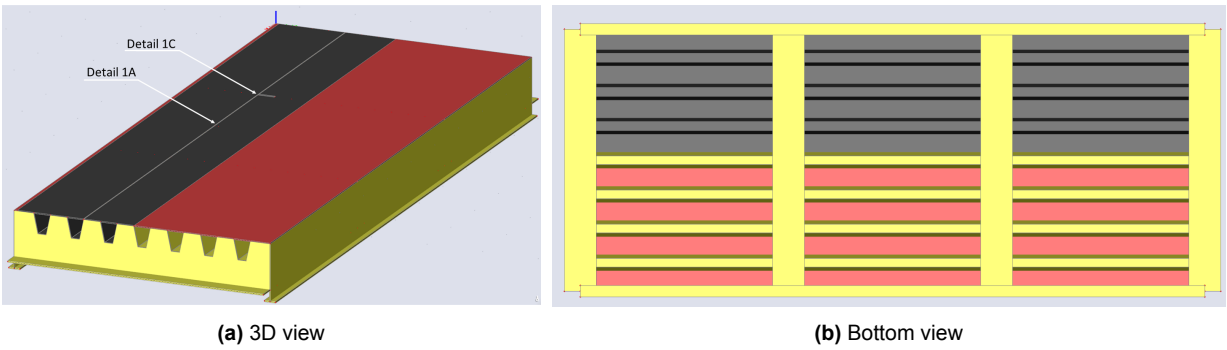
(b) Bottom view

Figure 6.14: 3D and bottom view of the different mesh regions. Each color corresponds to a mesh area described in Table 6.4. An example is given in Figure 6.15.
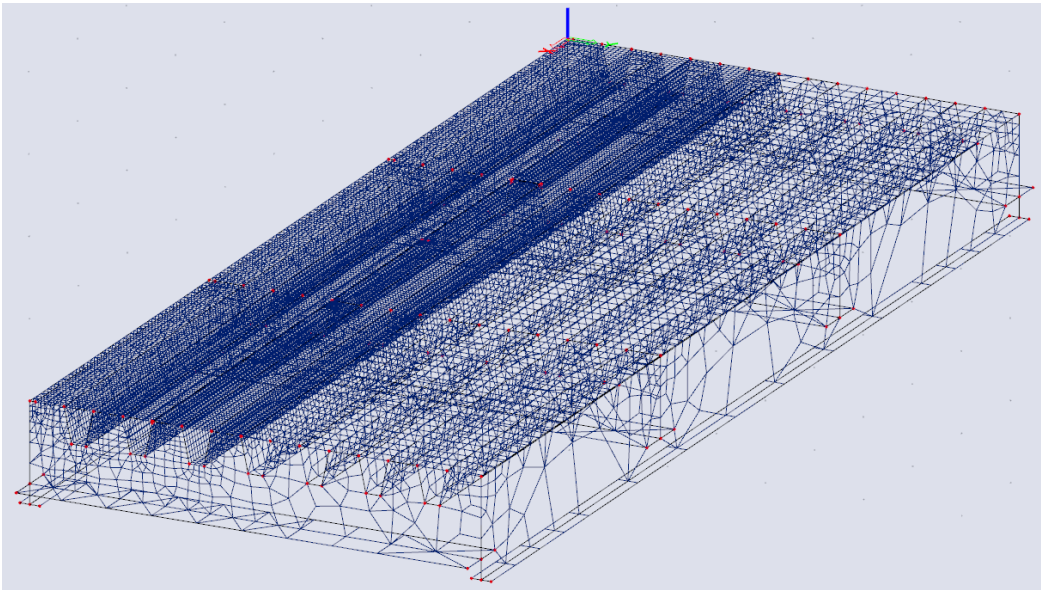
Figure 6.15: Example of different meshing regions.

Table 6.4: Distinguished mesh regions and their description.

Mesh area	description
A	The three stiffeners and deckplate area closest to the considered detail
B	Deckplate area other than area A
C	Main girders and crossbeams

The same influence line of the previously used model has been compared for multiple different mesh designs. The configuration and run times of the different mesh designs can be seen in Table 6.5, and their results on the influence lines of detail 1A and 1C are displayed in respectively Figure 6.16 en 6.17.

Table 6.5: Designs to test influence mesh regions and runtimes. The design names correspond to the legends in Figures 6.16 and 6.17.

Design name	Mesh size in mm per region			Runtime in seconds
	A	B	C	
Design 1	50x50	50x50	50x50	953.7
Design 2	50x50	50x50	1000x1000	556.7
Design 3	50x50	100x100	1000x1000	369.2
Design 4	50x50	150x150	1000x1000	329.5
Design 5	50x50	200x200	1000x1000	299.8
Design 6	50x50	1000x1000	1000x1000	280.5
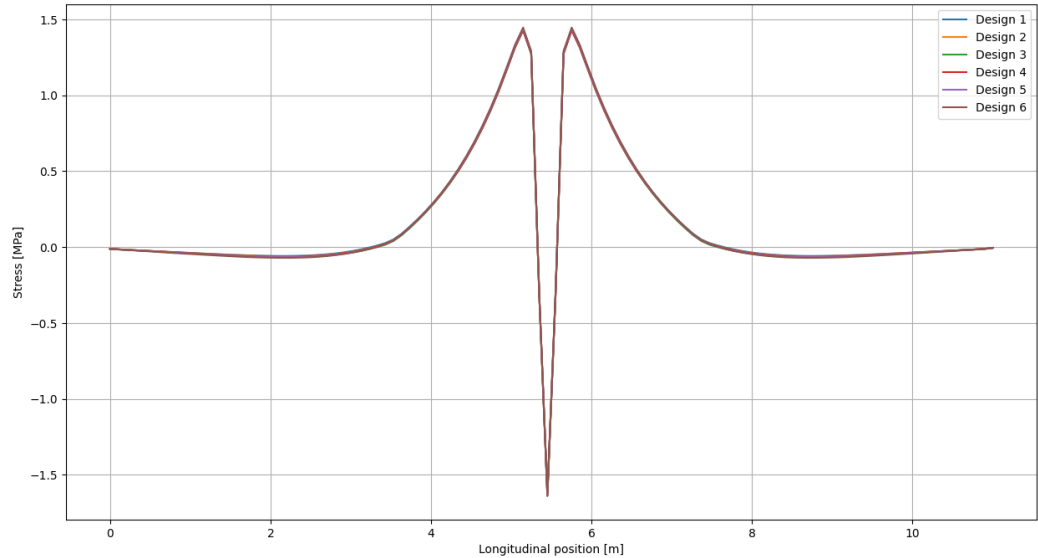
Figure 6.16: Influence line of detail 1A of different designs.
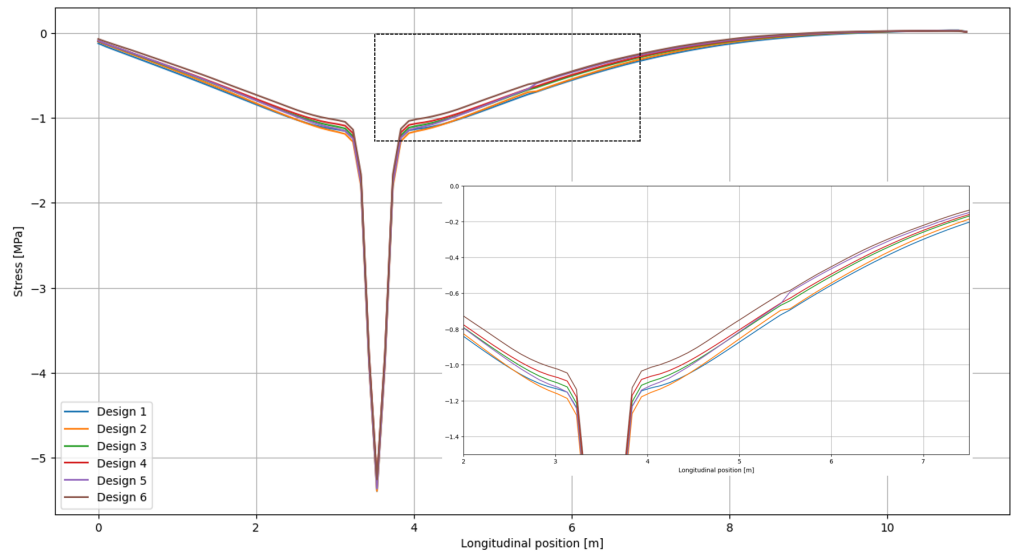
Figure 6.17: Influence line of detail 1C of different designs.

Based on these figures, concluded can be that for detail 1A, solely meshing region A significantly impacts the results, as all designs yield remarkably similar outcomes. Detail 1C seems to differ more regarding the designs. This can be explained by the extra stiffness of the crossbeam causing detail 1C to be influenced by global behaviour. It is observed in Figure 6.17 that the peak stress is similar in the different designs. However, around 200 to 3500 millimeter away from the peak stress at the crossbeam, some slightly different results are obtained. Designs 5 and 6 differ the most in this region. Designs 3 and 4 differ significantly less, and Designs 1 and 2 are particularly similar. The differences with respect to the designs with small meshes are displayed in Table 6.6.

Table 6.6: Maximum differences of the designs with respect to the design with accurate 10x10 mm mesh.

Mesh configu-ration	Max abs diff w.r.t. Mesh config 1[Mpa]	Difference in % of max stress peak	Max abs diff w.r.t. Design with mesh 10x10 mm [MPa]	Difference in % of max stress peak
1	0,00	0,00%	0,03	0,55%
2	0,02	0,36%	0,05	0,91%
3	0,04	0,73%	0,07	1,27%
4	*0,05*	*0,91%*	*0,08*	*1,45%*
5	0,09	1,64%	0,12	2,18%
6	0,12	2,18%	0,15	2,73%

Design 4 is regarded as the best balance between accuracy and calculation time. This design differs at most 1.45% from the accurate designs with mesh size 10x10 or 5x5 mm for the considered model. But has a feasible calculation time of 329.5 seconds for one wheel traversal. Accounting for one full multi-path model, thus one transversal distribution of 5 lanes with all 3 wheels; this would result in a calculation time of around 4942 seconds, or around 82 minutes. This is already satisfying sub research question 4a and 4b, as this is within a tenfold of minutes.

However, faster calculation times can be achieved as another simplification which can be implemented is the use of symmetry for the loading conditions, see Section 6.8. For this, the so-called elastic mesh function of SCIA engineer is needed as the meshing algorithm without it would be influenced significantly by the load placement, which is undesirable. This elastic mesh automatically avoids really small mesh angles [52] and is therefore considered more accurate. Additionally, a check of one load placement has been executed in Annex 6.7. Although a check of only one load placement can not be conclusive, it does increase the certainty of the assumption that the elastic mesh is generally more accurate.

6.7.3. Sensitivity for deviations
It is known that fatigue damage numbers are quite sensitive for a change in stresses. Also, due to the choice of mesh, it is demonstrated in section 6.7.2 that deviations can occur of 1.45% of the highest stress peak. It should be noted that this 1.45% can vary dependent on the design and on the influence lines of the wheels.

It should also be noted that the local behaviour around the vicinity of the detail seems accurate, and maximum deviations occur outside this local region. Therefore, designs with more global effects in influence lines, as visible in Figure 6.17, are expected to have a bigger possible deviation in stresses than designs with less global effects in influence lines, as illustrated in Figure 6.18, and used as example in Table 6.7. Therefore, quantifying this difference with only one design cannot be conclusive. However, it can give an indication of an order in which the damage number varies when stresses deviate. To illustrate this sensitivity on the damage number, a benchmark model is run with different deviations of the stresses, see Table 6.7 .

Table 6.7: Sensitivity of damage number to changing stresses.

Multiplier of stresses	1	1,01	1,015	1,02	1,03
Damage number	0.748	0,788	0,808	0.828	0.889
% Damage increase	-	5,3	8.02	10.7	18.9

This table shows the sensitivity of damage numbers to a change in stresses. Although stresses only might deviate 3 percent, this can result in an increase of damage numbers of around 20 percent. With the estimated maximum difference of 1.45% in the parametric model, the difference in damage numbers would be around 8%. It should be noted that this difference is when all stresses are multiplied with the given factor.
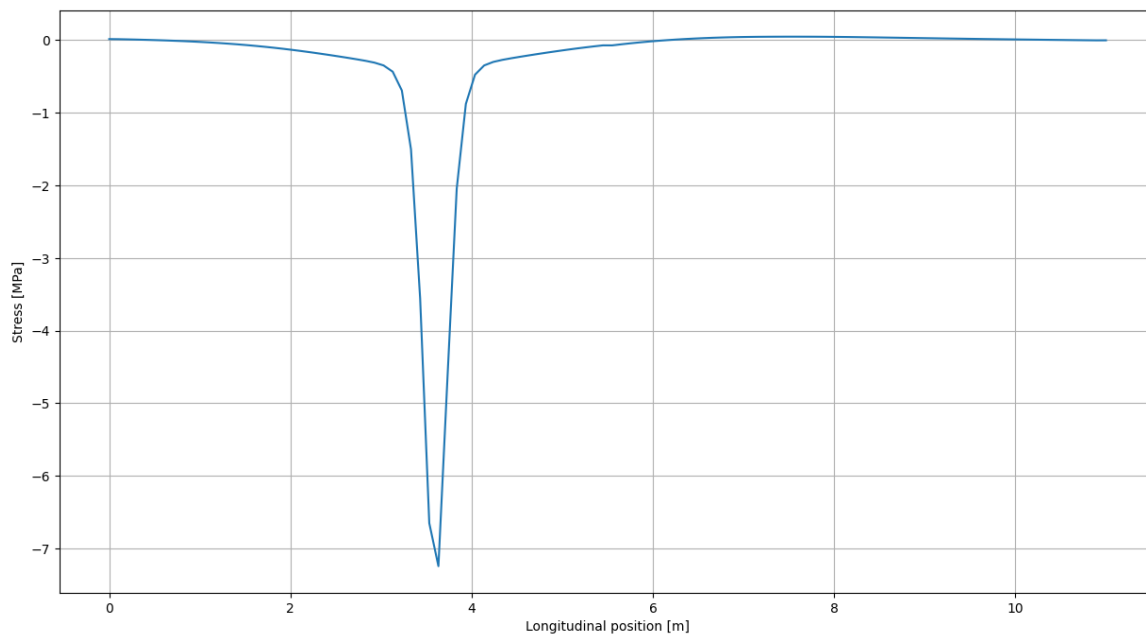
Figure 6.18: Example of an influence line with large local effects and little global effects (see Figure 6.17 for an example of an influence line with more global effects).

6.8. Loading

The loading accounts for a significant part of the computational time of the model. Fatigue load model 4a from the Eurocode has been applied to the model. This means that a complete verification of one detail for an OSD requires the incorporation of 3 transversal load distributions [2], each having 5 lateral weaves on which 3 distinguished wheel types should be placed in small steps over the length of the bridge, as stated in Section 4.2. Unfortunately, as concluded by Zou et al.[34], the effect of stress reversals from these lateral weaves cannot be ignored as this may result in overestimated fatigue life. For the parameterized model this means a total of 4995 load cases. To calculate this amount of load cases takes about 5 hours of calculation time, disregarding the time it takes to read out stresses and calculate damage numbers. Fortunately, due to the perfect symmetry of the parametric model and the load cases. Symmetry can be taken advantage of to reduce the necessary load cases.

6.8.1. Symmetry

Symmetry can be used to half the load cases, and thereby save approximately half of the computational time. This would mean the time it takes to calculate one wheel over the length of the bridge is approximately 160 seconds, see section 6.7.2. Meaning that the calculation time for one transversal distribution with the lateral weaves takes about 40 minutes. Which indicates that sub research question 4a and 4b are satisfied, as this is within a tenfold of minutes.

The implementation of symmetry is done as follows: Instead of reading out the stresses of all load cases over the full length of the bridge at only the detail position of the bridge, the stresses up to half the length could be read out at both the original detail and one additional detail exactly mirrored in the halfway line of the bridge. Why this is possible is illustrated in Figure 6.19, where the red dots indicate the points at which the stresses are obtained from the FEM model. Additionally, a comparison of damage numbers between a model with and without the use of symmetry is executed, See Table 6.8 . For this comparison, the relevant benchmark model obtained in section 7.2 is used.
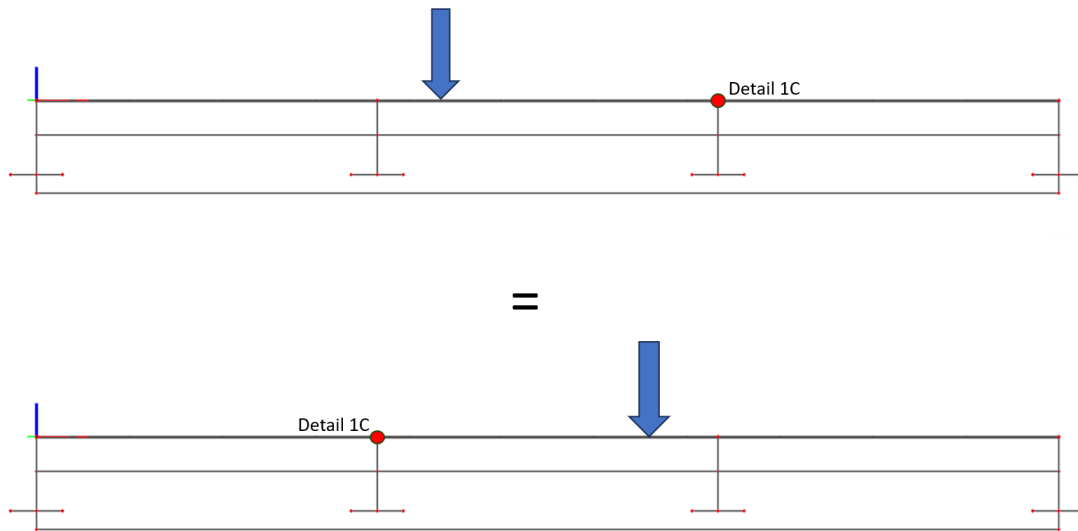
Figure 6.19: Illustration use of symmetry for loads.

Table 6.8: Damage numbers comparison.

Design	Damage number	Runtime in minutes
Benchmark without loading symmetry	0.748	± 85
Benchmark with loading symmetry	0.760	37.4

The damage number has remained roughly the same, while the model's speed has more than doubled, as shown in Table 6.8. This improvement is not only due to reducing the pure calculation time, but also because the time required for SCIA to export the XML files has significantly decreased. With half the load cases, the file size is also considerably smaller.

6.8.2. Including second wheel

For all load cases, both wheel loads of one axis have been used to compute the stress at the details. This second wheel, which does not directly ride above the detail, is additionally incorporated as the stresses can be influenced by this load. This is shown by determining the maximum stress of the benchmark model for wheel A and the wheel load on the middle of the trough, once with the second wheel and once without. See the different wheel configurations in Figure 6.20, results are displayed in Table 6.9. The table shows a 4.6 % increase in stresses when the second wheel is ignored, which would be very conservative.

(a) Additional second wheel ignored.

(b) Additional second wheel incorporated.
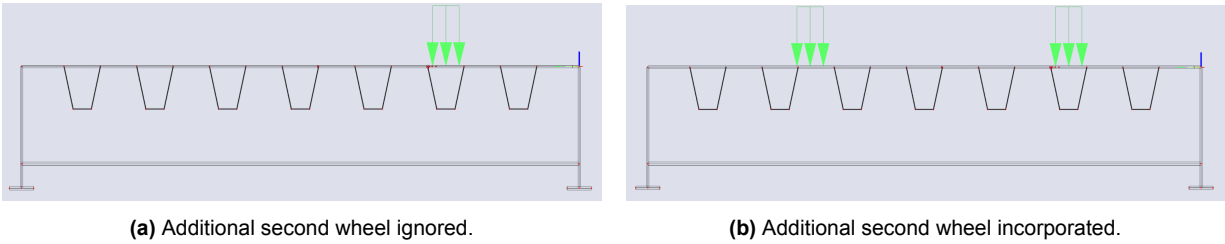
Figure 6.20: Configuration of wheels.

Table 6.9: Stresses from the two configurations.

Load con-figuration	Stresses [MPa]		
	point A	*point B*	*Hot Spot Stress*
Second wheel incorporated	-2.066	-5.647	**-7.11**
Second wheel ignored	-1.926	-5.376	**-7.44**

7

Parameter Sensitivity Analysis Preliminaries

This chapter focuses on the preliminary steps needed for conducting a parameter sensitivity analysis. It starts with identifying the critical details within the OSDs that significantly influence their fatigue performance. The chapter then outlines the process of creating a benchmark model, which serves as a reference point for the PSA. Detailed characteristics and parameters of this benchmark model are discussed. Finally, the chapter explains the methods used to analyze the data obtained from the parameter sensitivity analysis.

7.1. Determination of governing details

The parameter sensitivity analysis is will be executed per detail. However, conducting a sensitivity analysis for all the included details is considered infeasible due to the runtime of the model and the time constraints of this thesis. For the relevancy of this research, the most governing details should be investigated. This section illustrates the workflow of the determination of the most governing details.

7.1.1. Location

First of all, the locations where the details should be checked have to be determined. The ROK [2] states that load model 4a should be applied everywhere inbetween the outer vehicle barriers. This ensures that a rearrangement of the driving lanes on a bridge does not lead to problems. In this theoretical case the assumption is made that the driving lanes are not rearranged, and that the trucks drive in the center of the theoretical driving lane. This is required to reduce the needed load cases and thus computational power of the parametric model. For the considered details this means that a significant amount of locations do not need to be checked, and only the directly ridden details in the deckplate can be considered. An illustration of the directly ridden details are given in section 6.5 of the previous chapter.

Transversal positions

The assumption of the theoretical driving lane reduces the possible governing details significantly. However, the transversal position of the details are still not definite, as different designs mean different potential governing detail positions. As stated, in this research the directly ridden details are considered. Due to the huge influence of local loads, the highest damage numbers in the bridge are expected to be found at transversal positions closest to the load of the wheels. The transversal location can change per detail. Details 1A, 1C, 2A and 2B have the same transversal location, as have 5, 6A and 6B. It should be noted that the transversal positions can also change for different designs.

Details 1A, 2A and 2B are all details at the intersection of the trough and deckplate, and 1C is at the trough, crossbeam and deckplate intersection. The assumed governing transversal location for these details is at the intersection of the trough and deckplate closest to the wheel of the truck driving in the middle of the theoretical lane. To be conservative and adhere to the ROK, the loads are then moved to the three possible transversal distributions as described in section 4.2. This process is illustrated in Figure 7.1.

Details 5, 6A and 6B are details at the intersection of the crossbeam to the deckplate. These considered details are likewise incorporated between the troughs closest to the wheel of the truck driving in the middle

of the theoretical driving lane. Afterwards, the loads are again modified, similarly to details 1A, 1C, 2A and 2B. See Figure 7.1 for the determination of the transversal detail position.

(a) For details 1A, 1C, 2A and 2B.

(b) For details 5, 6A and 6B.
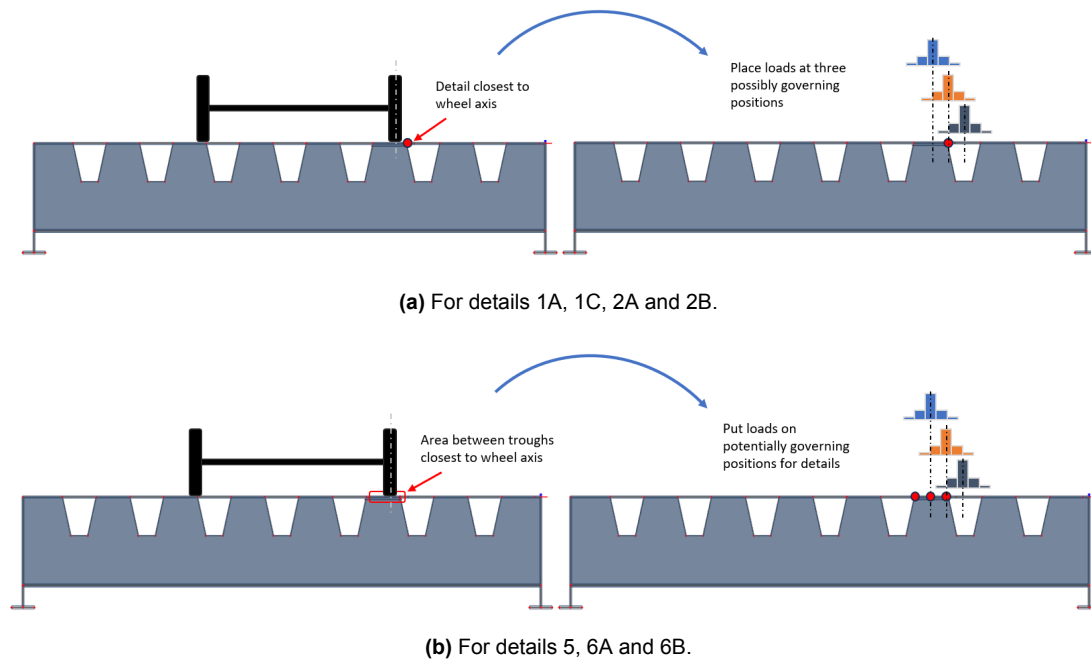
Figure 7.1: Transversal detail position and load placement for different details.

It should be noted that the load of a wheel can be exactly inbetween two troughs. When this occurs, the inspected details are the ones at the trough closest to the main girder as this gives the highest stresses and damage numbers. Additionally, the load distributions are also shifted towards this position.

Longitudinal positions
The longitudinal placement should additionally be investigated, as incorporating details over the full bridge is needless as expectations about the governing position are given in the ROK [2]. On top of that, this requires tremendous computational power. Details 1A, 2A and 2B are expected to have the same longitudinal position, as have details 1C, 5, 6A and 6B.

Details 1A, 2A and 2B can be placed over the full length of the bridge, with the exception of locations within 150 mm of a crossbeam for detail 1A and 2A, as stated in the ROK [2]. Additionally, the ROK states that for detail 2A the highest stresses are expected in the middle of the span. The investigated positions are shown in Figure 7.2, these positions are based on expectations of the ROK, and a balance of considering enough details and the computational time of the model. Additionally, due to symmetry, the details can be placed at only one half of the length of the bridge.
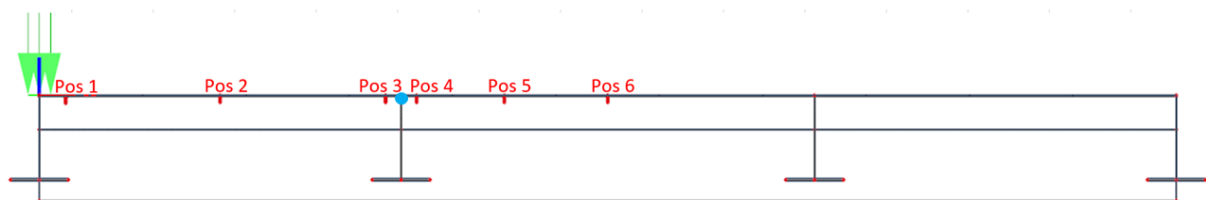
Figure 7.2: Considered longitudinal detail positions for details 1A, 2A and 2B. Details 1C, 5, 6A and 6B are incorporated at the first crossbeam (blue dot).

The longitudinal location of details 1C, 5, 6A and 6B are all at the crossbeam, see Figure 7.2. Due to the symmetry over the length of the bridge only two crossbeams should be considered. In the generalization

process of the bridge, see section 6.1, the intersection of the end-crossbeam, troughs and deckplate also has been simplified. To consider relevant detail places as much as possible, only the middle crossbeams are investigated. It is assumed that this does not change the determination of governing details, as the dynamic amplification factor is a constant with a value of 1.15, see Section 4.4, instead of the linear decreasing dynamic amplification factor defined in the Dutch National Annex 1991-2 NB [32]. The locations are shown in Figure 7.2.

7.1.2. Domain check

To be able to find the governing details, damage numbers over the full design domain should be checked. When the value of the damage numbers of certain details seem to be consistently greater, it can be assumed that these details are the governing.

To perform this domain check, the lightest, and thus most flexible, OSD design is checked in combination with one extremely stiff and heavy design. When the same details will have high damage numbers in both designs, these details are considered governing over the full domain. The parameters of these flexible and stiff OSD bridge designs are given in Table 7.1. Additionally, the designs are shown in Figure 7.3.

Table 7.1: OSD parameter dimensions (in mm) and mass of the designs at the end of the design spectrum.

	t_{dp}	t_{tr}	$w_{tr,top}$	$w_{tr,bot}$	ctc_{tr}	h_{tr}	$t_{cb,web}$	$ctc_{cb,mid}$	$Mass\,[kg]$
Light and flexible design	10	6	300	100	600	325	12	4000	12427
Heavy and stiff design	30	8	150	100	250	400	20	3600	29175

(a) Light and flexible design.

(b) Heavy and stiff design.
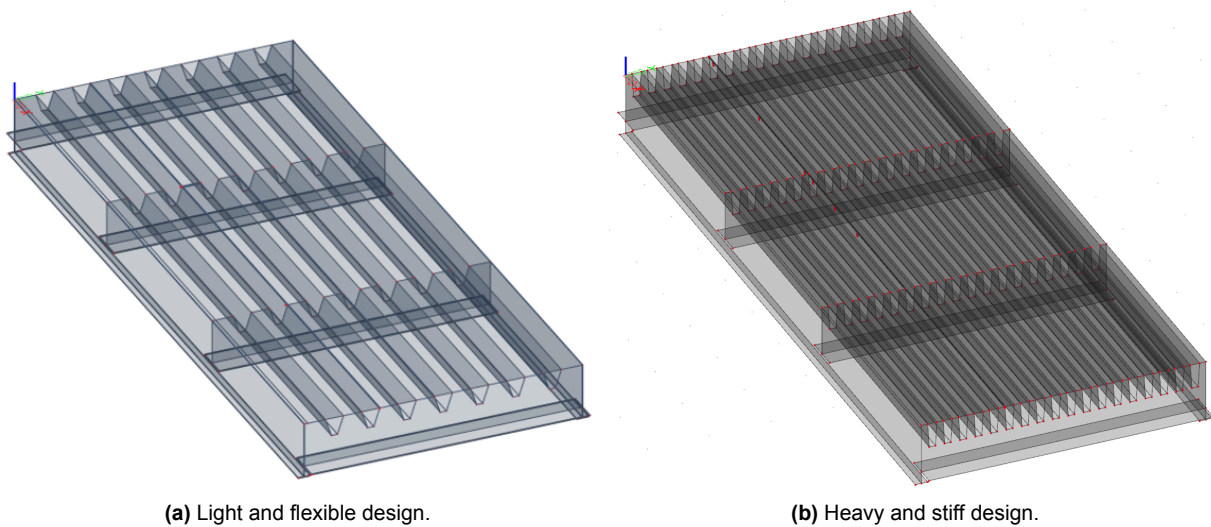
Figure 7.3: Illustration of OSD designs at the ends of the design spectrum.

7.1.3. Results

All damage numbers of the details at the indicated positions as in section 7.1.1 are computed. The results can be found in Annex C and are summarized in Table 7.2 and Table 7.3 below. The damage numbers of the heaviest design are zero for almost all details. To still create an appropriate comparison between the details, the damage number without a fatigue cut-off limit is computed. This allows for a comparison which, like normal fatigue verification, still includes the occurring stresses and detail categories. The table contains the highest damage numbers of all locations per detail. From Tables 7.2 and 7.3, two conclusions can be drawn.

Table 7.2: Highest damage number and corresponding load distribution and location in the bridge per detail for the light and flexible design.

Detail	Max damage	Load distribution position	Longitudinal detail pos (Figure 7.2)	Transversal detail pos
		Flexible design		
1A	173,5	Trough leg	6	At trough leg
1C	551,6	Trough middle	At crossbeam	At trough leg
2A	13,7	Between troughs	5	At trough leg
2B	172,4	Trough middle	5	At trough leg
5	201,7	Between troughs	At crossbeam	Between troughs
6A	382,68	Between troughs	At crossbeam	Between troughs
6B	149,42	Between troughs	At crossbeam	Between troughs

Table 7.3: Highest damage number and corresponding load distribution and location in the bridge per detail for the heavy and stiff design.

Detail	Max damage	Load distribution position	Longitudinal detail pos (Figure 7.2)	Transversal detail pos
		Stiff design		
1A	2,90E-06	Between troughs	2	At trough leg
1C	8,27E-03	Trough middle	At crossbeam	At trough leg
2A	3,36E-04	Between troughs	1	At trough leg
2B	2,07E-03	Trough middle	1	At trough leg
5	1,02E-04	Trough middle	At crossbeam	Position 1 from Figure C.2
6A	5,15E-03	Trough middle	At crossbeam	Position 1 from Figure C.3
6B	1,32	Trough middle	At crossbeam	Position 1 from Figure C.3

Firstly, it can be concluded that even for the most stiff design, detail 6B does not suffice, as the damage number with a cutoff limit is 1.18. This is remarkable, it would be intuitive for the most stiff design within the limits of the ROK to be conservative and have small damage numbers for the details. Apparently, detail 6B should not occur in this design space.

Detail 6B however can occur in other Orthotropic Steel Decks, but in designs with other traffic categories or a lower amount of passing trucks (N_{obs}) per year. Considering a traffic category of 'short distance' instead of the in this research considered 'medium distance', changes the damage number from 1.18 to 0.74. Additionally, changing the N_{obs} accounts for a decrease of the damage number linearly. So, if half of the trucks are considered, the damage number also halves. Besides, projects are observed where at governing positions the crossbeam to deckplate weld is locally realized with fully penetrated butt welds. As the parametric model does not have this functionality. The assumption will from now on be made that instead of double sided fillet welds, butt welds are applied on this theoretical model, and then detail 6B does not occur in the bridge, as this detail is only applicable in case of double sided fillet welds. Additionally, the category of detail 6A increases from 90 to 100 MPa, resulting in a drop of the damage numbers of this detail.

Secondly, disregarding detail 6B due to reasons stated above, it is observed that detail 1C has the highest damage numbers in both the flexible and stiff design. It is concluded that detail 1C is governing within the design domain. A parameter sensitivity of detail 1C will be executed first due to the detail's relevancy. More details are verified for relevancy when a start design (benchmark) for the parameter sensitivity analysis is identified.

7.2. Obtaining benchmark model

A benchmark model is sought for to start the one-at-a-time sensitivity analysis. As detail 1C is determined to be governing, this benchmark model is based on the damage numbers of detail 1C. To find this benchmark model, an iterative strategy is applied. First, within the domain, damage numbers of multiple designs with rather different weights are determined. Thereafter the domain is made smaller, and the damage numbers of different designs are again determined. This process is repeated until a great benchmark design is found with a reasonable damage number. A reasonable damage number for this fatigue design is assumed to be inbetween 0.6 and 0.90. The upper limit being 0.9 due to possible small deviations in stresses, as discussed in section 6.7.2. The first iteration resulted in Figure 7.4 .
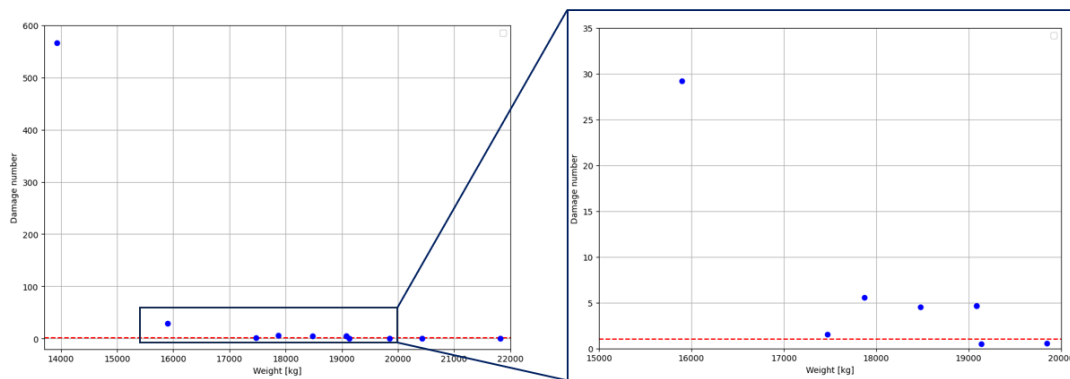
Figure 7.4: First iteration of designs in the search for the benchmark model.

A second iteration can be executed with a smaller domain based on the results of the first iteration. It is observed that a Unity Check lower than 0.9 could logically be obtained somewhere in the range of 17 - 18 tons in terms of weight. To obtain a relevant benchmark, the second iteration should have many designs inside this range. See Figure 7.5, the chosen benchmark is the indicated design, with a Damage Number of 0.76.
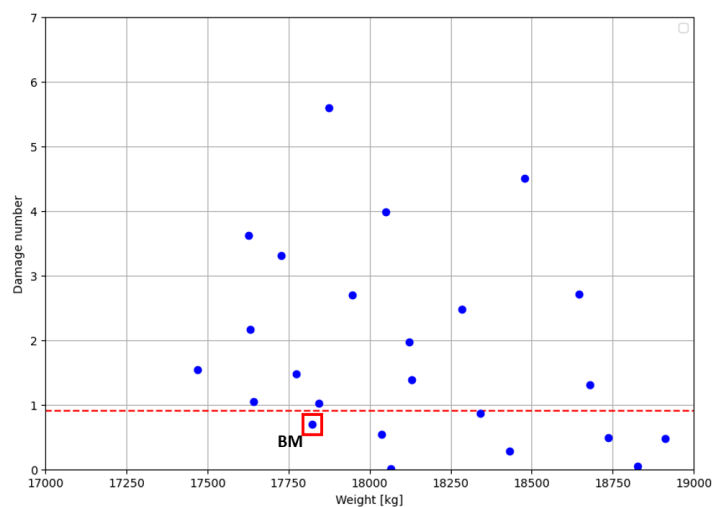
Figure 7.5: Second iteration of designs in the search for the benchmark model (BM).

7.3. Benchmark model

In the previous Section a benchmark model is obtained to execute the Parameter Sensitivity analysis of detail 1c. The parameter values of the benchmark model are displayed in Table 7.4. To gain insight into the weight per component of the deck, a diagram is added in the illustration of the Benchmark, see Figure 7.6

Table 7.4: OSD parameter dimensions (in mm) and mass of benchmark model.

	t_{dp}	t_{tr}	$w_{tr,top}$	$w_{tr,bot}$	ctc_{tr}	h_{tr}	$t_{cb,web}$	$ctc_{cb,mid}$	$Mass\,[kg]$
Benchmark model	21	6	300	150	600	350	20	3666	17822.5
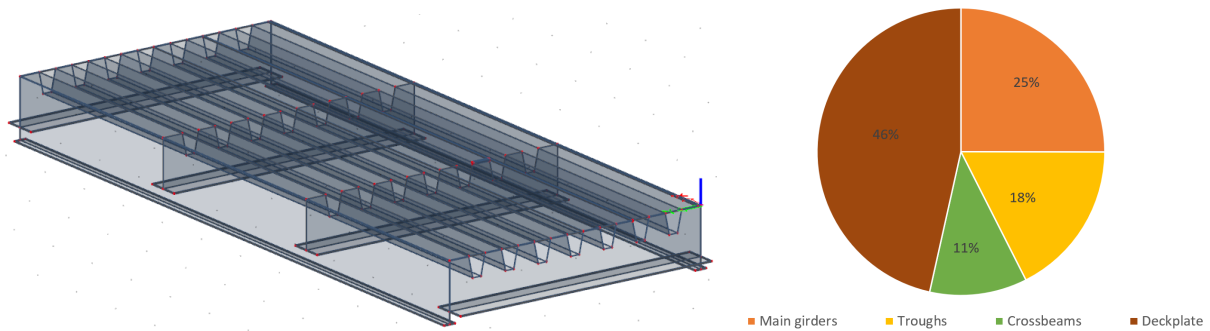
Figure 7.6: Benchmark model and its weight distribution.

As depicted in Figure 7.6, the deckplate significantly influences the total weight of the entire bridge, contributing to 46% of it and having the biggest impact on the weight. The main girders make up 25% of the weight, followed by the troughs at 18%, and the crossbeams at 11%. It should be noted that these percentages change when different designs are considered.

For the determination of this benchmark model only detail 1C is taken into account. To observe what happens with other details in the bridge when a design is only optimized for one detail, the damage numbers of the details other than 1C are determined for the same positions on the bridge. These tables are found in Annex D, a summary of the maximum damage number per detail is showed in Table 7.5.

Table 7.5: Highest damage number and corresponding load distribution and location in the bridge per detail for the benchmark model.

Benchmark design				
Detail	**Max damage**	**Load distribution position**	**Longitudinal detail pos (Figure)**	**Transversal detail pos**
1A	1,66	Trough leg	2	At trough leg
1C	0,75	Troug middle	At crossbeam	At trough leg
2A	0,03	Trough leg	2	At trough leg
2B	0,01	Trough leg	2	At trough leg
5	0,47	Between troughs	At crossbeam	Middle between troughs
6A	0,44	Between troughs	At crossbeam	Middle between troughs

Observed from Table 7.5 is that detail 1A has a damage number greater than 1, when a benchmark model is sought for only as a function of the damage of detail 1C. Detail 1A is additionally considered as an important detail in this research, and is incorporated in the parameter sensitivity analysis. To obtain possible governing locations of this detail, the damage numbers are displayed per transversal load distribution and per position. Note that these longitudinal positions are the same as in Figure 7.2.

Table 7.6: Damage numbers of detail 1A of the benchmark model.

Position (see Figure 7.2)	between troughs	above trough leg	trough middle
1	0,17	0,38	0,11
2	0,40	1,66	0,38
3	0,15	0,65	0,11
4	0,11	0,56	0,08
5	0,34	1,34	0,30
6	0,37	1,46	0,30

In Table 7.6 damage numbers per location and load configuration are stated for detail 1A. All positions checked result in considerable higher damage numbers when the transversal weaves are placed above the trough leg. It can be assumed that this transversal load placement is governing. The longitudinal detail position governing location 2 at the middle of first to crossbeams according to Table 7.6. This is also similar as for the stiff design in Section 7.1.2. For the flexible design, the damage numbers indicate that the position at midspan is governing, see appendix C. In the parameter sensitivity analysis, longitudinal detail position 2 and 6 will be incorporated.

7.4. Data Analysis

This section introduces the data analysis which is executed in chapter 8. The focus is on the one-at-a-time parameter sensitivity study, and the influence of traffic types on the bridge. Also the Normalized Root Mean Square Error (NRMSE) is introduced to quantify a goodness of fit.

7.4.1. OAT

With the obtained benchmark model a one-at-a-time parameter sensitivity study can be executed. A one-at-a-time (OAT) parameter sensitivity analysis is a method used to understand how the variation in individual input parameters affects the output of a model. In this case the input parameters are the different geometries of the bridge, and the output is the damage number, and also a certain weight. This OAT analysis helps to identify which parameters are the most influential on the model's behavior, and influences of the eighth variables can be researched. Furthermore, the effect of traffic categories on the stresses in the bridge can be studied.

It is important to note that the used OAT techniques explore a small fraction of the design space [53]. Therefore, they do not capture the full complexity of the whole bridge, but show accurate local behaviour for details. It can be researched whether this local behaviour holds for more points in the bridge.

In this OAT analysis, one parameter is varied while keeping all others constant. After which a line is fitted to quantify this influence of the parameter on the damage numbers of the researched detail.

7.4.2. Normalized Root Mean Square Error

In the parameter sensitivity analysis functions are fitted to quantify the relations of the parameters on the damage number of the bridge. However, it should be noted that these fits cannot be assumed to be accurate [54]. Just by observing one can see if a line fits okay or not. However, it might not be easy to compare two fitted functions. Therefore a value is needed to quantify how well a certain function fits some data. This is done with the Root Mean Square Error.

The Root mean Square Error is the standard deviation of the residuals, which are the differences between predictions and targets. This value is a measure of how spread out the residuals are. In other terms, it tells how concentrated the data is around the fitted line, and thus how good the fit is. See Formula 7.1.

$$RMSE = \sqrt{\frac{\sum_{i=1}^{n}(p_i - t_i)^2}{n}} \tag{7.1}$$

In this formula, p_i are the predictions of the function and t_i are the targets. As in this research the damage number is on the y-axis when data points are fitted, the root mean square directly tells something about the error in the prediction of the damage numbers. This value is the average model prediction error of the damage number. When using the RMSE, a model with high damage numbers will have a greater error while this model could percentage wise be more accurate. In order to be able to compare goodness of fits to each other, the RMSE is normalized by its mean [55]. This is called the Normalized Root Mean Square Error, see Formula 7.2.

$$NRMSE = \frac{RMSE}{\bar{t}} \tag{7.2}$$

8

Parameter Sensitivity Analysis Results

In this chapter the results of data analysis are discussed. For each parameter of the parametric model a OAT analysis is executed for both detail 1C as detail 1A. The results are discussed per parameter.

8.1. Single parameter influences

In the sensitivity analysis, each parameter is varied while the other parameters are held constant. The parameters are varied over a certain domain, provided in Table 8.1. The results are displayed in figures with the damage numbers of the design on the y-axis, and the parameter varied on the x-axis. For information regarding the weight of the design, a top horizontal axes displaying the weight of each design and the weight change relative to the Benchmark Model (BM) is added. To quantify the influence of the deckplate thickness on the damage number, a function is fitted, being either a polynomial or exponential. The functions are displayed in the legend of the figure, together with their domain. Furthermore, to quantify the goodness of fit of the function, the Normalized Root Mean Square Error (NRMSE) is stated, as discussed in section 7.4.2.

Table 8.1: Parameters and their domain for the PSA.

Symbol	Min (mm)	Max (mm)	Step size [mm]
t_{dp}	17	24	1
t_{tr}	6	8	1
$t_{cb,web}$	12	20	2
$w_{tr,top}$	150	400	50
$w_{tr,bot}$	100	200	25
ctc_{tr}	490	610	10/20
h_{tr}	325	400	25
$ctc_{cb,mid}$	3000	4000	100

It should be noted that the damage numbers mentioned in the upcoming section reflect the impact after trucks from traffic category 2 have traversed the bridge for 100 years. Where each year 500.000 passing trucks are considered, corresponding to the traffic category 2 according to the Eurocode [51].

8.1.1. Detail 1C

Firstly the influence of the parameters on detail 1C is discussed. An initial overview is provided for the parameters in Figure 8.1. In the figure, all parameters are presented from their minimal value to their maximal value, observed in Table 8.1.
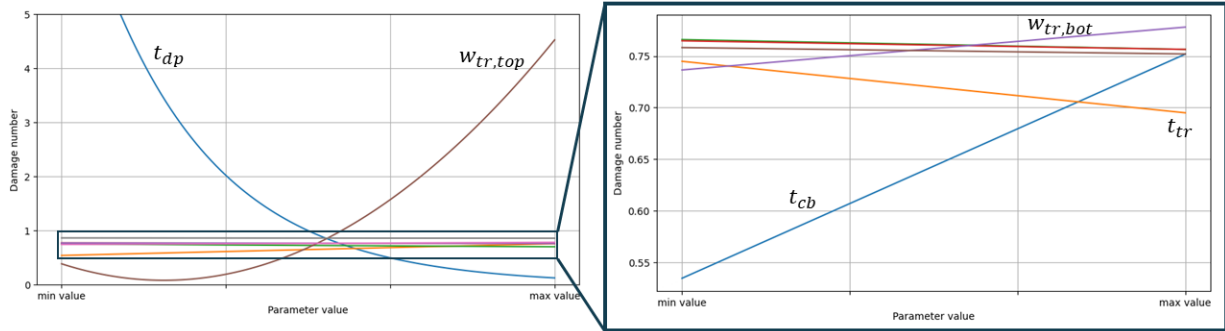
Figure 8.1: Overview of parameter influence on detail 1C.

The analytical schematisation of detail 1C is additionally presented in Figure 8.2 for overview. This analytical solution clearly demonstrates the significant impact of deckplate thickness and trough width, as these are the only parameters considered.
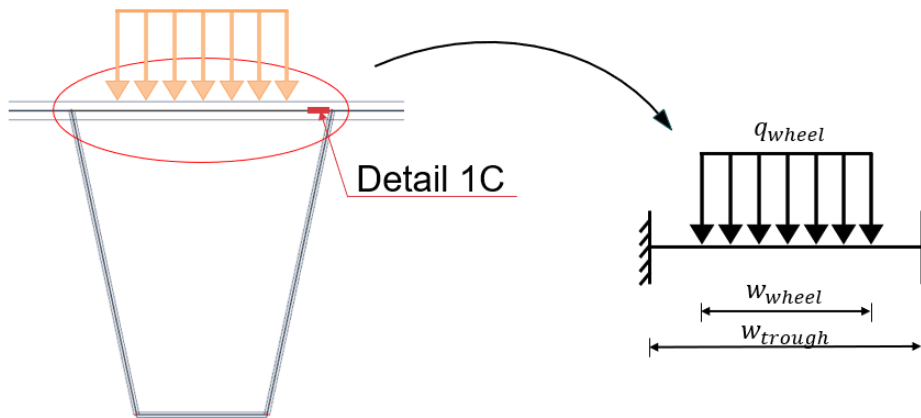
Figure 8.2: Analytical schematisation for detail 1C.

In the coming paragraphs, all single parameter influences on detail 1C are analysed. Starting at the most influential parameter, which is the deckplate thickness, and continuing in descending order of the influence of the parameter on the damage of detail 1C.

Deckplate thickness

The deckplate thickness is known to be a significant factor in both the weight of the bridge and the damage numbers of directly ridden details in the bridge. The damage number per value of deckplate thickness is given Figure 8.3.

(a) Polynomial function fitted.

(b) Exponential function fitted.
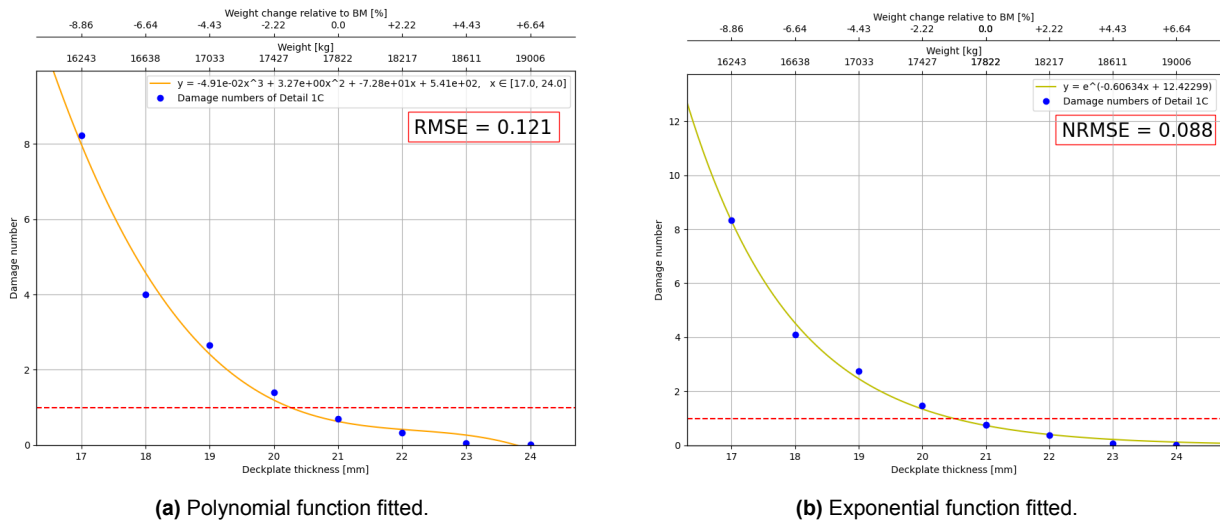
Figure 8.3: PSA of deckplate for damage of detail 1C, two different function fits.

It is observed that an exponential function fits better than a polynomial as the NRMSE is lower for the exponential function. See Figure 8.3. Concluded is that a linear line on log scale fits the data well, see Figure 8.4.
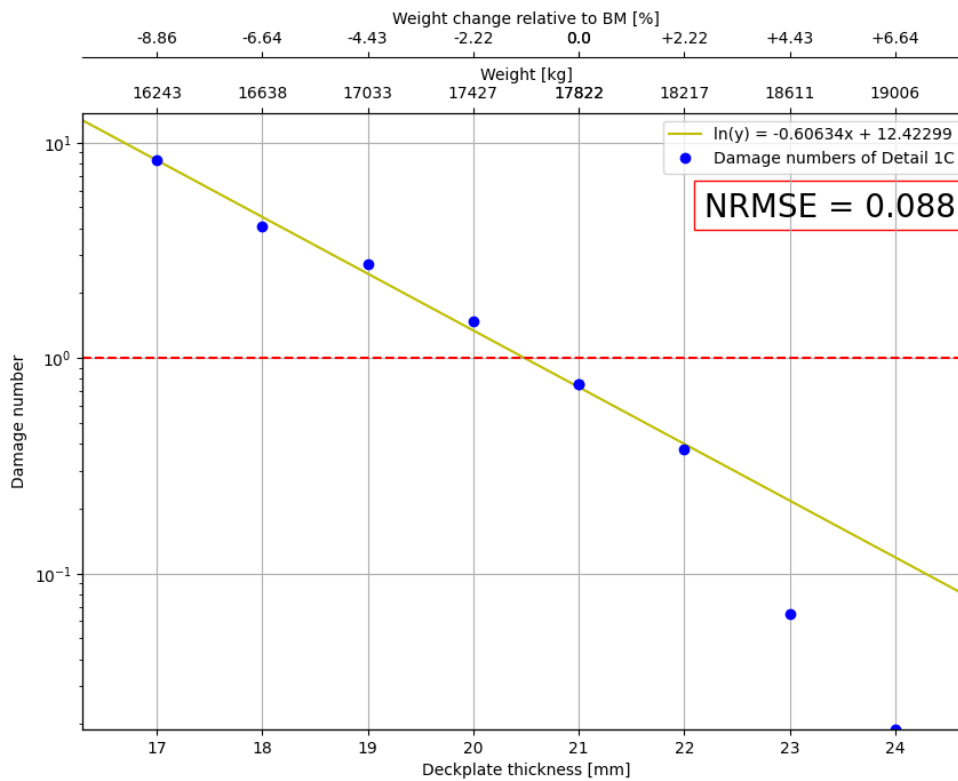
Figure 8.4: Damage numbers vs deckplate thickness and weight for detail 1C.

In Figure 8.4, the influence of the deckplate thickness on the weight is clearly significant. The mass of the structure reduces with 2.22% when the deckplate thickness is reduced with 1 mm. Furthermore, it is observed that the relation between the damage number and the deckplate thickness is substantial. The fit is accurate with a low NRMSE score of 0.088. It seems linear in logarithmic space when the damage number is higher than 0.4. Below this damage number of 0.4, it seems like another linear correlation can be identified in logarithmic space. After the last point the damage will be zero when increasing the deckplate thickness further. Therefore on logarithmic scale a third linear line can then be identified going vertically down, sharing remarkable similarities with a regular S-N curve. An effort is taken to try and find relations between these figures, this is done in Appendix E. It is concluded that the hypothesis involving the three straight lines is questionable, and that no further investigation is necessary as the absolute error at thes points is small.

Trough top width
The second most influential parameter on detail 1C is the top width of the trough. The influence of this parameter on detail 1C is displayed in Figure 8.5. A third order polynomial fits the data best. However, when only the damage numbers which are nonzero are incorporated in the fit, a second order polynomial appears as a better fit. Indicating that the relation between damage number and trough top width is a combination between a quadratic, linear and a constant term. This is as expected due to the fact that the length of the top width of the trough has a quadratic and a linear relationship with the stresses retrieved from detail 1C. This can be explained by referring to the analytical model, see Figure 8.2. The top width of the trough is the length between the clamped supports, and the bending stress at the position of 1C has a quadratic relationship with this length when a uniform q-load is applied over the full length of the clamped beam. However, due to the load not being applied over the full length of the beam an additional linear term occurs.

(a) Full domain.

(b) Domain $w_{top,tr}$ > 249 mm.
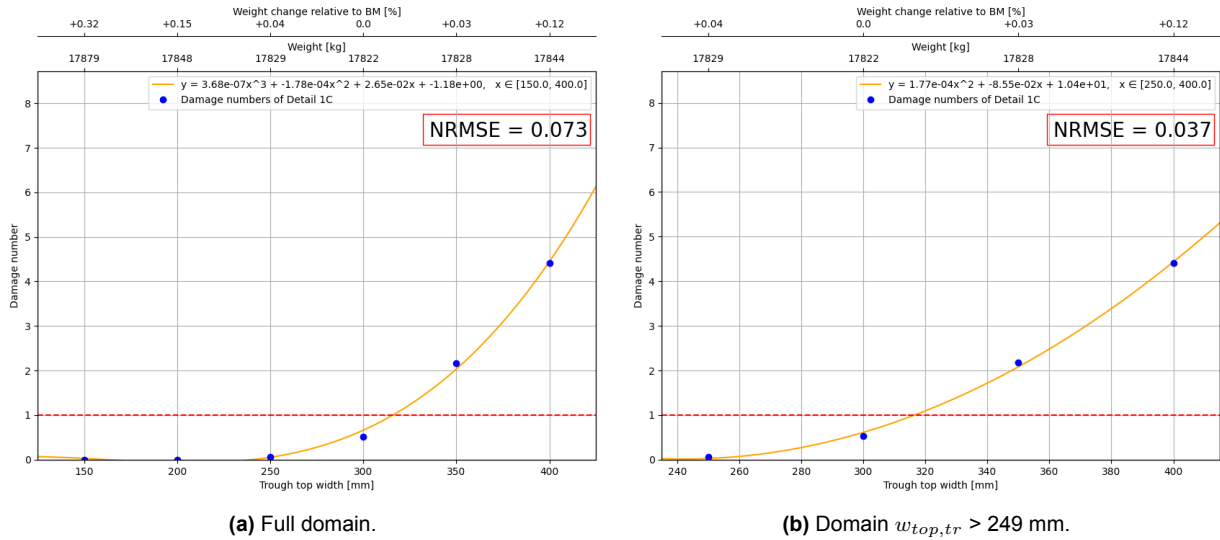
Figure 8.5: Influence of the top width of the trough on detail 1C.

The influence of the top width of the trough on the damage is significant, as an increase of 50 mm of the top trough width of the benchmark model results in a damage increase of 181%. While the influence on the weight is minimal, as no troughs are added or removed because the trough center-to-center distance remains the same.

Crossbeam thickness

Another influential parameter of detail 1C is the crossbeam thickness. This parameter is varied between values of 12 mm and 20 mm. Which is the design domain prescribed by the ROK. The damage numbers of detail 1C for the different values of the crossbeam thickness are displayed in Figure 8.6.
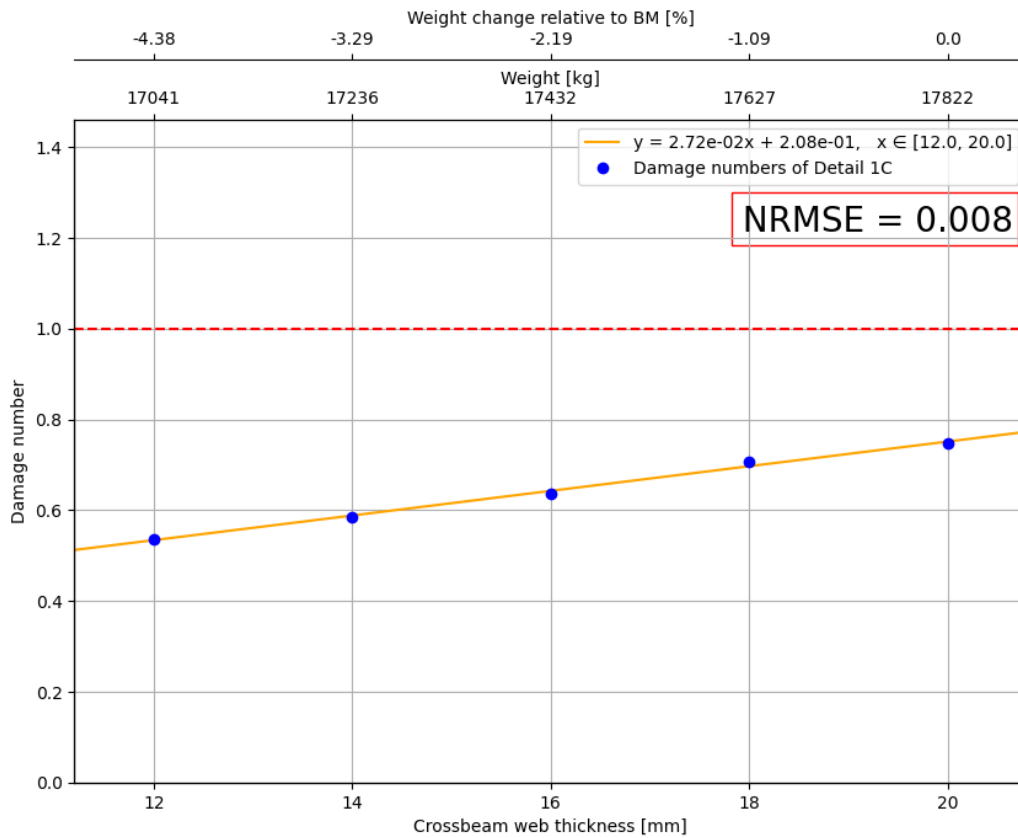
Figure 8.6: Influence of the crossbeam web thickness on detail 1C.

It is concluded that a decrease of the crossbeam web thickness leads to a decrease in stress for detail 1C. The decrease in crossbeam web thickness leads to a decrease in stiffness of the intersection of the crossbeam web, trough leg and deckplate, and this means a decrease of stresses in the deckplate adjacent to this intersection. This parameter affects the damage maximally 30% of the benchmark model damage number. The crossbeam thickness influences additionally the weight of the bridge by about 1.10% per 2 mm of thickness. It is seen that this parameter does influence the damage of the detail, while it does not occur in the analytical solution of detail 1C. A better analytical solution could be to switch the schematised clamps of the beam by springs.

Trough thickness

The trough thickness in an OSD is only allowed to vary from 6 to 8 mm according to the ROK [2]. Figure 8.7 shows the influence of the trough thickness on detail 1C. An increase in trough thickness results in a damage number of maximum 6% lower, while increasing the total weight of the bridge by 5.84%. The trough thickness has a slight influence on the damage while it has a big influence on the weight. To optimize a bridge design for detail 1C, this parameter should be minimized.
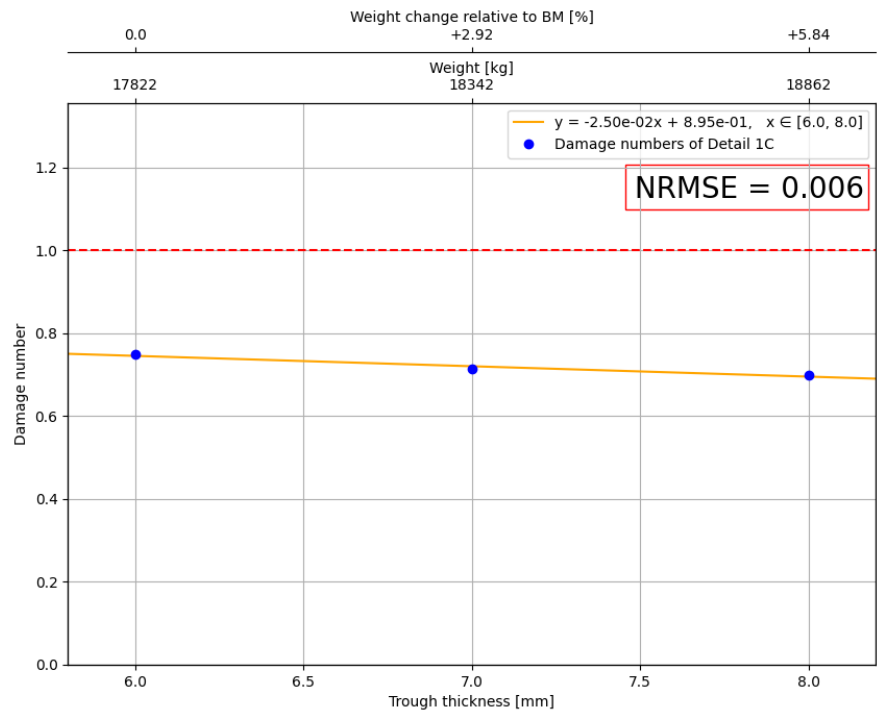
Figure 8.7: Influence of trough thickness on detail 1C.

Trough bottom width
The value of the trough bottom width is restricted between 100 and 200 mm. The influence of this parameter is illustrated in Figure 8.8. A wider trough bottom results in a moderately higher damage number for detail 1C.
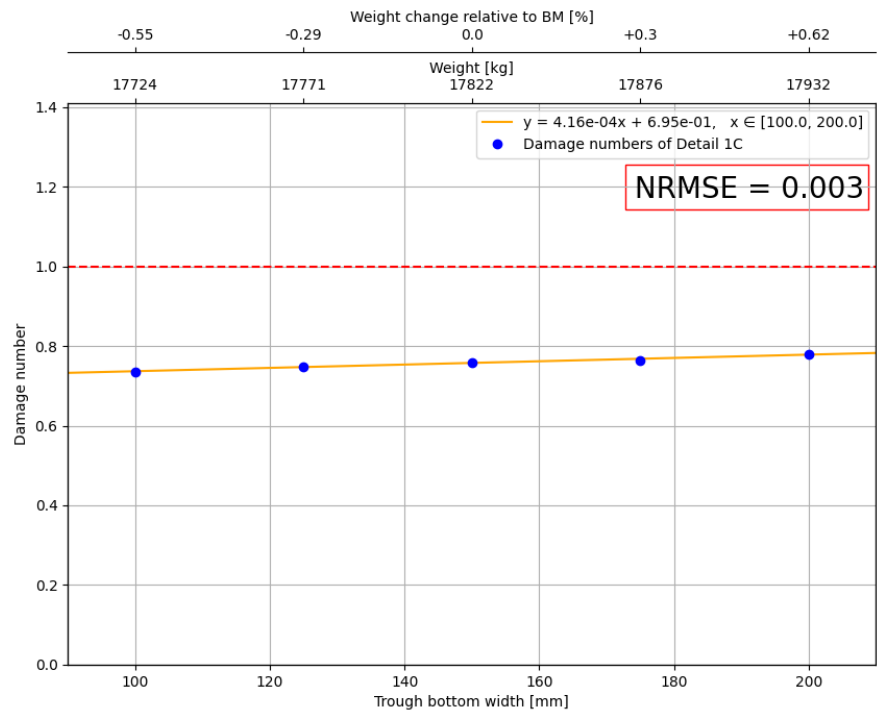
Figure 8.8: Influence of trough bottom width on detail 1C.

The effect on detail 1C can be explained by considering the analytical schematisation, see Figure 8.2. In this analytical model, to adhere to reality the clamped supports should be replaced by rotational springs. When the bottom width of the troughs increases, the intersection between the trough leg, deckplate and crossbeam stiffens, as the flexural and torsional stiffness slightly increases, and the rotational spring will behave more like a fully clamped spring. This increases the bending moment and therewith stresses at detail 1C. However, this accounts for a minimal influence of the trough bottom width on detail 1C, as the influence on the damage number is maximally about 6% of the damage number of the benchmark model.

Crossbeam center to center

The parameter which is varied in this research is the center to center distance of the middle crossbeam, and with it the center to center distance of the first and last two crossbeams. Detail 1C is not influenced by the center to center, this is expected as the stiffness around this detail does not change because the detail shifts along with the crossbeam, see Figure 8.9.
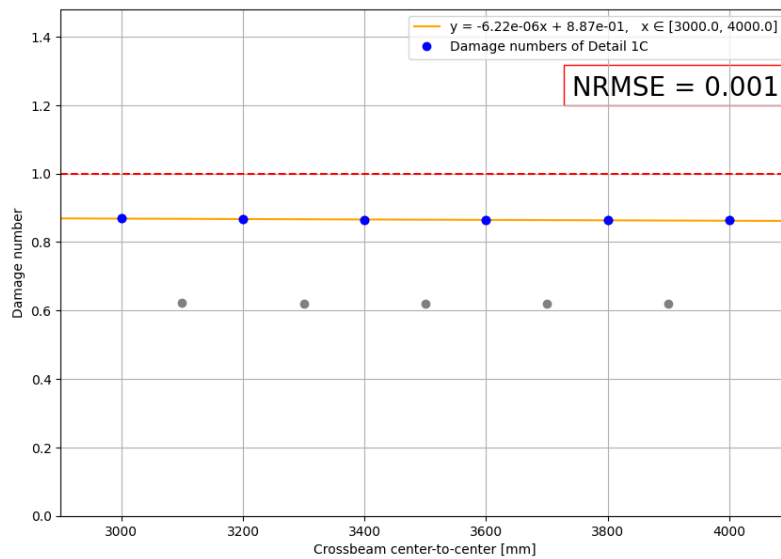
Figure 8.9: Influence of crossbeam middle center to center distance.

When the crossbeam center to center is divisible by 200, the maximum damage occurs. For other values a load is not directly placed above detail 1C due to a bug in the model, and therefore fewer points can be used as the load should be place exactly on top of the considered detail. The variation of the damage number is clearly deductible from Figure 8.9. The influence of this bug is 0.24 absolutely, which is 27% of the maximum damage number. This is a significant amount, as expected based on the large influence of local loads.

The influence of the crossbeam center to center can still be derived from these results, see Figure 8.9. It is illustrated in this figure that the crossbeam center-to-center does not influence detail 1C as the damage number does not change for different values of the crossbeam center-to-center.

Trough center to center

Figure 8.10 shows the impact of the trough center-to-center distance on detail 1C. The fluctuations in damage numbers are due to the shifting of the detail from the left to the right trough leg within the bridge for different trough center-to-center distances, visible in Figure 8.10. This shift occurs because the number of troughs changes with varying center-to-center distances. The magnitude of this shift is so large that the assumption of the governing transversal location of the detail should be questioned. Further investigation regarding this assumption is done in chapter 9. The trough center-to-center distance has a significant impact of the weight as decreasing the parameter value with 80 mm can lead to a weight increase of 4.45%. In the Figure the line is fitted based on the damage numbers obtained from detail 1C positioned at a left trough leg. The parameter does not seem to affect the damage number of detail 1C when detail 1C is regarded at a left trough leg closest to the load position.
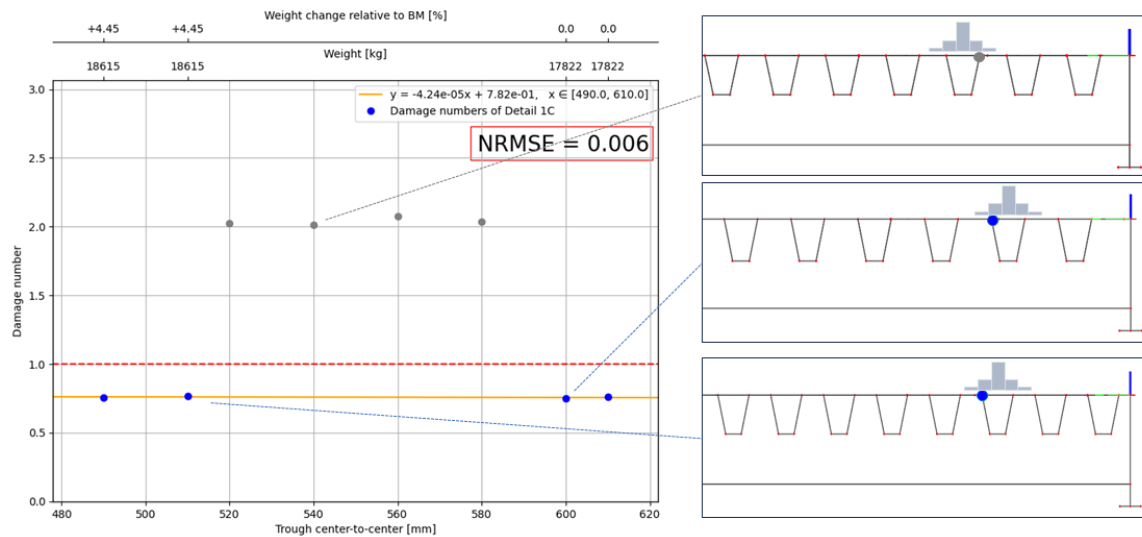
Figure 8.10: Influence of the trough center-to-center distance on detail 1C.

Trough height

The height of the trough affects the stiffness of the span between the crossbeams. As detail 1C is at the crossbeam, the stiffness of the span, and therefore the trough height, does not influence this detail. See figure 8.11, it is verified that the trough height does not impact the damage of detail 1C.
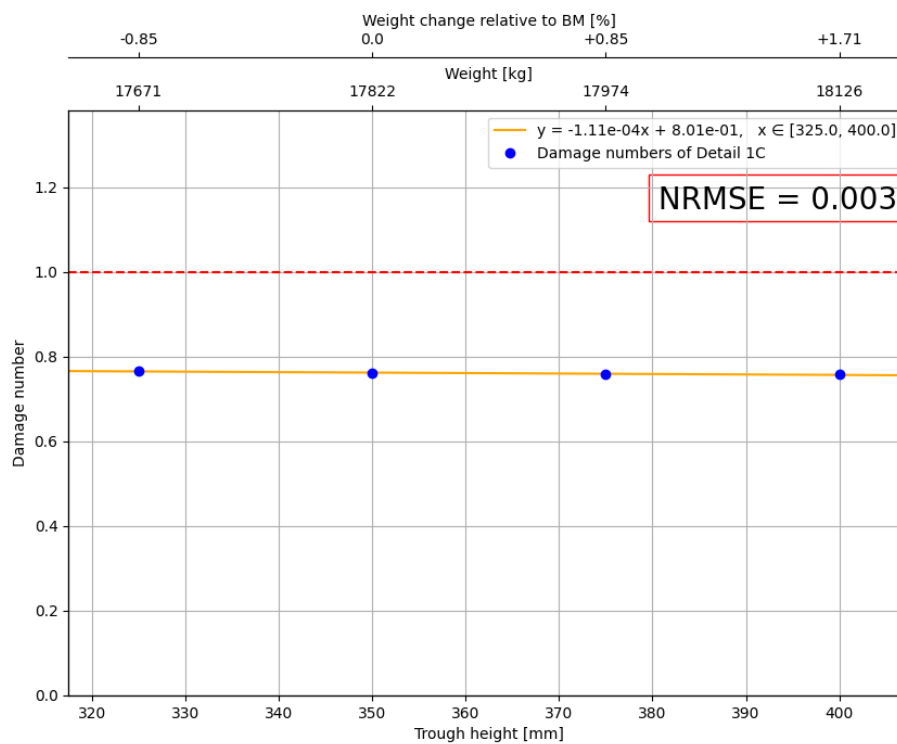
Figure 8.11: Influence of trough height on detail 1C.

8.1.2. Detail 1A

Before discussing the influence of the single parameters on the damage of detail 1A, an initial overview is provided for the parameters in Figure 8.12. In the figure, all parameters are presented from their minimal value to their maximal value, observed in Table 8.1.
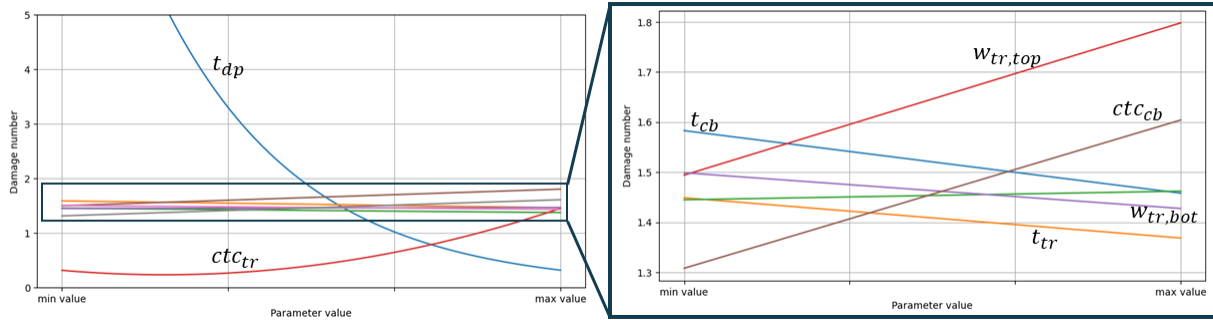
Figure 8.12: Overview of parameter influence on detail 1A.

No simple analytical solution exist for detail 1A. However, an analytical schematisation of detail 1A is presented in Figure 8.13. It should be noted that this simple analytical solution does not account for the full mechanical working. However, it can help to explain the influence of parameters on detail 1A.
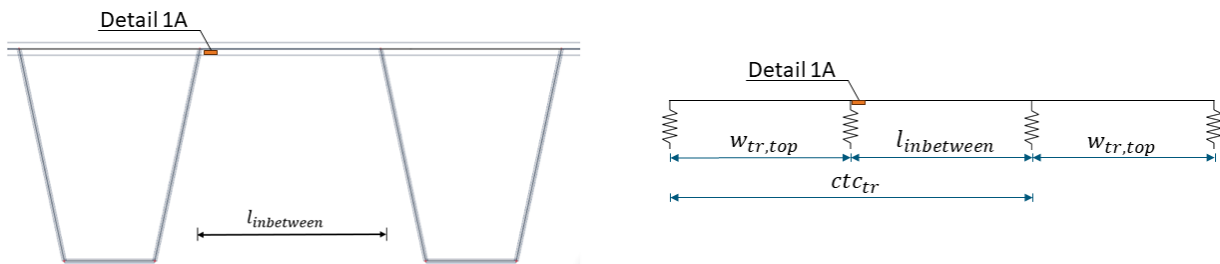
Figure 8.13: Analytical schematisation for detail 1A.

Damage of detail 1A is read out at two locations in the deck, as section 7.3 illustrated at two locations the damage in the OSD can be greater than 1. The positions are inbetween the first two crossbeams and between the middle two, the same as position 2 and position 6 in Figure 7.2, additionally illustrated in Figure 8.14.
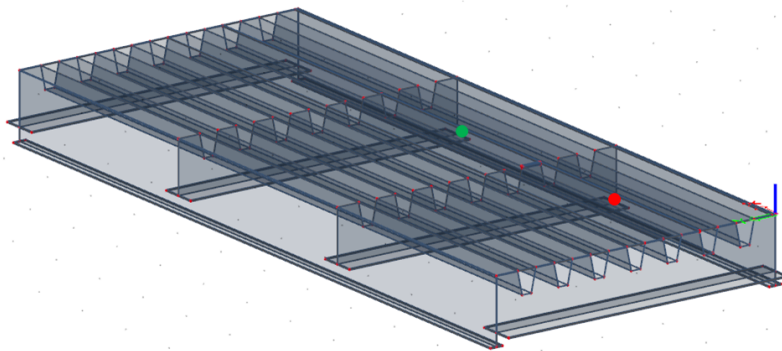
Figure 8.14: Considered positions in the PSA of detail 1A.

In the coming paragraphs, all single parameter influences on detail 1A are analysed. Similarly to detail 1C; starting at the most influential parameter, which is the deckplate thickness, and continuing in descending order of the influence of the parameter on the damage of detail 1A.

Deckplate thickness
The influence of the deckplate thickness on detail 1A is similar to the influence of it on detail 1C, see Figures 8.15 and 8.16. The influence of the deckplate is studied at both the position of the maximum damage, which lies for detail 1A inbetween the first two crossbeams, and at midspan. The positions of the details can be viewed in Figure 8.14.

(a) Linear space.

(b) Logarithmic space.
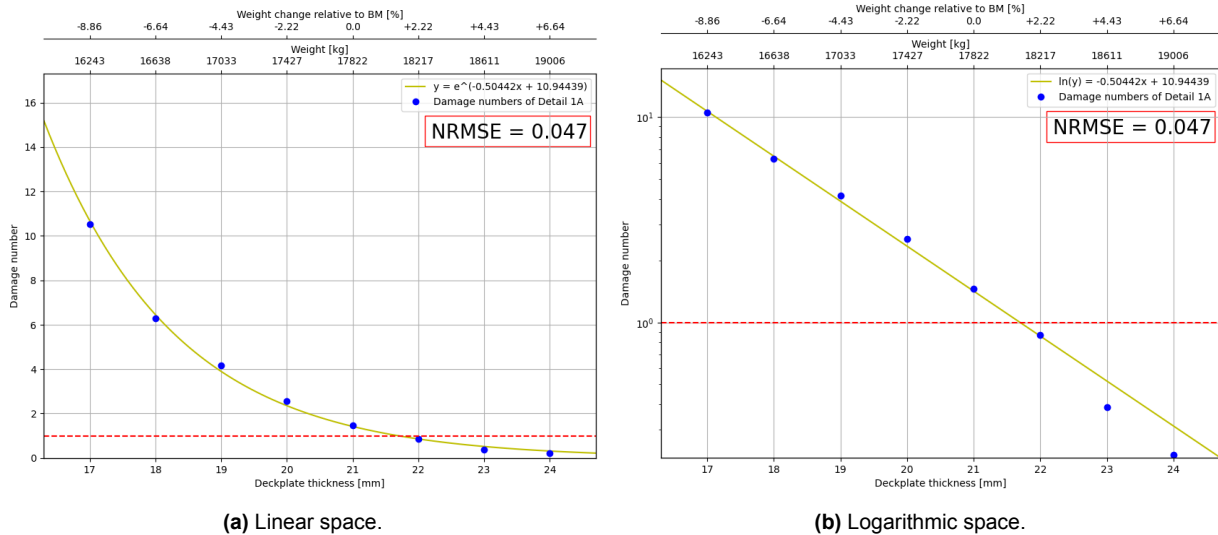
Figure 8.15: Damage numbers vs deckplate thickness and weight for detail 1A at midspan.

(a) Linear space.

(b) Logarithmic space.
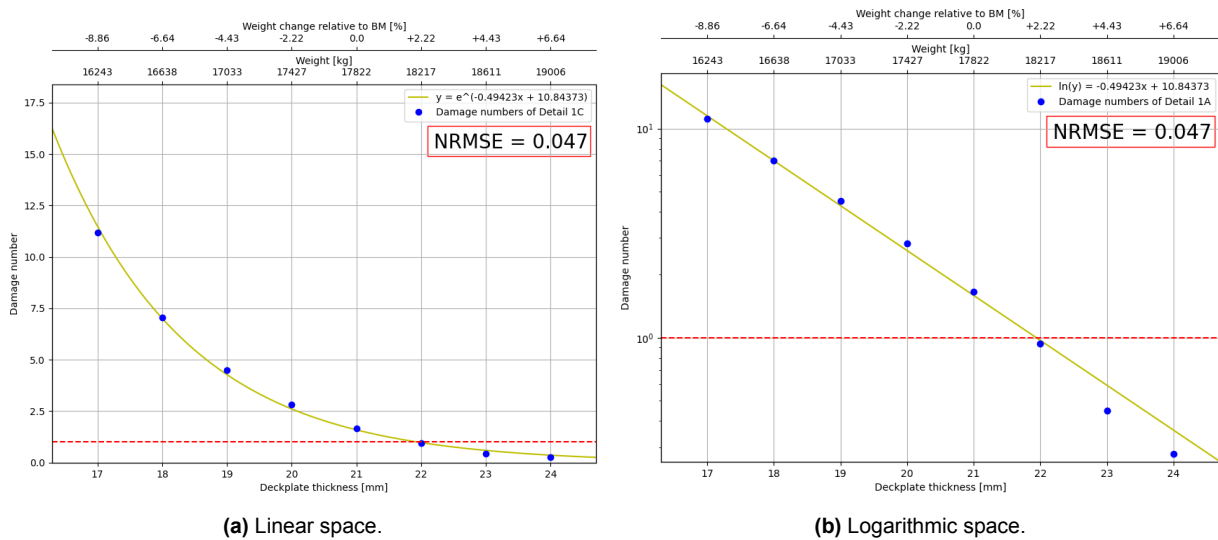
Figure 8.16: Damage numbers vs deckplate thickness and weight for detail 1A inbetween crossbeam 1 and 2.

Again, the influence of the deckplate thickness on the damage number is clearly significant and can be represented by an exponential and the influence on the weight is about 2.22% of the total weight per millimeter of deckplate. Additionally, it is observed that a linear line in logarithmic space fits detail 1A slightly better than detail 1C, as the NRMSE is even lower with a score of 0.047 for both positions in the bridge.

Trough center-to-center

The second most influential parameter on the damage of detail 1A is the trough center-to-center distance. The influence of this parameter can be represented by a second order polynomial, see Figure 8.17. Initially the damage decreases when the center-to-center distance increases, after a trough center-to-center value of 450 mm, the damage increases. Additionally, it can be observed that this parameter has a significant influence on the weight of the bridge, as a reduction of 100 mm can lead to an increase mass of 4.45%.
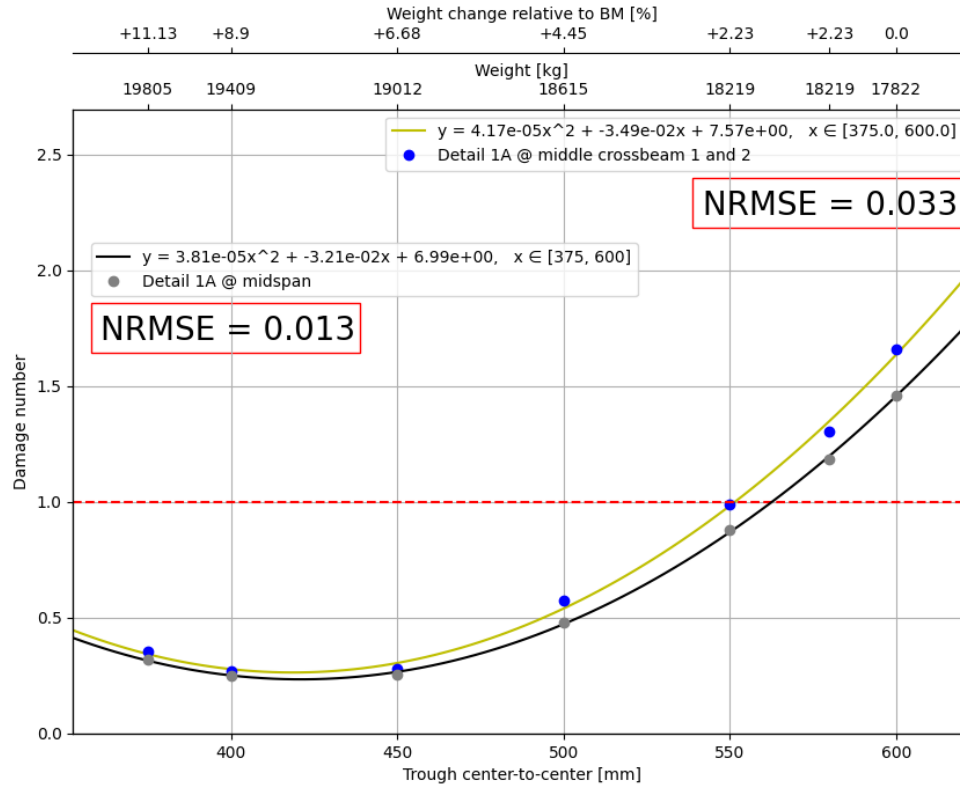
Figure 8.17: Influence of the trough center-to-center distance on detail 1A.

Changing the trough center-to-center distance affects the space between two troughs. From a trough center-to-center value of 450 mm and higher, as the trough center-to-center distance increases, the distance between the troughs increases, thereby decreasing torsional and flexural stiffness and load sharing between troughs. Resulting in more force flow towards the trough leg of detail 1A. Consequently, the stresses and damage number increases.

When the trough center-to-center decreases from 450 mm and onwards, the damage additionally increases. This initially might not make sense as more troughs result usually in less stresses and damage. However, when the trough center-to-center distance is decreased, a stiffer deck is obtained. This stiffness attracts force in the midspan between crossbeams, and in this case, the stresses at detail 1A can increase while the span ($l_{inbetween}$ in Figure 8.13) decreases.

Trough top width

The influence of the top width of the trough on detail 1A is visible in Figure 8.19. A smaller top width of the trough induces smaller stresses and thus damage numbers at both places of detail 1A. However, a trough top width of 150 mm, which makes the troughs rectangular in shape, is the exception. As a larger damage number is obtained for this rectangular stiffener design. At the left of the Figure, the top trough width is very small while the trough center-to-center distance stays the same. This is visualized in Figure 8.18.
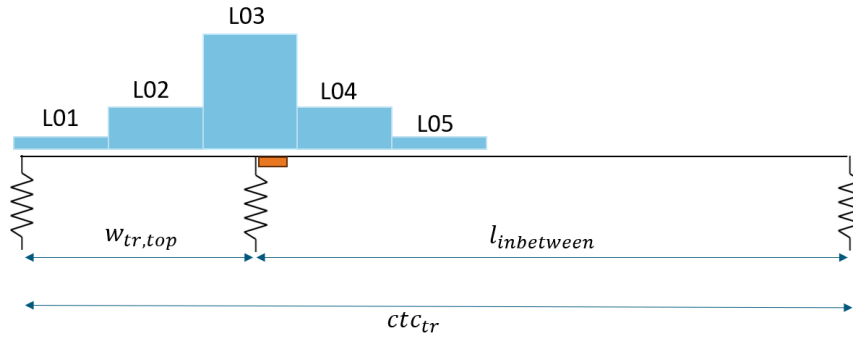
Figure 8.18: schematisation of very small top width of the trough.
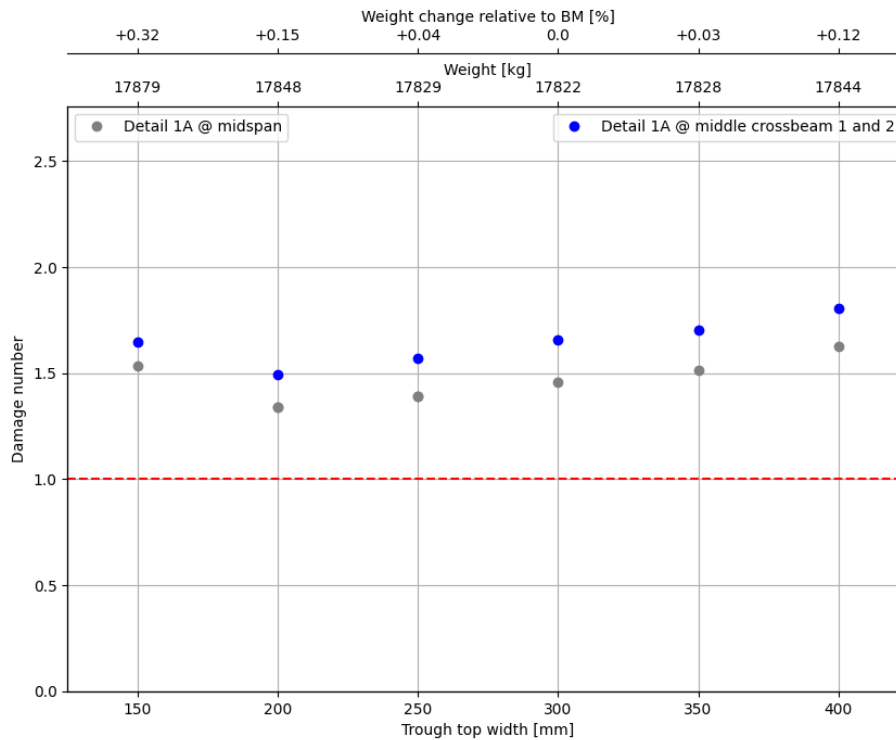
Figure 8.19: Influence of the trough top width on detail 1A.

Starting at the left end of Figure 8.19, the schematisation looks like illustrated in Figure 8.18. In this design, it is observed that traffic lane 4 and 5 produce stresses almost as high as lane 3. When initially increasing the trough top width, the stresses of these lanes reduce quickly as the distance inbetween the troughs reduces. This results in initially in a lower damage number when the trough top width is increased.

However, when increasing the top trough width from 200 mm and further, the decrease in $l_{inbetween}$ means that the middle spring further moves right. This results in an increase of force transfer from the middle support towards the right support. Consequently, the damage number increases as additionally the stresses increase.

A linear fit is suggested without considering the design with the rectangular stiffeners for a top trough width of 150 mm, as this design falls outside the parameter's design domain. Figure 8.20 is then obtained. This parameter is accurately represented by a linear fit.
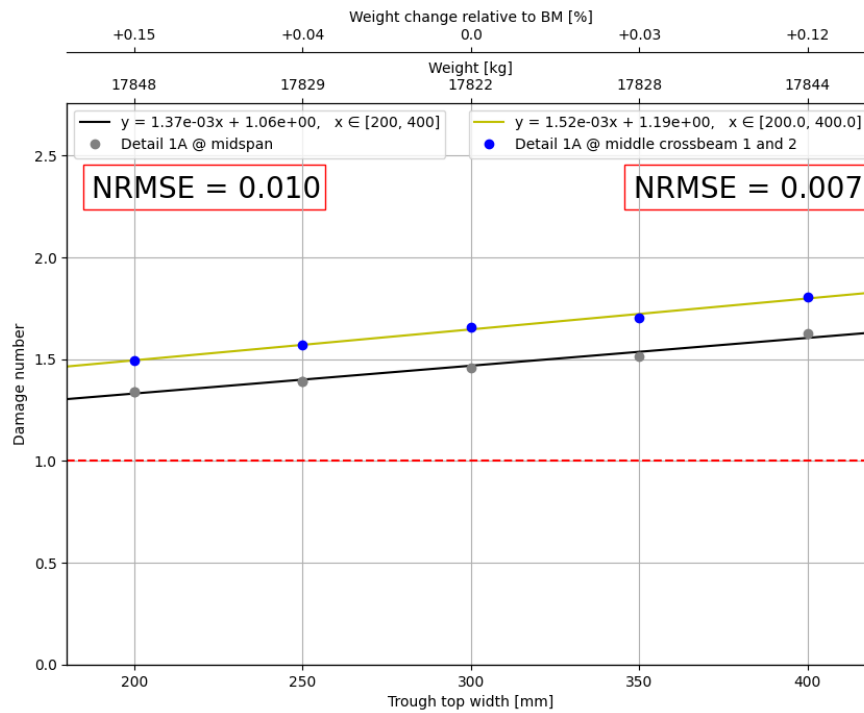
Figure 8.20: Influence of the trough top width on detail 1A.

Crossbeam center-to-center

As detail 1A lies in the middle of the span between crossbeams, different behaviour is expected than detail 1C. As detail 1A is incorporated between the first two crossbeams and between the middle crossbeams, the optimal center to center distance for the OSD regarding detail 1A can be found. The influence of the crossbeam center-to-center is displayed in Figure 8.22a. In this figure, the x axis displays information about both the span between the middle crossbeams and the first two crossbeams. The weight of the designs remain the same as always four crossbeams are used.
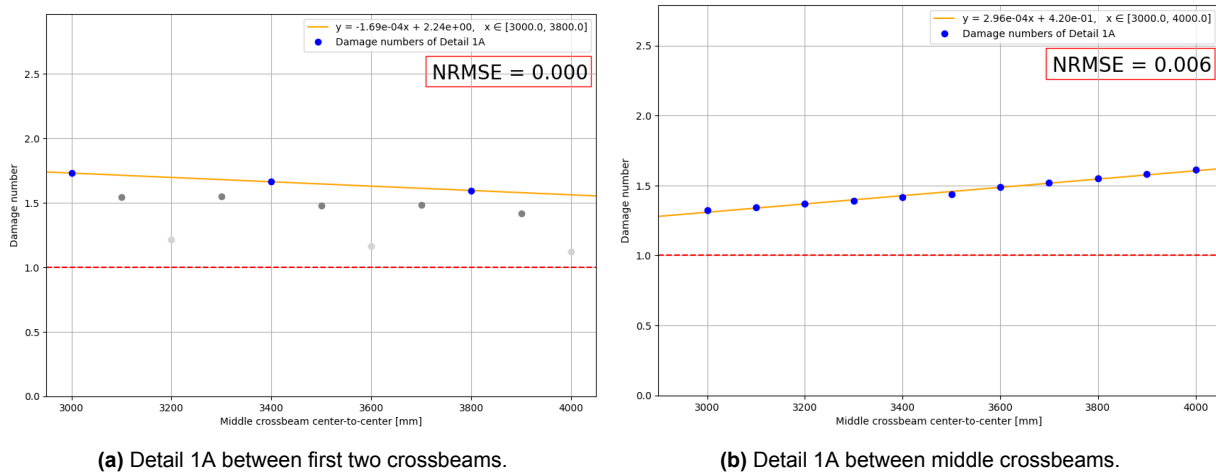
(a) Detail 1A between first two crossbeams.

(b) Detail 1A between middle crossbeams.

Figure 8.21: Damage numbers vs crossbeam center-to-center distance for detail 1A.

In Figure 8.21a, again fewer points are able to be used due to the bug in the model as the load was placed 25 and 50 mm away from the details. This accounts for the dots with respectively gray and light gray colors. Similarly as for the influence of the crossbeam center-to-center distance on detail 1C, the difference between having a longitudinal load position exactly on top of detail 1A and 50mm away from the detail is about 27%.

By having incorporated detail 1A at the center of both the middle crossbeams (see Figure 8.21b and the first crossbeams, the ideal crossbeam positions could be found for this design. The damage of both positions are set against each other, see Figure 8.22b. Observed from this figure can be that detail 1A at the span between the first two crossbeams is most governing at the majority of the domain. Additionally, observed can be that for the Benchmark configuration, the ideal span between the outer crossbeams is about 3550 mm, and the ideal span of the middle crossbeams is 3900 mm. In this the damage numbers of the two positions are equal, leaving this equilibrium point means always that the damage of one detail location will increase.

(a) Positions of detail 1A.   **(b)** Influence of crossbeam center to center distances.
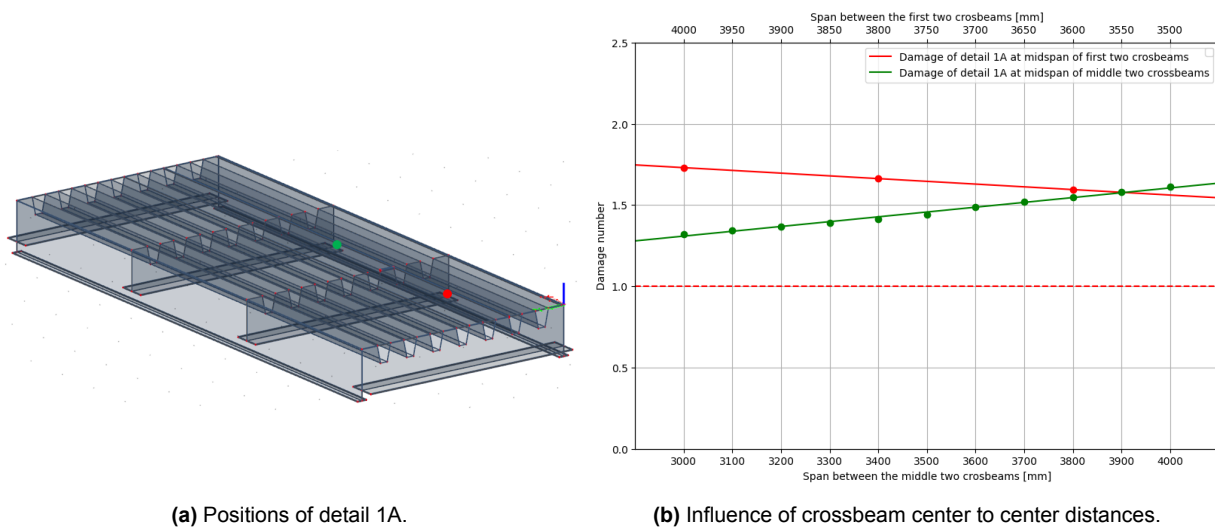
Figure 8.22: Position of details and influence of crossbeam center to center distances.

Crossbeam web thickness

Detail 1A shows behaviour opposite to detail 1C regarding the influence of the crossbeam web thickness. For both detail 1A at midspan and at the middle between crossbeam 1 and 2, a lower crossbeam web thickness causes higher damage numbers, as this lower web thickness causes increased flexibility and decreased rotational stiffness of the crossbeams, causing also higher deformation and stresses inbetween the crossbeams. From Figure 8.23 it follows that the crossbeam web thickness has a minimal influence on detail 1A.
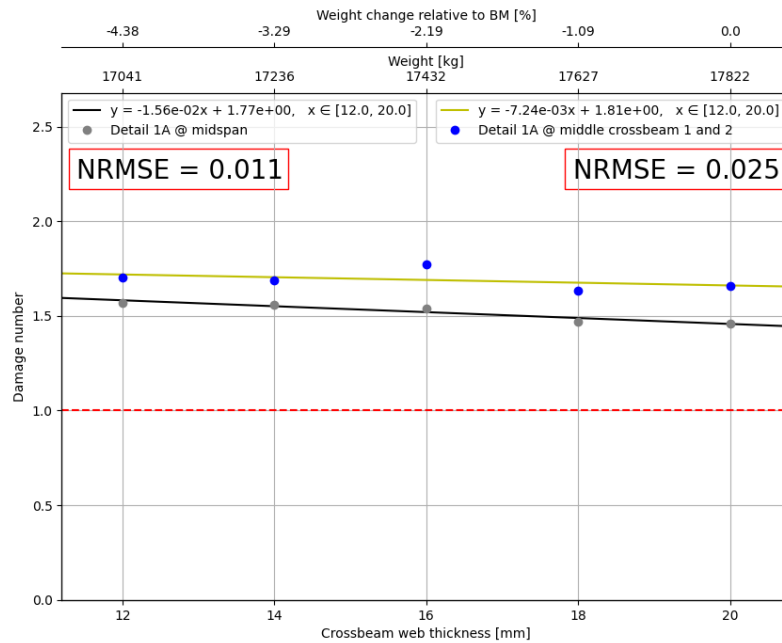
Figure 8.23: Influence of the crossbeam web thickness on detail 1A at the position between the first two crossbeams and at midspan.

Trough thickness

The influence of the trough thickness is very similar for both details. The trough thickness in an OSD is only allowed to vary from 6 to 8 mm according to the ROK [2]. Figure 8.24 shows the influence of the trough thickness on detail 1A. An increase in trough thickness results in a lower damage number of maximum 0.05 lower, while increasing the total weight of the bridge by 5.84%.
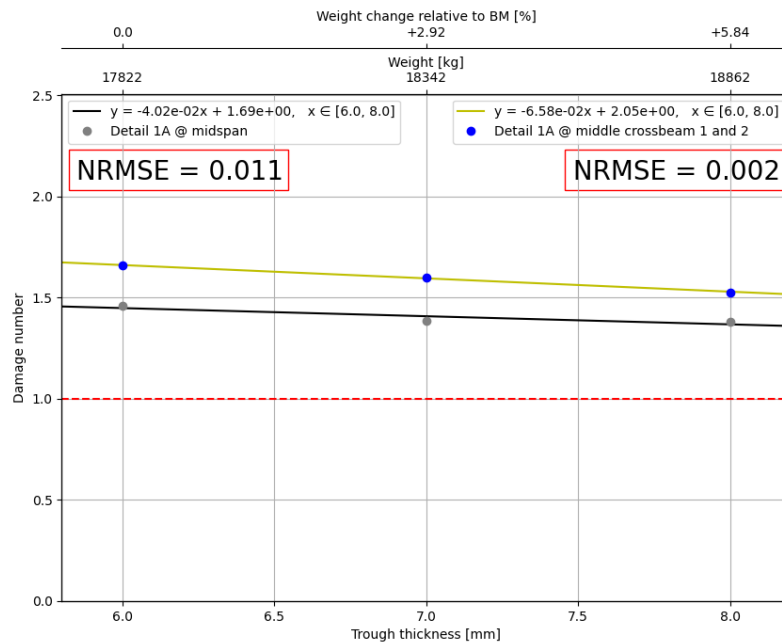
Figure 8.24: Influence of trough thickness on detail 1A.

Trough bottom width

The value of the trough bottom width is restricted between 100 and 200 mm. The influence of this parameter is illustrated in Figure 8.25. A wider trough bottom results in a moderately lower damage number for respectively detail 1A.
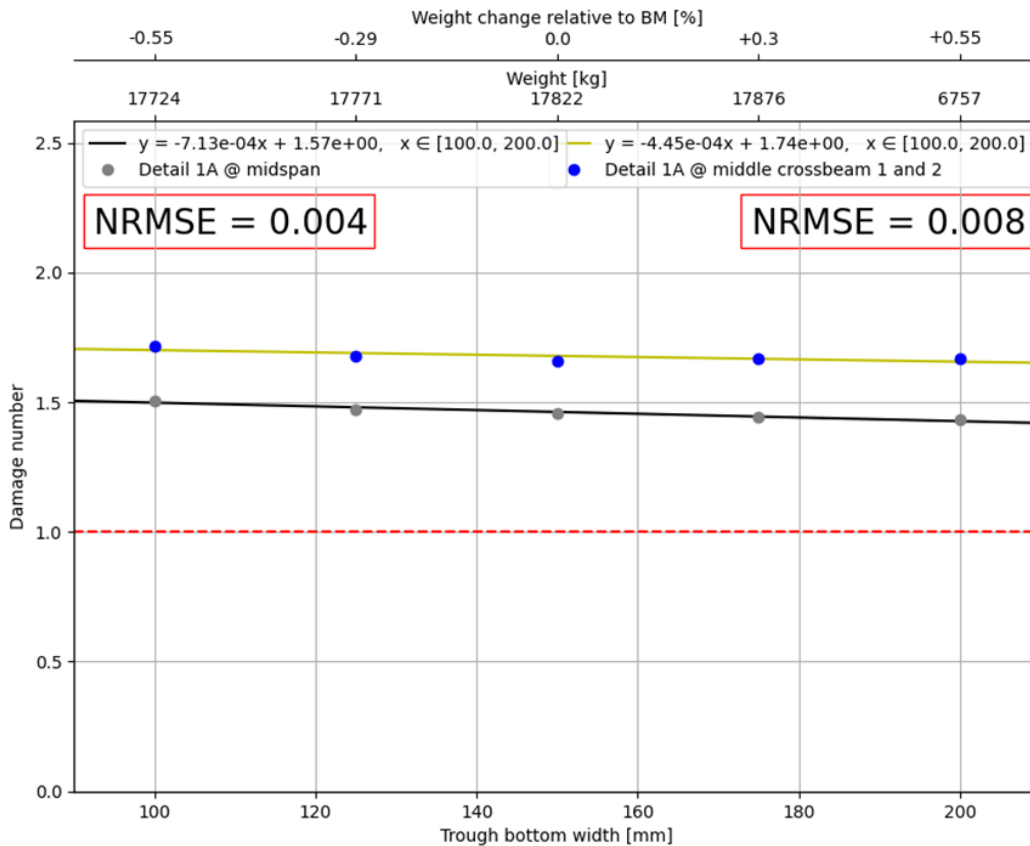
Figure 8.25: Influence of trough bottom width on detail 1A.

The influence of the trough bottom width on detail 1A is maximally about 3% of the benchmark damage number. The trough bottom width additionally does influence the weight only slightly, changing the total weight of the bridge by about 0.3% when the trough bottom width is changed by 20 mm.

Trough height

The height of the trough affects the stiffness of the span between the crossbeams. Nonetheless, the influence of the trough height on detail 1A is extremely small within its domain. The maximal influence over the parameter's domain is less than 1% of the total damage, and therefore considered negligible. The trough height does influence the weight of the bridge by about 0.85% of the total weight of the brigade per 25 mm.
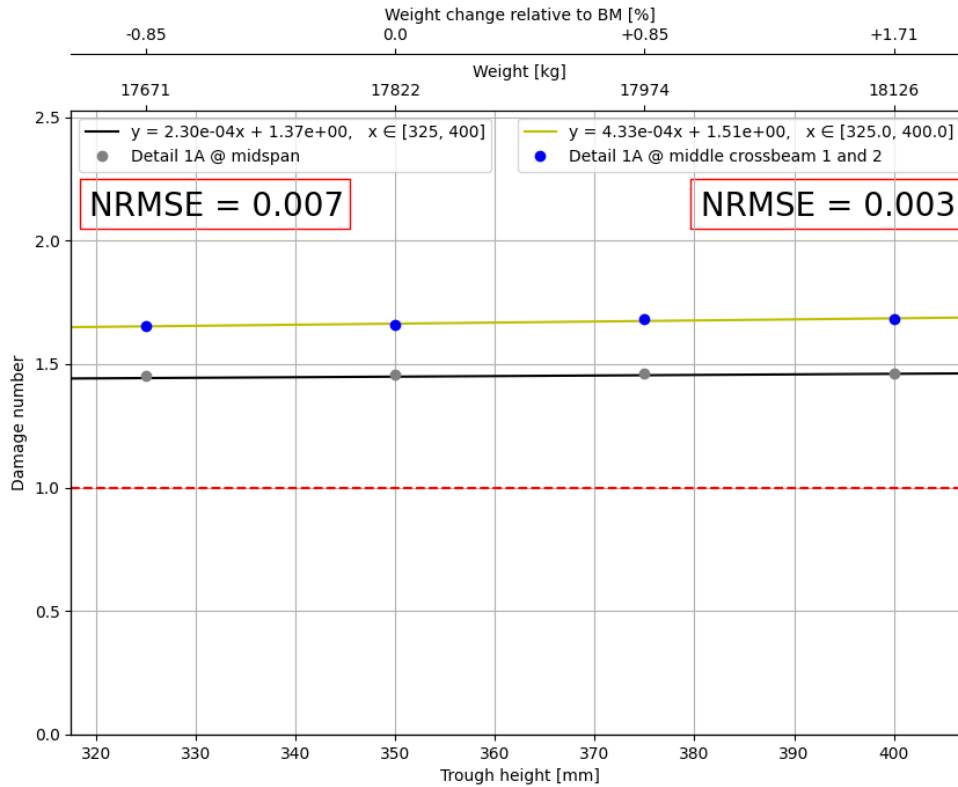
Figure 8.26: Influence of trough height on detail 1A.

8.2. Overview parameter influences

The impact of individual parameters on the different designs is shown in tables below. Table 8.2 first presents the absolute influence of the parameters on detail 1A and 1C. Tables 8.3 and 8.4 provide a more in-depth analysis and introduce a new parameter: weight-effectiveness. Weight-effectiveness represents the weight of the bridge that must be added (+) or removed (-) to reduce the damage number by 0.1. However, it's worth noting that the damage number cannot always be reduced by exactly 0.1, if at all. Furthermore, it should also be considered that this is based on a derivative, which is a constant. This can only be valid for the entire domain if a linear relationship is present. If the relationship is not linear, a derivative of the line at the benchmark model is taken. Parameters with an influence of less than 5% of damage number of the benchmark or parameters which do not influence the weight have a '-' in the weight-effectiveness column.

Table 8.2: Overview of absolute influence of parameters on detail 1A and 1C.

Parameter	Researched domain [mm]	Absolute Influence on damage of detail 1A	Absolute Influence on damage of detail 1C
t_{dp}	[17, 24]	**11,12**	**8,31**
ctc_{cb}	[3000, 4000]	**0,61**	0,01
t_{cb}	[12, 20]	0,11	**0,21**
t_{tr}	[6,8]	0,14	0,05
ctc_{tr}	[375, 600]	**1,37**	0,01
h_{tr}	[325, 400]	0,03	0,01
$w_{tr,top}$	[200, 400]	**0,31**	**4,40**
$w_{tr,bot}$	[100, 200]	0,07	0,04

Table 8.3: Parameter influence overview for detail 1C.

Parameter	Parameter domain [mm]	Damage domain [-]	Fit	Derivative @ BM D/mm	Weight-effectiveness @ BM
t_{dp}	[17; 24]	[0,02; 8,33]	$D = e^{(-0.622t_{dp}+12.68)}$	-0,594	66,6
ctc_{cb}	[3000; 4000]	[0,86; 0,87]	$D = -6.22e^{-6}ctc_{cb} + 0.887$	-6.22e-6	-
t_{cb}	[12; 20]	[0,55; 0,76]	$D = 0.0272t_{cb} + 0,208$	0,0272	-357,11
t_{tr}	[6; 8]	[0,69; 0,76]	$D = -0,025t_{tr} + 0,895$	-0,025	2081,60
ctc_{tr}	[375, 600]	[0,75; 0,77]	$D = -4.24e^{-5}tr_{ctc} + 0.782$	-4.24e-5	-
h_{tr}	[325; 400]	[0,76; 0,77]	$D = -1.11e^{-4}h_{tr} + 0,801$	-1.11e-4	-
$w_{tr,top}$	[250; 400]	[0; 4,5]	$D = 0,00018w_{tr,top}^2 - 0,086w_{tr,top} + 10.4$	0,022	-0,049
$w_{tr,bot}$	[100; 200]	[0,74; 0,78]	$D = -4.16e^{-4}w_{tr,bot} + 0.695$	-4.16e-4	-

Table 8.4: Parameter influence overview for detail 1A.

Parameter	Parameter domain	Damage domain	Fit	Derivative @ BM D/mm	Weight-effectiveness @ BM
t_{dp}	[17, 24]	[0,39; 11,51]	$D = e^{(-0.504t_{cb}+10.94)}$	-2,61	15,02
ctc_{cb}	[3000, 4000]	[1,12;1,73]	$D = -0.00017cb_{ctc} + 2.24$	-0,00017	-
t_{cb}	[12; 20]	[1,63; 1,70]	$D = -7.24e^{-3}t_{cb} + 1.81$	-7.24e-3	-
t_{tr}	[6, 8]	[1,52; 1,66]	$D = -0.04t_{tr} + 1.7$	-0,04	1301
ctc_{tr}	[375, 600]	[0,28; 1,65]	$D = 0.000042tr_{ctc}^2 - 0.0035tr_{ctc} + 7.57$	0,0469	16,95
h_{tr}	[325; 400]	[1,66; 1,68]	$D = 4,33e^{-4}h_{tr} + 1.51$	4.33e-4	-
$w_{tr,top}$	[200, 400]	[1.5; 1,8]	$D = 0.0014w_{tr,top} + 1.06$	0,0014	10,18
$w_{tr,bot}$	[100; 200]	[1.66; 1,72]	$D = -4.45e^{-4}w_{tr,bot} + 1.74$	-4.45e-4	-

8.3. Influence of traffic types

Traffic types are given by the Eurocode and have been discussed in Section 4.2. Three traffic types are distinguished: Local distance traffic, medium-long distance traffic and long distance traffic. Further in this study, they will be revered to as respectively Traffic type 1, 2 and 3, or in short TT1, TT2 and TT3. To research the influence of the different traffic types, multiple important parameters have been investigated for the distinguished traffic types. For each traffic category, the Eurocode and ROK prescribe a certain amount of trucks passing the bridge (N_{obs}). However, to be able to study solely the influence of traffic categories, the amount of trucks passing the bridge is held constant at 500.000 trucks per year. It is worth noting that a change in this amount linearly affects the damage number.

Not all parameters are interesting to study. Parameters with limited influence on the damage numbers show similar influence of traffic types of the Benchmark model over the full domain. Thus, not all parameters are incorporated. The most influential parameter will be investigated; the deckplate thickness. See Figure 8.27 and Tables 8.5 and 8.6. Further Tables and Figures of the influence on the trough center-to-center distance and crossbeam thickness can be found in Annex F.

(a) Detail 1C. **(b)** Detail 1A (inbetween crossbeam 1 and 2).
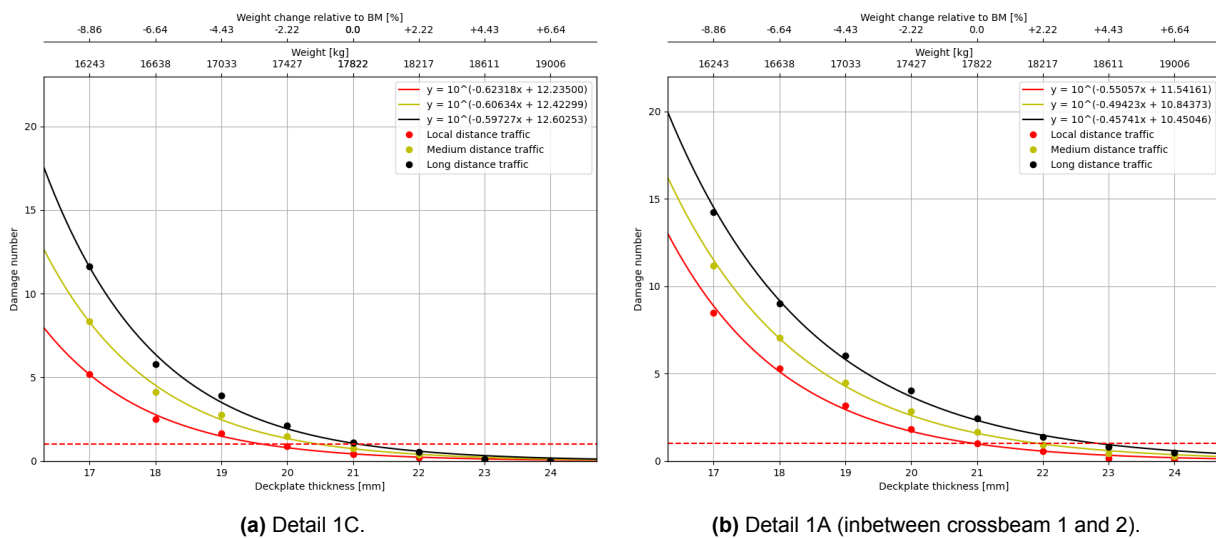
Figure 8.27: Influence of traffic categories on bridge response to different deckplate thicknesses for detail 1C and 1A.

Table 8.5: Damage numbers and differences per deckplate thickness and traffic type for Detail 1C.

t_{dp} [mm]	Damage numbers per traffic type*			Absolute differences			Percentual increase TT3 w.r.t. TT1
	TT1	TT2	TT3	TT3-TT1	TT2-TT1	TT3-TT2	
17	5,21	8,33	11,6	6,39	3,12	3,27	123%
18	2,51	4,11	5,8	3,29	1,6	1,69	131%
19	1,64	2,74	3,91	2,27	1,1	1,17	138%
20	0,87	1,48	2,14	1,27	0,61	0,66	146%
21	0,43	0,76	1,11	0,68	0,33	0,35	158%
22	0,22	0,38	0,54	0,32	0,16	0,16	145%
23	0,03	0,07	0,11	0,08	0,04	0,04	267%
24	0,01	0,02	0,04	0,03	0,01	0,02	300%

* TT1 = Local distance traffic; TT2 = Medium-long distance traffic; TT3 = Long distance traffic

Table 8.6: Damage numbers and differences per deckplate thickness and traffic type for Detail 1A inbetween crossbeam 1 and 2.

| t_{dp} [mm] | *Damage numbers per traffic type** | | | *Absolute differences* | | | |
	TT1	TT2	TT3	TT3-TT1	TT2-TT1	TT3-TT2	Percentual increase TT3 w.r.t. TT1
17	8,46	11,17	14,24	5,78	2,71	3,07	68%
18	5,30	7,04	9,03	3,73	1,74	1,99	70%
19	3,16	4,49	6,05	2,89	1,33	1,56	91%
20	1,81	2,83	4,04	2,23	1,02	1,21	123%
21	1,03	1,66	2,42	1,39	0,63	0,76	135%
22	0,56	0,94	1,38	0,82	0,38	0,44	146%
23	0,15	0,45	0,79	0,64	0,30	0,34	427%
24	0,09	0,28	0,49	0,40	0,19	0,21	444%

* TT1 = Local distance traffic; TT2 = Medium-long distance traffic; TT3 = Long distance traffic

A higher damage number has higher absolute differences between the different traffic types, as can be expected. It is observed that the absolute difference between TT3 and TT2 is always greater than the difference between TT2 and TT1. Furthermore, it is observed that generally, the lower the damage number becomes, the higher the percentual increase of TT3 with respect to TT1. However, this is not necessarily the case, as Table F.4 in Annex F shows opposite behaviour. Around the benchmark model, the model with a deckplate thickness of 21 mm, the difference between the local distance traffic and long distance traffic is about 158% of the local distance traffic for detail 1C, and 135% or 116% for detail 1A. Indicating that this is different for each detail and detail position. No further conclusions can be drawn from this analysis.

8.4. Degree of parameter interaction

The parameter sensitivity is analyzed using a one-at-a-time approach. As a result, interactions between parameters are not mapped, even though they occur in reality. The aim of this verification is to examine whether a great interaction exists between parameters around the benchmark model. To achieve this, damage numbers from a new model based on the generalized case study are determined through the lines of the parameter sensitivity study and trough a new run of the parametric model. This allows for a comparison to check whether a parameter interaction is noticeable.

Firstly, the model must be defined. See Table 8.7 for the parameters of this model. It can be observed that all parameters differ from the benchmark model, except for the trough top width and center-to-center distance. These parameters remain unchanged as they are often employed with a value of respectively 300mm and 600mm.

Table 8.7: OSD parameter dimensions (in mm) and mass of the invesigated design.

t_{dp}	t_{tr}	$w_{tr,top}$	$w_{tr,bot}$	ctc_{tr}	h_{tr}	$t_{cb,web}$	$ctc_{cb,mid}$	$Mass\ [kg]$
20	7	300	170	600	375	16	3400	17799

The damage for both details is estimated through a parameter sensitivity study. To determine the damage number from the PSA, the new parameter values are entered in the fitted lines. The difference between this new value and the original damage of the benchmark model is calculated. These differences are obtained for all parameters, as done for detail 1C and both places of detail 1A in respectively Table 8.8, Table 8.9 and Table 8.10.

Table 8.8: Usage of PSA for determining difference in damage number between the benchmark model and the new design for detail 1C.

Parameter	Original value [mm]	New value [mm]	Damage by PSA fit	Damage original	Δ_{damage}
t_{dp}	21	20	1,344	0,760	0,584
ctc_{cb}	3666	3400	0,760	0,760	0,000
t_{cb}	20	16	0,643	0,760	-0,117
t_{tr}	6	7	0,745	0,760	-0,015
ctc_{tr}	600	600	0.760	0,760	0.000
h_{tr}	350	375	0,759	0,760	-0,001
$tr_{w,top}$	300	300	0.760	0,760	0.000
$tr_{w,bot}$	150	170	0,766	0,760	0,006
				Δ_{sum}	0,457

Table 8.9: Usage of PSA for determining difference in damage number between the benchmark model and the new design for detail 1A at midspan.

Parameter	Original value [mm]	New value [mm]	Damage by PSA fit	Damage original	Δ_{damage}
t_{dp}	21	20	2,354	1,458	0,896
ctc_{cb}	3666	3400	1,426	1,458	-0,032
t_{cb}	20	16	1,520	1,458	0,062
t_{tr}	6	7	1,408	1,458	-0,050
ctc_{tr}	600	600	1.458	1,458	0.000
h_{tr}	350	375	1,456	1,458	-0,002
$tr_{w,top}$	300	300	1.458	1,458	0.000
$tr_{w,bot}$	150	170	1,449	1,458	-0,009
				Δ_{sum}	0,865

Table 8.10: Usage of PSA for determining difference in damage number between the benchmark model and the new design for detail 1A inbetween crossbeam 1 and 2.

Parameter	Original value [mm]	New value [mm]	Damage by PSA fit	Damage original	Δ_{damage}
t_{dp}	21	20	2,609	1,658	0,951
ctc_{cb}	3666	3400	1,665	1,658	0,007
t_{cb}	20	16	1,694	1,658	0,036
t_{tr}	6	7	1,589	1,658	-0,069
ctc_{tr}	600	600	1.658	1,658	0.000
h_{tr}	350	375	1,672	1,658	0,014
$tr_{w,top}$	300	300	1.658	1,658	0.000
$tr_{w,bot}$	150	170	1,664	1,658	0,006
				Δ_{sum}	0,946

These calculated differences can be added to the original value of the benchmark model to obtain the estimation of the new damage value. As already pointed out in section 8.1, due to a bug in the model the damage number of detail 1C has observed to be 0.760 instead of 0.862, as the longitudinal load was not exactly placed on the detail. Therefore, the estimation of the damage number of detail 1C should be adjusted by a factor of $0.862/0.760 = 1.134$, to account for the bug in the model, see Table 8.11. The FE model damage value is also displayed in this table.

Table 8.11: Difference in Damage numbers between the FE model and the estimation based on the PSA.

Detail	Original value	$\Delta_{damage,sum}$	Estimated value	Correction	FE model value	Difference
1C	0,760	0,457	1,217	1,377	1,485	0,108
1A @ midspan	1,458	0,865	2,323	-	2,333	0,010
1A inbetween cb 1 and 2	1,658	0,946	2,604	-	2,527	-0,077

As observed, the difference between the PSA-based estimation and the FE model value is minimal. Only detail 1C seems to deviate slightly. This makes sence as not much parameter interaction is expected to influence the results, because the design in Table 8.7 do not difference much from the benchmark model. However, it is expected that a design further away from the benchmark model has a greater parameter interaction. See Table 8.12 for a design further away from the benchmark model.

Table 8.12: OSD parameter dimensions (in mm) and mass of the design further away from the benchmark model.

t_{dp}	t_{tr}	$w_{tr,top}$	$w_{tr,bot}$	ctc_{tr}	h_{tr}	$t_{cb,web}$	$ctc_{cb,mid}$	$Mass\ [kg]$
17	8	250	180	600	400	12	3000	17047

Similar tables to calculate the differences as previous are generated, these are visible in Appendix G. The result of the parameter interactions are displayed in Table 8.13.

Table 8.13: Difference in Damage numbers between the FE model and the estimation based on the PSA for the design further away from the benchmark model.

Detail	Original value	$\Delta_{damage,sum}$	Estimated value	Correction	FE model value	Difference
1C	0,760	6,561	7,321	8,284	3,428	-4,856
1A @ midspan	1,458	9,386	10,844	-	9,493	-1,351
1A inbetween cb 1 and 2	1,658	9,868	11,526	-	10,173	-1,353

As expected, the difference between the designs is observed to grow as the parameters of the new design are further from the parameters of the benchmark model design. Nevertheless, for detail 1A the estimations are still in the same order, being on average conservative with about 13.5%. Although the estimation for detail 1C is conservative, it is not accurate due to parameter interactions occurring in reality. For detail 1A less parameter interaction is observed than for detail 1C. This can be explained: Detail 1C observes a greater parameter interaction as the two most influential parameters are varied, while for Detail 1A the second most influential parameter is not changed, and the parameter interaction observed is significantly less. Nevertheless, it is demonstrated that the parameter interaction is present, especially between the most influential parameters of the details.

Model Validation

In this chapter the parametric model is validated in several ways. Firstly assumptions made in the creation of the model are validated. Secondly, a comparison for detail 1C with the analytical model is drawn. In the last section, the parametric FE model is used to determine damage numbers in the original case study bridge. This damage numbers are compared to the damage numbers coming from manual calculations of the actual used FE model to determine the influence of the boundary conditions on detail 1A and 1C.

9.1. Validation of assumptions

This section validates three assumptions made in the development of the parametric model. Firstly the transverse load distribution of 1C is verified. After which the assumptions about the transversal detail location of both details is checked.

9.1.1. Transverse load distribution

In Chapter 8 the governing detail is found. This governing detail showed the highest stresses in both the flexible and rigid design for the same transversal load distribution; the distribution exactly above the middle of the trough. It is assumed that this distribution is always governing in this design domain. To verify this, damage numbers of the benchmark model are compared for the three possible transversal distributions. The distributions are shown in Figure 9.1, Table 9.1 gives their damage numbers. The damage number for the distribution above the trough middle is the largest, which demonstrates the validity of the assumption in the benchmark model.

(a) Above trough middle.   **(b)** Above trough leg.   **(c)** In between troughs.
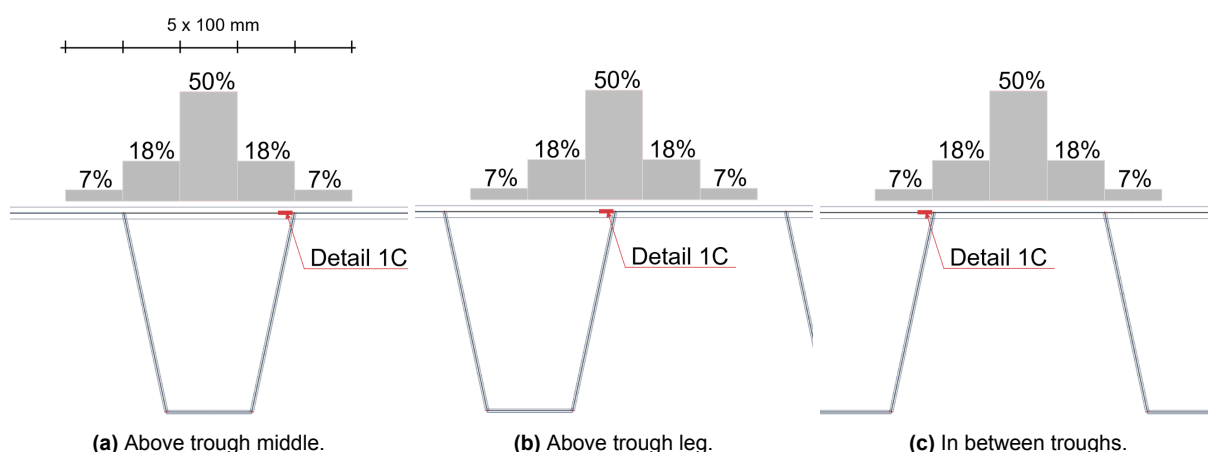
Figure 9.1: Different load distributions.

Table 9.1: Benchmark damage numbers of different load distributions.

Distribution	Above trough middle	Above trough leg	In between troughs
Damage number	0.76	0.28	0.08

9.1.2. Transverse location of detail 1C

From the data analysis of the ctc_{tr} for detail 1C, it is found that a certain domain of points might be progressive due to the assumption that the governing detail is always closest to the load. It should be checked whether the detail closest to the load is actually governing. It is checked whether this assumption does hold for the benchmark model. This is done by placing the load exactly where the trucks are expected; which is exactly in the middle of the road, and determining the damage for multiple trough legs around this load. See Figure 9.2 and corresponding Table 9.2.
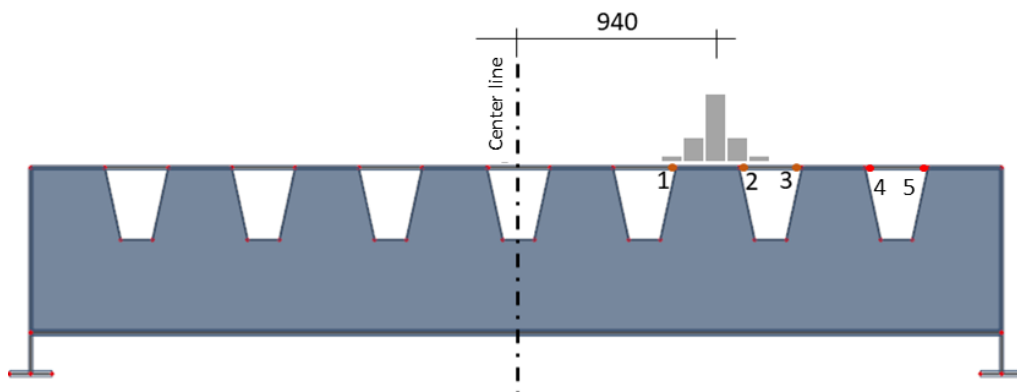
Figure 9.2: Tested detail locations for detail 1C.

Table 9.2: Damage numbers corresponding to the locations indicated in Figure 9.2.

Detail location	1	2	3	4	5
Damage	0,18	0,14	0,59	0,00	0,00

The assumption that the maximum damage occurs at the trough leg closest to the load distribution does not hold for the benchmark model. Although, it can be noted that damage numbers obtained from placing the loads exactly where the trucks are expected, see Table 9.2, are still below the value found of detail 1C for the position 2 in Figure 9.2 when placing the load distribution in the middle of the trough. The quantity of the damage number of position 3 in Figure 9.2 is remarkable. It is questioned whether more troughs behave this way. To research this, the maximum damage numbers of all trough legs for detail 1C are determined by the parametric FE model. These damage numbers are displayed transversely along the bridge in Figure 9.3.
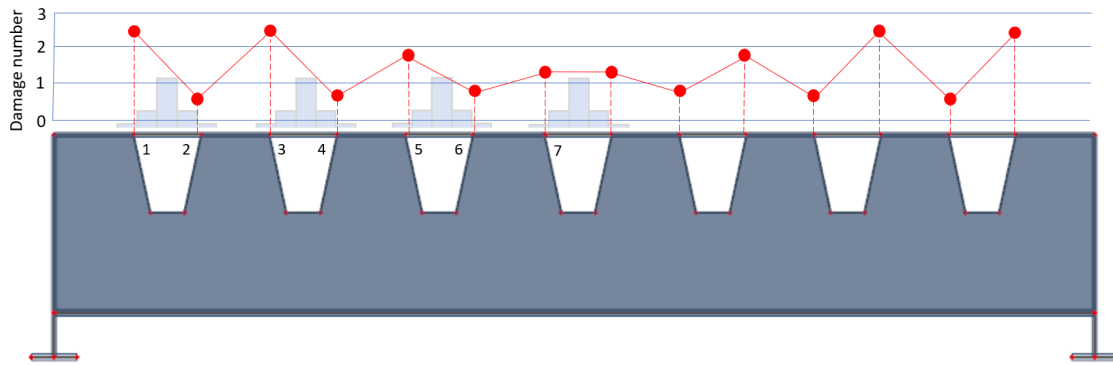
Figure 9.3: Damage numbers of detail 1C over the width of the bridge for the BM. The governing load distributions for detail 1C are additionally displayed in light blue.

Table 9.3: Damage numbers corresponding to the locations indicated in Figure 9.3.

Detail location	1	2	3	4	5	6	7
Damage	2,22	0,72	2,23	0,76	1,87	0,98	1,28

When the investigated trough is closer to the main girders, the difference in damage numbers between its two legs increases. This difference is significant, with variations within a trough leg reaching nearly three times the lowest value in that trough. This is due to a difference in stiffness between the trough legs, except for the middle trough leg, which is symmetrical. At the first trough leg the damage is somewhat lower than expected based on the other results, it is assumed that this is due to a slightly different mesh configuration. When the trough leg closest to the main girder is observed, only two trough beams are refined instead of the usual three. This is because the parametric model refines the troughs next to the considered trough whenever possible, and at the trough closest to the main girder only has 1 adjacent trough, so only two troughs get refined. Nevertheless, the damage is expected to be maximal at the trough leg closest to the main girder.

The difference in damage numbers can be explained by looking at the loading causing the highest damage, which is truck C directly above the center of a trough, see Figure 9.5. For this loading, the stiffer side of the trough, takes more loading than the less stiff part. The quantity of the stresses on each side depends on the stiffness distribution between the legs. Which is more skewed closer to the main girder. Concluded from this analysis can be that detail 1C is always governing at trough leg closest to the main girder.

9.1.3. Transverse location of detail 1A
To check whether the assumption that the maximum damage occurs at the trough leg closest to the load distribution does hold for detail 1A in the benchmark model, the same check as in the previous section is executed for detail 1A positioned inbetween crossbeam 1 and 2, which is the governing one. The same positions are used as in Figure 9.2. The damage obtained at these points is displayed in Table 9.4.

Table 9.4: Damage numbers of detail 1A corresponding to the locations indicated in Figure 9.2.

Detail location	1	2	3	4	5
Damage	0.22	0,54	0,00	0,00	0,00

It can be derived from Table 9.4 that the assumption about the maximum damage occurring at the trough leg closest to the load distribution does hold for detail 1A. It seems that the variation in damage numbers between the trough legs of the same trough is not present for detail 1A. The damage numbers over the width of the bridge are studied anyway, see Figure 9.4.
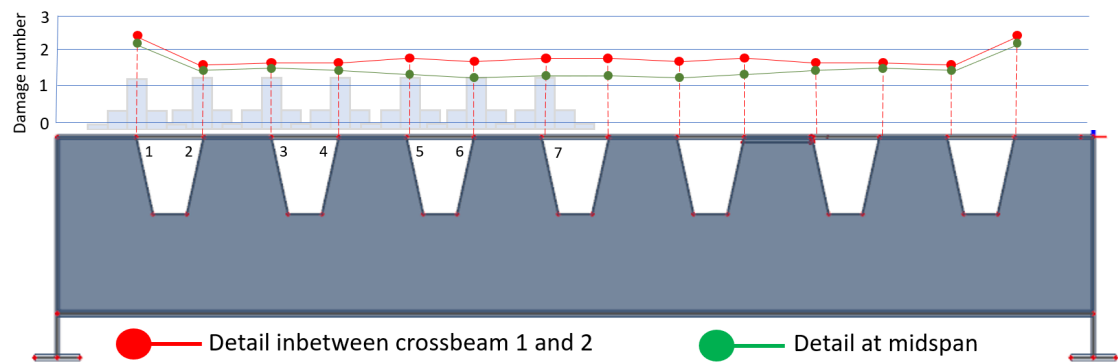
Figure 9.4: Damage numbers of detail 1A over the width of the bridge for the BM. The governing load distributions are additionally displayed in light blue.

Table 9.5: Damage numbers corresponding to the locations indicated in Figure 9.4.

Detail location	1	2	3	4	5	6	7
Damage at midspan	2,12	1,46	1,48	1,46	1,33	1,32	1,34
Damage inbetween cb 1 and 2	2,36	1,63	1,66	1,66	1,87	1,84	1,87

For detail 1A, the maximum damage number in the bridge can be found at the trough leg closest to the main girder. The damage numbers for detail 1A show less variation compared to detail 1C in the transverse direction of the bridge.

9.2. Comparison with analytical model

The Dutch national annex of EN 1993-2 [56] gives several analytical methods. One of them is for detail 1C of the ROK [2], at the intersection of the trough, deckplate and crossbeam. The simplified analytical model is represented by a beam with clamped supports at both ends, illustrated in Figure 9.5. The analytical solution for wheel type a of 70 kN is shown below, the comparison with the FE model is also drawn. It can be noted that there are parameters affecting detail 1C which are not accounted for in the analytical model, like the thickness of the crossbeams or troughs, which make an impact on the stresses
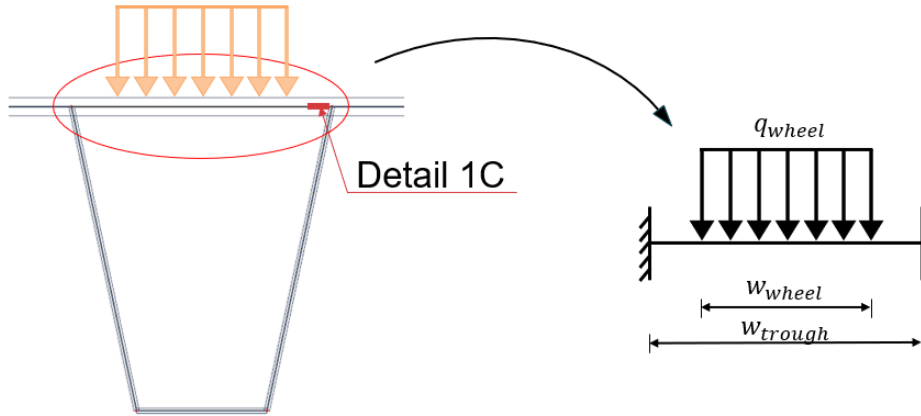
Figure 9.5: Analytical model of detail 1C.

To compare the models, the load on wheel A was considered. See the calculations below.

$$q_{wheel} = \frac{Q_k}{2 * b_{wheel} * l_{wheel}} = \frac{70}{2 * 0.22 * 0.22} = 723.14 \, [kN/m^2] \tag{9.1}$$

The bending moment at the location of detail 1C can be determined using various methods. When analyzed with a 1D FE Model, a moment of 4.896 kNm/m is obtained. This value can then be used to calculate the stress.

$$\sigma = \frac{6M}{t^2} = \frac{6 * 4.896}{0.021^2} = -66.62 \, [MPa] \tag{9.2}$$

The calculated stress of the analytical model is the pure bending occurring at the place of detail 1C, which is at the bottom of the deckplate at the trough leg. Since in reality also stress concentrations occur at this position, a Stress Concentration Factor (SCF) is introduced in the national annex of EN 1993-2 [56]. Without an asphalt layer, this factor is calculated according to equation 9.3.

$$SCF = 1.2975 - 0.00938t_{dp} = 1.2975 - 0.00938 * 21 = 1.1005 \tag{9.3}$$

$$\sigma_{SCF} = -66.62 * 1.1005 = -73.3 \, [MPa] \tag{9.4}$$

This value can be compared to the hot spot stress coming from the FE model, which shows stresses of -51.96 MPa at trough leg 4 in Figure 9.3, of which -5.1 MPa is axial stress and -47.1 MPa bending. It is observed that the analytical solution gives much higher stresses for this detail, as expected, even considering that the FE model includes both bending and normal stresses while the analytical model only includes bending stresses. The other trough leg (leg 3, see Figure 9.3) of the same trough should also be verified, as section 9.1.2 shows big differences between the two trough legs of the same trough. The stresses of the analytical model remain the same, while stresses of -61.65 MPa are found at this trough leg in the FE model, indicating that the analytical solution is truly conservative for both trough legs.

9.3. Comparison with Goereese bridge

The FE model used for the design of the Goereese bridge is used to execute a short validation of the influence of the support conditions. For both detail 1A and 1C one point on the bridge is chosen and damage numbers are compared for these details.

The trough leg at which these details are investigated is chosen at random. The longitudinal position of the details are based on where the highest damage is expected for the chosen trough leg. The locations of the details are indicated in Figure 9.6. The damage of both models is calculated with the method of the ROK[2], and reported in Table 9.6.

(a) Original Goereese FE model.　　　　　　　　(b) Parametric model.
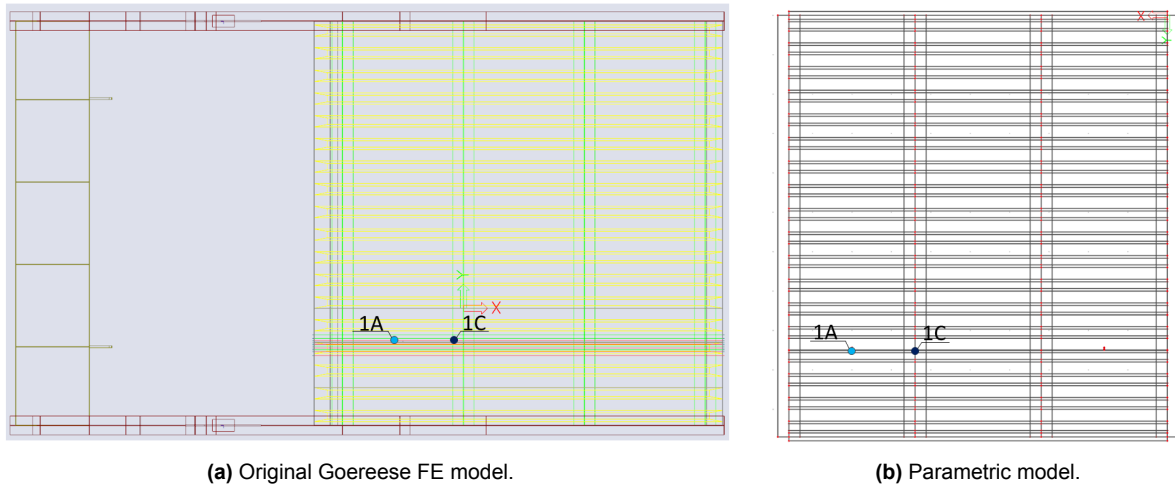
Figure 9.6: Original Goereese model vs the Parametric model.

Table 9.6: Difference in Damage numbers between the parametric tool and the original FE model of the Goereese bridge.

	Damage detail 1A	Damage detail 1C
Manual calculation (ROK 1.4) [57]	0.114	0.744
Manual calculation (ROK 2.0)	2,487	1,478
Calculation by parametric tool (ROK 2.0)	2,508	1,365

The observed difference between the Original Goereese bridge and the generalized parametric model is 0.113 for detail 1C, and 0.021 for detail 1A. While a single comparison for each detail is not enough to draw definitive conclusions, it does support the assumption that boundary conditions do not impact the damage number of these details significantly. This assumption stems from the fact that the details are mostly influenced by local loads.

Furthermore it is seen that the damage numbers of both details at this random trough leg in the bridge are greater than one. This means that the bridge according to the new ROK rules does not have a service life of 100 years, while designed for it. Nonetheless, it should be noted that a big difference can be obtained when incorporating the new Dutch regulations (v2.0) instead of the old (v1.4) and the Eurocode used at the time of designing the Goereese bridge, as significant changes in the fatigue verification have been incorporated in the ROK[2]. The stress extraction method has been updated, the wheel imprints should be reduced and the detail categories have also been modified. Furthermore, instead of calculating damage per truck, the focus should now be on the impact of a representative number of trucks, in random order, across different transverse positions.

Part III

Research Outcome

10

Conclusion and recommendation

10.1. Conclusion

This thesis aimed to enhance the understanding of fatigue performance in Orthotropic Steel Decks (OSDs) by developing a parametric model to perform a sensitivity analysis, with the ultimate long-term objective of enhancing material efficiency trough a deeper understanding of the OSD. By focusing on the Goereese bridge as a case study, this research provided valuable insights into the critical design parameters influencing fatigue life in OSDs, and the goal of optimizing the deck. Furthermore, this research showed the possibility of developing an accurate parametric FE model, able to determine damage in 7 directly-ridden details. Developing and using the Parametric model contributed to answering the main research question, which is formulated as:

How can a parametric model be developed to assess the fatigue performance of Orthotropic Steel Deck bridges and what insights can be gained from analyzing the influence of key design parameters?

This main research question comprises of two distinguished questions: the practical question of how to develop a usable model, and the investigative question of what insights can be gained by analyzing the key design parameters of an OSD. Therefore, this research question is addressed in two parts

1. To obtain a usable model, simplifications of the mesh, assumed locations and loading scheme were a necessity. The mesh could be split into 3 different mesh areas and a local mesh refinement of 0.25 times the deckplate thickness. Hereby, area A should have the smallest mesh size and area C should have the largest mesh size. This reduced computational time by 289% while increasing the expected uncertainty by about 1.5% of the maximum stress peak. Additionally, symmetry in the loading conditions could be exploited to reduce computational time by about 127%. Due to these simplifications, a model with one detail had an average runtime of about 45 minutes. This proved to be sufficiently fast for executing a Parameter Sensitivity Analysis.

2. Conducting an OAT parameter sensitivity analysis yielded significant insights into the impact of eight parameters on the damage of details 1A and 1C, as well as their effect on the weight of the bridge. Conclusions regarding the parameter influences on these details were drawn. The following paragraphs will sum up conclusions about each detail separately for the different considered parameters.

   Findings for parameter influences on Detail 1C; The weld root crack at intersection deckplate, crossbeam and trough:

   – The deckplate thickness and trough top width influence the damage of this detail primarily, having a respective exponential and quadratic influence on the damage number. A deckplate thickness greater than 21 mm results in damage numbers smaller than 1. A 1 mm decrease of the deckplate thickness yields a damage number increase of about 100 %. A 50 mm increase in trough top width results in a damage number increase about 280 %. The deckplate thickness affects the weight of the bridge significantly, the total weight increases with 2.22% when the thickness is increased by 1 mm. The influence of the top trough width on the weight of the bridge is negligible.

84

- The crossbeam thickness is not included in the analytical solution of detail 1C, yet the parameter does influence the damage moderately. Increasing the parameter value will increase the damage number. Within the possible values of the thickness (12-20mm), the damage on 1C can vary around 30%. The crossbeam thickness influences the total weight of the bridge by 1.10% per 2mm of thickness.

- The thickness and bottom width of the trough have a minimal impact on the damage of detail 1C, with both parameters affecting the damage by up to 6% within their respective domains. While the bottom width's influence on weight is negligible, the thickness significantly affects it. An increase of 1 mm in thickness results in a 2.92% rise in the total weight.

- The trough center-to-center, trough height and crossbeam center-to-center have negligible impact on the damage number of detail 1C.

Findings for parameter influences on Detail 1A; The weld toe crack at intersection deckplate and trough:

- The deckplate thickness has the greatest influence of the parameters on detail 1A, having an exponential influence on the damage number. A 1 mm decrease of the deckplate thickness yields a damage number increase of about 70%. The influence on the total weight is 2.22% per 1 mm of deckplate. Similarly as for detail 1A, A deckplate thickness greater than 21 mm results in damage numbers smaller than 1.

- The trough center-to-center has the second greatest influence on the damage number of detail 1A. The influence can be represented by a second order polynomial. A decrease in the center-to-center distance generally accounts for a decrease in the damage number. The influence of the parameter on the weight is significant, causing a 2.23 % increase in weight when a trough is added, which happens roughly every 45 mm when the value is decreased.

- The top trough width and crossbeam center-to-center additionally influence the damage of detail 1A. Both parameters account for a maximum difference in damage number of 0.3 over the parameter domain, which is 20% of the damage number. The crossbeam center-to-center does not affect the weight of the bridge, the effect of the top trough width is negligible.

- The crossbeam thickness, trough thickness and trough bottom width influence the damage of detail 1A marginally. Within the possible values of the parameters, the damage of 1A varies maximally around 8% of the damage number of the benchmark (0.12).

- The influence of the trough height on the damage number is negligible. The influence on the weight is 0.85% of the total weigth per 25 mm of trough height.

The main research question has been answered by the preceding paragraphs, the remainder of this section discusses further findings of this thesis.

- The load placement exactly above the middle of a trough is the governing transversal position for detail 1C and results in the highest stresses and damage numbers.

- Disregarding the second wheel of an axle increases the maximum stresses about 5% for detail 1C.

- A difference in stiffness exists between two trough legs of the same trough at detail 1C. The stiffness distribution over two trough legs of one trough influences the damage numbers and governing position of detail 1C significantly. The greatest difference is obtained at the trough closest to the main girder, where the trough leg closest to the main girder had a damage value of 2.22, and the other leg a value of 0.72.

- The governing transversal location of details 1C and 1A is positioned at the trough leg closest to the main girder when no assumptions are made about the theoretical driving lane.

- Regarding detail 1C, when incorporating the theoretical driving lane, it is recognized that the detail at the trough leg closest to the center of the load distribution does not have to be the governing detail.

- The influence of the different Traffic Types (TTs) is highly different per detail and damage value. Generally a lower damage number accounts for smaller absolute differences between the TTs, but accounts for a higher percentual increase of the differences.

- The case study Goereese bridge has damage numbers higher than one due to new rules in version 2.0 of the ROK, when this was far below one in version 1.4.

10.2. Recommendations

A set of recommendations is given based on the research in this thesis. Recommendations obtained by the Parameter sensitivity analysis, the modelling approach of the parametric model and recommendations for future research are distinguished and described in separate sections.

10.2.1. Parameter sensitivity analysis

In the parameter sensitivity study multiple conclusions have been drawn, some have led to recommendations which are described in this section for detail 1A en 1C in future designs. These recommendations are purely about the design of the bridge regarding details 1A and 1C, other details are not included.

Recommendations regarding the design of detail 1C.

- It is recommended to optimize the deckplate thickness to the fullest extent (practically this means on mm scale), as small changes in this deckplate thickness can result in huge damage changes due to the exponential behaviour. Additonally, the deck plate has the largest impact on the weight of the bridge.
- When detail 1C appears to be governing, it is recommended to reduce the top width of the trough, as this parameter has a great influence on the damage number, but small influence on the weight.
- The minimal trough thickness value in the ROK [2] of 6 mm is recommended as this parameter has minimal influence on the damage number of detail 1C, but has a significant influence on the weight of the bridge.
- The minimal trough height value in the ROK [2] of 325 mm is recommended as the influence of this parameter on the damage number of detail 1C is negligible.
- To decrease the damage of detail 1C, the crossbeam thickness can be decreased. This parameter does slightly influence detail 1A, so a balance should be found for the value of this parameter. It is recommended to keep this parameter at the lower end of their domain, as this parameter has a great influence on the weight of the bridge.
- It is recommended to check detail 1C at the trough leg closest to the main girder, as here the highest damage is expected.

Recommendations regarding the design of detail 1A.

- For detail 1A, it is recommended to optimize the deckplate thickness to trough center-to-center ratio. These are the two details with the most influence on both the damage of 1A and the weight of the OSD. Finding a good balance is crucial as they interact with each other. A thinner deckplate results in a lighter bridge, but this requires a reduced trough center-to-center distance, which in turn increases the weight.
- The minimal trough thickness value in the ROK [2] of 6 mm is recommended as this parameter has a minimal influence on the damage number of detail 1A, but has a significant influence on the weight of the bridge. Reducing the trough thickness yields a lighter design.
- The minimal trough height value in the ROK [2] of 325 mm is recommended as the influence of this parameter on the damage number of detail 1A is negligible.
- It is recommended to check detail 1A at the trough leg closest to the main girder, as here the highest damage is observed.

10.2.2. Modelling simplifications

To ensure the the parametric model could be solved within an acceptable time, the computational size of the finite element model had to be reduced. Recommendations regarding the modelling of a parametric model of an OSD bridge can be given:

- Dividing the bridge into separate areas with specific mesh sizes significantly improves calculation time with limited impact on stress accuracy. Further research is recommended to establish guidelines for this approach and check further feasibility.
- Disregarding the multi-path model and incorporating all trucks into the middle lane can further speed up the parametric model. This method reduces the number of load cases and computational time, and is expected to increases conservatism, albeit with decreased accuracy. Research is needed to justify this simplification.

- In this thesis, the step size for placing longitudinal loads on the parametric model has been set to 0.1 meter. However, it is expected that such precision may not be necessary. Further research should explore the possibility of increasing the step size in specific domains of the bridge for certain details. This adjustment could lead to a further reduction in computational time for the parametric FE model.

10.2.3. Future work

From the research in this thesis, recommendations can be made for expanding this thesis research, relevant future research and application possibilities.

- To gain deeper insights into various detail or detail locations, this research could be expanded by incorporating additional details or conducting sensitivity studies on details besides 1A and 1C. When more details are added to the parametric model beyond the directly-ridden details, more parameters should be added as then parameters like the crossbeam height and flange thickness or the dimensions of the main girders are expected to have a greater affect on these details more influenced by global behaviour.

- This research did not account for a second traffic lane due to the generalization of the parametric FE model to a single lane. If the model is expanded to include a second traffic lane, further studies could be conducted to examine the effects of trucks in the additional lane.

- The Goereese bridge shows damage numbers higher than 1 for detail 1A and 1C when the fatigue verification is executed conform ROK version 2.0. It is recommended that this bridge will be carefully inspected during its lifetime as a possibility of cracking occurs. Additionally, it is expected that damage numbers higher than 1 occur in more bridges according to the fatigue verification of ROK version 2.0 [2]. It is suggested to recalculate bridges designed with ROK version 1.4 to check this.

- The Dutch Department of Waterways and Public Works (Rijkswaterstaat) aims to replace the current labor-intensive fatigue calculation method with a table that outlines the dimensions of OSDs for various traffic categories and commonly used forms of occurrence [2]. Further development and expansion of the parametric OSD model could support this goal by generating extensive data on different bridges

Discussion

This chapter evaluates the research done, addressing the assumptions, limitations and research and practical applications. In the first section the important assumptions in this thesis are discussed. The second section incorporates the discussion on the limitations of this thesis; the scope, the parametric tool and the parameter sensitivity analysis. The last section addresses the importance of this study and how this study can be used for further research.

11.1. Discussion on Assumptions

Throughout this research, the ROK has been used as the Dutch regulatory standard. According to the ROK [2], fatigue damage numbers should be verified for all possible detail positions in the bridge. However, due to the extensive calculation time required for the parametric FE model combined with fatigue verification, this was not feasible. To identify logical detail locations in the deck, estimated assumptions were made regarding the longitudinal and transverse positions of details in the bridge. These assumptions were based on literature, structural knowledge, and the experience of assisting engineers.

Assumption of governing transverse location of detail 1C
The governing transverse positions of details 1A and 1C were assumed to be the trough closest to the assumed loading position, which occurs when a truck drives exactly in the middle of the road. Chapter 9 confirmed that this assumption holds true for detail 1A. However, for detail 1C, the assumption does not hold, as the trough leg closest to the main girder at the considered trough was found to be governing.

It is noteworthy that the damage numbers obtained from placing the loads exactly where the trucks are expected (see Table 9.2) are still below 0.76. This is the damage value found for detail 1C at the assumed position (position 2 in Figure 9.2) when placing the load distribution in the middle of the trough to obtain maximum damage at this position. Therefore, if the assumption that all trucks drive in the middle of the road holds, the obtained damage number of 0.76 remains conservative. However, this assumption is impractical in real-world scenarios, and it cannot be validated whether this damage number is truly conservative. The method of the ROK [2] to account for all troughs is considered very conservative when no changes are made to the layout of the driving lanes on the bridge.

It is anticipated that the sensitivity study would largely produce similar results regarding the influence of the incorporated parameters on detail 1C, even if the investigated trough leg for the PSA were shifted one leg to the right, which is proved to be the governing trough leg. Although the fitted lines would be quantitatively be different, similar types of fit or explanations regarding the mechanical schemes would be obtained, additionally, similar conclusions about the influence of traffic types or degree of parameter interaction are expected.

Assumption of longitudinal loading position detail 1C
The longitudinal location of detail 1C is at the crossbeam. Due to the symmetry along the length of the bridge, only two crossbeams should be considered. In the generalization process described in section 6.1, the intersection of the end-crossbeam, troughs, and deckplate has also been simplified. To identify relevant detail locations for the PSA, the middle crossbeams are investigated. It should be noted that while the longitudinal detail can still be calculated at the first or last crossbeam, its applicability to real-world scenarios may be questionable

Assumption of loading distributions
The assumption of the loading distributions are validated for the benchmark model. This validation is too rash for the full domain and a more comprehensive validation could be done. It is however only for very few cases assumed that the a different loading distribution could be governing. One of the few cases is for the influence of the trough top width on detail 1A, as the lower end of this domain the distribution between two troughs is expected to be governing. However, it can also be noted that these trough top widths are usually not found in reality, therefore this assumptions is considered valid.

Assumption of automated welds
The assumption was made that automated welds were included in the design whenever possible, enhancing the detail categories of 2A and 2B. However, the damage numbers for these details were so small compared to those of 1A and 1C in the benchmark that this assumption does not affect the results. If using this framework for a more in-depth analysis of more details like 2A or 2B, this assumption should not be included in the parametric framework as it is not necessarily standard to include automated welds.

11.2. Discussion on Limitations

This sections discusses the limitations of this research, exploring constraints such as model scope, computational restrictions, and simplifications. This evaluation aims to clarify the boundaries of the research and the potential impacts on its findings.

Scope
The parametric FE tool made and the parameter sensitivity analysis executed is limited by the scope of this research. This research focuses on directly-ridden details of orthotropic steel decks with continuous trapezoidal troughs without cut-outs, additionally with an thin epoxy layer instead of an asphalt layer. This implies that the conclusions do not apply to different bridge types.

Parametric tool
The parametric tool created initiates an XML file and connects with the FEM software SCIA Engineer. The FEM analysis and the transfer back into the XML file causes the model to have a fairly long computational time of approximately 45 minutes for 1 detail. This limits the optimization possibilities of the model. With the current running time, only manual optimizations can be done, as optimisation algorithms often take many runs and this becomes infeasible. Another limitation is that the parametric tool can only incorporate the 7 directly-ridden details discussed in this study. It can be noted that all parameters in the OSD can be adjusted, thus a more in-depth parameter sensitivity analysis could be executed for other parameters in the future. Another limitation of the tool is that the design is restricted to have two main girders at the sides, and supports on those main girders.

Parametric Sensitivity Analysis
The Parameter sensitivity analysis is only executed with a one-at-a-time analysis. This means that no interaction between parameters can be observed, while this parameter interaction is definitely present. A small check of the parameter interaction is executed to show the interaction is there, this however does not indicate something about the way the important parameters interact. Additionally, this does not capture the complexity of the influence of parameters on the bridge.

11.3. Importance and usability

This thesis aimed to enhance the understanding of parameter influence in the Orthotropic steel Deck, to contribute to the greater goal of assessing possibility for more efficient OSDs. The study offers valuable insights into how key parameters influence the fatigue life and damage of the bridge regarding the toe crack at the intersection of the deckplate and trough and the root crack at the intersection of the deckplate, trough and crossbeam. The study could additionally be expanded to further enhance the understanding of more parameters across various details.

Furthermore this thesis shows insights into how fatigue verifications can be automated without compromising much on the accuracy. The tool can be used by multiple parties, the framework of this tool shows much potential in the practical aspect, it can be expanded, used and optimised even further to allow for many other things, like possibility of incorporating more details, optimizing a design or possibility of making a

preliminary design. This could be helpful for design teams or advisors. Also researchers could make use of it to further study optimizations in the OSD, and give recommendations to achieve more efficient material use in many of the OSD bridges in the world.

References

[1] Canam-Bridges. "Orthotropic Steel Deck". In: (2024). URL: https://www.canambridges.com/products/orthotropic-steel-deck/.

[2] Rijkswaterstaat. "Richtlijnen Ontwerp Kunstwerken". In: 2600 GB, Delft, Dec. 2021. URL: https://www.rijkswaterstaat.nl/zakelijk/werken-aan-infrastructuur/bouwrichtlijnen-infrastructuur/kunstwerken.

[3] Robert Connor et al. "Manual for Design, Construction, and Maintenance of Orthotropic Steel Deck Bridges". In: (Feb. 2012).

[4] Menke Henderikus Kolstein. "Fatigue Classification of Welded Joints in Orthotropic Steel Bridge Decks". In: (Mar. 2007).

[5] Francesco M Russo et al. "Design and evaluation of steel bridges for fatigue and fracture – reference manual". In: (2016).

[6] Mattia Mairone et al. "Fatigue performance analysis of an existing orthotropic steel deck (OSD) bridge". In: Infrastructures 7.10 (2022), p. 135.

[7] Fbp de Jong. "OVERVIEW FATIGUE PHENOMENON IN ORTHOTROPIC BRIDGE DECKS IN THE NETHERLANDS". In: 2004. URL: https://api.semanticscholar.org/CorpusID:110577750.

[8] Wouter De Corte. "Parametric study of floorbeam cutouts for orthotropic bridge decks to determine shape factors". In: Bridge Structures 5.2-3 (2009), pp. 75–85.

[9] Abdullah Fettahoglu. "Effect of cross-beam on stresses revealed in orthotropic steel bridges". In: Steel and Composite Structures, An International Journal 18.1 (2015), pp. 149–163.

[10] Ye Xia et al. "Optimization of design details in orthotropic steel decks subjected to static and fatigue loads". In: Transportation research record 2331.1 (2013), pp. 14–23.

[11] H.W. van der Laan. "Structural Optimization of Stiffened Plates - Application on a Orthotropic Steel Bridge Deck". In: (2021). URL: https://repository.tudelft.nl/islandora/search/%20?collection=research.

[12] Wei Huang et al. "Nonlinear Optimization of Orthotropic Steel Deck System Based on Response Surface Methodology". In: Research 2020 (2020). DOI: 10.34133/2020/1303672. eprint: https://spj.science.org/doi/pdf/10.34133/2020/1303672. URL: https://spj.science.org/doi/abs/10.34133/2020/1303672.

[13] Mads Baandrup et al. "Parametric optimization of orthotropic girders in a cable-supported bridge". en. In: J. Bridge Eng. 24.12 (Dec. 2019), p. 04019118.

[14] Coen Stellinga. "Deciding where to verify the fatigue resistance of an orthotropic steel bridge deck". In: (2023). URL: https://repository.tudelft.nl/islandora/search/%20?collection=research.

[15] European Committee for Standardization. "NEN-EN 1993-1-9+C2(nl) - Eurocode 3: Ontwerp en berekening van staalconstructies - Deel 1 - 9: Vermoeiing". In: NEN Connect (Sept. 2012).

[16] H. De Backer. "Innovative Bridge Design Handbook". In: (2016).

[17] European Steel Design Education Programme. "Structural system: bridges". In: 2018. URL: http://fgg-web.fgg.uni-lj.si/~/pmoze/ESDEP/master/wg15b/l0300.htm.

[18] Man-Chung Tang. "A new concept of orthotropic steel bridge deck". In: vol. 7. 7-8. Taylor & Francis, 2011, pp. 587–595. DOI: 10.1080/15732479.2010.496996. eprint: https://doi.org/10.1080/15732479.2010.496996. URL: https://doi.org/10.1080/15732479.2010.496996.
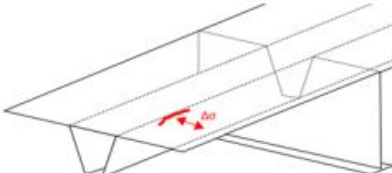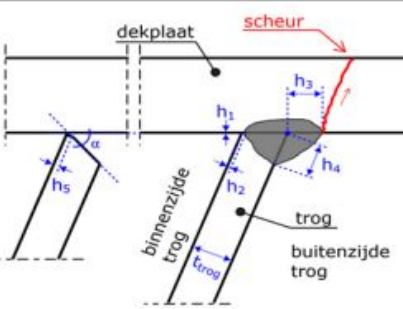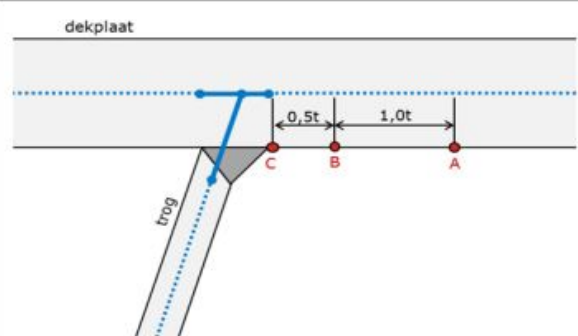
[19] Roman Wolchuk. "Steel Orthotropic Decks: Developments in the 1990s". In: vol. 1688. 1. 1999, pp. 30–37. DOI: `10.3141/1688-04`. URL: `https://doi.org/10.3141/1688-04`.

[20] Roman Wolchuk. "Lessons from Weld Cracks in Orthotropic Decks on Three European Bridges". In: Journal of Structural Engineering 116.1 (1990), pp. 75–84. DOI: `10.1061/(ASCE)0733-9445(1990)116:1(75)`. eprint: `https://ascelibrary.org/doi/pdf/10.1061/%28ASCE%290733-9445%281990%29116%3A1%2875%29`. URL: `https://ascelibrary.org/doi/abs/10.1061/%28ASCE%290733-9445%281990%29116%3A1%2875%29`.

[21] Justin M Dahlberg et al. Guide for Orthotropic Steel Deck Level 1 Design. Tech. rep. United States. Federal Highway Administration. Office of Bridge Technology, 2022.

[22] Sufian H. Natsheh et al. "Built-Up Closed-Rib Steel Orthotropic Bridge Decks". In: CivilEng 3.4 (2022), pp. 960–978. DOI: `10.3390/civileng3040054`. URL: `https://www.mdpi.com/2673-4109/3/4/54`.

[23] René Tinawi et al. "Orthotropic bridge decks with closed stiffeners — Analysis and behaviour". In: Computers & Structures 7.6 (1977), pp. 683–699. DOI: `https://doi.org/10.1016/0045-7949(77)90023-2`. URL: `https://www.sciencedirect.com/science/article/pii/0045794977900232`.

[24] Eric J. Mittemeijer. "Fundamentals of Materials Science". In: (Jan. 2021). DOI: `10.1007/978-3-030-60055-6`.

[25] Jaap Schijve. "Fatigue of structures and materials". In: (Oct. 2008).

[26] R.E. Smallman et al. "Modern physical metallurgy". In: (Sept. 2013).

[27] "NEN1993-1-9: Eurocode 3: Design of steel structures, part 1-9 fatigue". In: (2012).

[28] Correia José A F O. et al. "Mechanical fatigue of metals: Experimental and simulation perspectives". In: (2019).

[29] Christoffer Wesley et al. "Fatigue Analysis for Orthotropic Steel Deck Bridges". In: (2015).

[30] Boris Fuštar et al. "Review of Fatigue Assessment Methods for Welded Steel Structures". In: Advances in Civil Engineering 2018 (Apr. 2018), pp. 1–16. DOI: `10.1155/2018/3597356`.

[31] "prNEN-EN 1993-1-9 - Eurocode 3: Ontwerp en berekening van staalconstructies - Deel 1-9: Vermoeiing". In: NEN Connect (Mar. 2023).

[32] "NEN-EN 1991-2+C1/NB". In: NEN Connect (Nov. 2019).

[33] "NEN 8701+A1". In: NEN Connect (Aug. 2020).

[34] Shengquan Zou et al. "Effect of stress reversals on fatigue life evaluation of OSD considering the transverse distribution of vehicle loads". In: Engineering Structures 265 (2022), p. 114400. DOI: `https://doi.org/10.1016/j.engstruct.2022.114400`. URL: `https://www.sciencedirect.com/science/article/pii/S0141029622005144`.

[35] European Committee for Standardization. "prTS 1993-1-901 Fatigue design of orthotropic bridge decks with the hot spot stress method (Final draft)". In: (2023).

[36] Jorrit Rodenburg et al. "Generic method of local thickening in shell element FEM models for orthotropic bridge decks". In: ce/papers 6 (Sept. 2023), pp. 2540–2545. DOI: `10.1002/cepa.2691`.

[37] Brian M. Kozy et al. "Proposed Revisions to AASHTO-LRFD Bridge Design Specifications for Orthotropic Steel Deck Bridges". In: Journal of Bridge Engineering 16.6 (2011), pp. 759–767. DOI: `10.1061/(ASCE)BE.1943-5592.0000214`. eprint: `https://ascelibrary.org/doi/pdf/10.1061/%28ASCE%29BE.1943-5592.0000214`. URL: `https://ascelibrary.org/doi/abs/10.1061/%28ASCE%29BE.1943-5592.0000214`.

[38] Sayantan Pandit. "Finite element modelling of open longitudinal stiffener to crossbeam connection in OSD bridges for hot-spot stress determination". In: (2020). URL: `https://repository.tudelft.nl/islandora/object/uuid:9a4fd919-b0d0-443d-a66b-f42a3fe73f10?collection=education`.

[39] D.J. van der Ende. "Finite element analysis of the closed stiffener to crossbeam connection in OSDs using the hot spot stress approach". In: (2020). URL: `https://repository.tudelft.nl/islandora/object/uuid:0d49d337-0772-4a1b-9c8d-b0ef77ab8e58?collection=education`.

[40] Mustafa Aygül et al. "Modelling and fatigue life assessment of orthotropic bridge deck details using FEM". In: International Journal of Fatigue 40 (2012), pp. 129–142. DOI: `https://doi.org/10.1016/j.ijfatigue.2011.12.015`. URL: `https://www.sciencedirect.com/science/article/pii/S0142112311003434`.

[41] Erkki Niemi et al. "Structural hot-spot stress approach to fatigue analysis of welded components". In: IIW doc 13 (2018).

[42] Boris Fuštar et al. "High-Frequency mechanical impact treatment of welded joints". In: Gradevinar 72/2020 (July 2020). DOI: `10.14256/JCE.2822.2019`.

[43] Petra Beld. "Improvements for the prediction of the fatigue life of the deck plate in orthotropic steel decks: A design optimization study". In: (2019). URL: `https://repository.tudelft.nl/islandora/search/%20?collection=research`.

[44] Mikkel Pedersen. "Introduction to Metal Fatigue - Concepts and Engineering Approaches". In: (Dec. 2018). DOI: `10.13140/RG.2.2.25216.28163`.

[45] A. F. Hobbacher. "Recommendations for Fatigue Design of Welded Joints and Components". In: (Dec. 2015). DOI: `10.1007/978-3-319-23757-2_7`.

[46] Heng Fang et al. "Structural optimization of rib-to-crossbeam joint in orthotropic steel decks". In: Engineering Structures 248 (2021), p. 113208.

[47] Abdullah Fettahoglu. "Optimizing rib width to height and rib spacing to deck plate thickness ratios in orthotropic decks". In: Cogent Engineering 3.1 (2016), p. 1154703.

[48] Google maps. "Goereese bridge location". In: (2024). URL: `https://www.google.com/maps/@51.8239384,4.0374343,14.75z?entry=ttu`.

[49] Google maps. "Goereese bridge in use". In: (2024). URL: `https://www.google.com/maps/@51.8233102,4.0403038,3a,75y,315.33h,83.84t/data=!3m6!1e1!3m4!1sKc01hqasyWyW1BWlSWGX6A!2e0!7i16384!8i8192?entry=ttu`.

[50] Water- en Wegenbouw en de Verkeerstechniek Centrum voor Regelgeving en Onderzoek in de Grond-. Wegontwerp bubeko met HWOwegontwerp 2013 - regionale stroomwegen. Tech. rep. 2013. URL: `https://kennisbank.crow.nl/Kennismodule#14130`.

[51] Koninklijk Nederlands Normalisatie-instituut. "NEN-EN 1993-1-1+C2+A1". In: NEN Connect (Dec. 2016).

[52] SCIA Engineer. "Parameters of FE mesh". In: (2024). URL: `https://help.scia.net/22.0/en/index.htm#analysis/mesh_setup/mesh_setup.htm%3FTocPath%3DAnalysis%7CGenerating%2520the%2520FE%2520mesh%7C_____1`.

[53] Andrea Saltelli et al. "Global sensitivity analysis: the primer". In: (2008).

[54] Lorenzo Mentaschi et al. "Why NRMSE is not completely reliable for forecast/hindcast model test performances". In: Geophysical Research Abstracts. Vol. 15. 2013.

[55] Saskia A. Otto. How to normalize the RMSE. 2019. URL: `https://www.marinedatascience.co/blog/2019/01/07/normalizing-the-rmse/`.

[56] "NEN-EN 1993-2+C1/NB". In: NEN Connect (Mar. 2015).

[57] Antea Group nl. Rapport Goereese brug. Tech. rep. 2011.

Part IV

Appendix

A

Considered details

Detail-nummer	Beschrijving	Detail-categorie	N_D	N_L	m_1	m_2	Detailcategorie specifieke eisen
(1a)	Dekplaatscheur vanuit de lasteen van de trog-dekplaatlas in het veld tussen de dwarsdragers.	125	5	100	3	5	$t_{dekplaat} \geq 18mm$
		125	5	100	3	5	$15mm \leq t_{dekplaat} \leq 17mm$
		140	5	100	3	5	$10mm \leq t_{dekplaat} \leq 14mm$

Algemene eisen m.b.t. uitvoering	
Spleet	$h_1 = 0mm$ $h_1 < 0,5mm$ (<10% van de lengte)
MDF[1]	$h_{2,gemiddeld} \leq 1,0$ mm $h_{2,maximaal} \leq 1,5$ mm
Lasuitbouw[1]	$h_3 = t_{trog}$ +/- 1mm $h_4 = t_{trog}$ +/- 1mm

Lasgeometrie[1]
De las moet vloeiend aanliggen aan het dek en het trogbeen.
Doorslag van de las aan de binnenzijde van de trog is niet toegestaan.

Voorbewerking
Trogbeen afschuinen tot een lasopeningshoek van 50° tot 60°. h_5=1mm (h_5 is het niet afgeschuinde deel van het trogdeel).

NDO
Visueel: 100 %; MT: alle lasaanzetten + 10 % van de laslengte als steekproef te kiezen op basis van de visuele inspectie.

Spanningsanalyse:

Lineaire extrapolatie vanuit A & B naar C. Mesh-afmeting $\leq 0,5t_{dekplaat}$. Extrapolatie vanaf de elementknopen.
Toetsing dient uitgevoerd te worden over de gehele lengte van de trog-dekplaatlas met uitzondering van de eerste 150mm vanaf een dwarsdrager.

Opmerkingen

[1] De MDF (maximale doorlasfout), lasuitbouw en lasgeometrie dienen geverifieerd te worden middels productieproeven conform ROK par. 7.20.

Detail-nummer	Beschrijving	Detail-categorie	N_D	N_L	m_1	m_2	Detailcategorie specifieke eisen
(1c)	Dekplaatscheur vanuit de laswortel van de trog-dekplaatlas ter plaatse van een dwarsdrager bij doorgestoken troggen.	200	20	300	3	5	$t_{dekplaat} \geq 18mm$
		188	25	200	3	5	$15mm \leq t_{dekplaat} \leq 17mm$
		167	30	100	3	5	$10mm \leq t_{dekplaat} \leq 14mm$

Algemene eisen m.b.t. uitvoering	
Spleet	$h_1 = 0mm$
	$h_1 < 0{,}5mm$ (<10% van de lengte)
MDF[1]	$h_{2,gemiddeld} \leq 1{,}0$ mm
	$h_{2,maximaal} \leq 1{,}5$ mm
Lasuitbouw[1]	$h_3 = t_{trog} +/- 1mm$
	$h_4 = t_{trog} +/- 1mm$

Lasgeometrie[1]
De las moet vloeiend aanliggen aan het dek en het trogbeen.
Doorslag van de las aan de binnenzijde van de trog is niet toegestaan.
Voorbewerking
Trogbeen afschuinen tot een lasopeningshoek van 50° tot 60°. $h_5 = 1mm$ (h_5 is het niet afgeschuinde deel van het trogdeel).
NDO
Visueel: 100 %; MT: alle lasaanzetten + 10 % van de laslengte als steekproef te kiezen op basis van de visuele inspectie.

Spanningsanalyse:

Lineaire extrapolatie vanuit A & B naar C. Mesh-afmeting $\leq 0{,}5t_{dekplaat}$, maar tussen knoop B en C dienen minimaal 2 elementen ($0{,}25t_{dekplaat}$) toegepast te worden. Extrapolatie is van de elementknopen in lijn met het lijf van de dwarsdrager/kamplaat (haaks op de trogwand). Indien hoek α kleiner is dan 80° of groter dan 100° dient de spanning bepaald te worden zowel loodrecht op de trog als parallel aan het lijf van de dwarsdrager/kamplaat (zie onderstaand Figuur). Spanningsrichting dient altijd gelijk te zijn aan de extrapolatierichting.

Opmerkingen
Bij dit detail horen aangepaste vermoeiingscurves. De cut-off limit ligt voor alle drie de categoriën ongeveer even hoog, echter ontwikkelen de dikkere platen minder snel schade dan de dunnere platen. Dit komt omdat het punt van schade (D=1) is afgestemd op het doorscheuren van de plaat. Voorbeeld, voor DC=200: $N_c=2miljoen$; $N_D=20miljoen$ (m=3); $N_L=300miljoen$ (m=5). Ter controle: met $\gamma_{Mf}=1{,}15$ ligt het afkaplimiet bij circa $0{,}235\sigma_C = 47$ MPa..

[1] De MDF (maximale doorlasfout), lasuitbouw en lasgeometrie dienen geverifieerd te worden middels productieproeven conform ROK par. 7.20.

Detail-nummer	Beschrijving	Detail-categorie	N_D	N_L	m_1	m_2	Detailcategorie specifieke eisen
(2a)	Las tussen het verstijverbeen en de dekplaat op een locatie tussen de dwarsdragers. Scheur in de trog geïnitieerd vanuit de lasteen.	180	5	100	3	5	automaatlas
		160	5	100	3	5	handlas (bij passtuk)

Algemene eisen m.b.t. uitvoering	
Spleet	$h_1 = 0$mm $h_1 < 0,5$mm (<10% van de lengte)
MDF[1]	$h_{2,\text{gemiddeld}} \leq 1,0$ mm $h_{2,\text{maximaal}} \leq 1,5$ mm
Lasuitbouw[1]	$h_3 = t_{\text{trog}} +/- 1$mm $h_4 = t_{\text{trog}} +/- 1$mm

Lasgeometrie[1]
De las moet vloeiend aanliggen aan het dek en het trogbeen.
Doorslag van de las aan de binnenzijde van de trog is niet toegestaan.

Voorbewerking
Trogbeen afschuinen tot een lasopeningshoek van 50° tot 60°. h_5=1mm (h_5 is het niet afgeschuinde deel van het trogdeel).

NDO
Visueel: 100 %; MT: alle lasaanzetten + 10 % van de laslengte als steekproef te kiezen op basis van de visuele inspectie.

Spanningsanalyse:

Lineaire extrapolatie vanuit A & B naar C. Mesh-afmeting ≤ 10mm. Extrapolatie vanaf elementknopen. Toetsing dient uitgevoerd te worden over de gehele lengte van de trog-dekplaatlas met uitzondering van de eerste 150mm vanaf een dwarsdrager. De hoogste spanning wordt verwacht in het midden van de overspanning.

Opmerkingen

De afstand van de extrapolatiepunten is vergroot om met een grote mesh te kunnen rekenen. Door de min of meer volledig lineaire spanningsopbouw richting de las heeft dit geen invloed op de resultaten. Als alternatief kan er bij gebruik van schaalmodellen de spanning direct afgelezen worden in C, voor detail 2b blijft extrapolatie wel nodig.

[1] De MDF (maximale doorlasfout), lasuitbouw en lasgeometrie dienen geverifieerd te worden middels productieproeven conform ROK par. 7.20.

Detail-nummer	Beschrijving	Detail-categorie	N_D	N_L	m_1	m_2	Detailcategorie specifieke eisen
(2b)	Las tussen het verstijverbeen en de dekplaat op een locatie tussen de dwarsdragers.	125	10	100	3	5	automaatlas
		112	10	100	3	5	handlas (bij passtuk)
	Scheur in de las geïnitieerd vanuit de laswortel	**Algemene eisen m.b.t. uitvoering**					

Spleet	$h_1 = 0$mm
	$h_1 < 0,5$mm (<10% van de lengte)
MDF[1]	$h_{2,gemiddeld} \leq 1,0$ mm
	$h_{2,maximaal} \leq 1,5$ mm
Lasuitbouw[1]	$h_3 = t_{trog}$ +/- 1mm
	$h_4 = t_{trog}$ +/- 1mm

Lasgeometrie[1]
De las moet vloeiend aanliggen aan het dek en het trogbeen. Doorslag van de las aan de binnenzijde van de trog is niet toegestaan.

Voorbewerking
Trogbeen afschuinen tot een lasopeningshoek van 50° tot 60°. h_5=1mm (h_5 is het niet afgeschuinde deel van het trogdeel).

NDO
Visueel: 100 %; MT: alle lasaanzetten + 10 % van de laslengte als steekproef te kiezen op basis van de visuele inspectie.

Spanningsanalyse:

De spanningswisseling dient bepaald te worden op basis van de normaalkracht en het moment in de schaalelementen loodrecht op de las. Beide dienen direct t.p.v. punt C te worden afgelezen, indien er getwijfeld wordt aan de resulaten kan er geëxtrapoleerd worden vanuit punt A en B. De spanningswisseling ter plaatse van de laswortel dient vervolgens bepaald te worden op basis van de keeldoorsnede (a) van de las gemeten loodrecht op het lasoppervlak (dit hoeft niet de kleinste keeldoorsnede te zijn). De excentriciteit t.g.v. van de keeldoorsnede t.o.v. hartlijn trog dient meegenomen te worden bij het bepalen van de spanningen t.p.v. de laswortel. Bij de toetsing dient MDF=1,5mm aangehouden te worden i.c.m. een lasuitbouw (h_3 en h_4) gelijk aan t_{trog}. Spanning in de las bepalen volgens onderstaande formule:

$$\sigma_{w,root} = \frac{N_{trog}}{a} + \frac{6}{a^2}\left(M_{trog} + N_{trog} \cdot e\right)$$

Opmerkingen
De afstand van de extrapolatiepunten is vergroot om met een grote mesh te kunnen rekenen. Door de min of meer volledig lineaire spanningsopbouw richting de las heeft dit geen invloed op de resultaten.

[1] De MDF (maximale doorlasfout), lasuitbouw en lasgeometrie dienen geverifieerd te worden middels productieproeven conform ROK par. 7.20.

Detail-nummer	Beschrijving	Detail-categorie	N_D	N_L	m_1	m_2	Detailcategorie specifieke eisen
(5)	Scheur in de dekplaat vanuit de teen van de las tussen de dekplaat en de kamplaat/dwarsdragerlijf	112	5	100	3	5	

Algemene eisen m.b.t. uitvoering

Lasgeometrie

De las moet vloeiend aanliggen aan het lijf van de dwardrager/kamplaat en dek dekplaat.

Hoeklassen

Lasuitbouw	$40° \leq \alpha \leq 50°$
Spleet	$h_1 \leq 1,0mm$
Keeldoorsnede	$a \geq 5mm$ en $a \geq 0,4t_{kamplaat}$
	(lasafmeting te vergroten met spleet h_1)

Stompe las (k-naad)

Lasuitbouw	$30° \leq \beta \leq 40°$
	$50° \leq \gamma \leq 60°$

Voorbewerking

Dwarsdrager/kamplaat afschuinen tot een lasopeningshoek (α) van 45° tot 50°.

Spanningsanalyse:

Lineaire extrapolatie vanuit A & B naar C. Mesh-afmeting $\leq 0,5t_{dekplaat}$, maar tussen knoop B en C dienen minimaal 2 elementen ($0,25t_{dekplaat}$) toegepast te worden. Extrapolatie loodrecht op de las.

Opmerkingen

Met $t_{kamplaat}$ kan zowel de plaatdikte van het lijf van de dwarsdrager als de kamplaat bedoeld worden.

Detail-nummer	Beschrijving	Detail-categorie	N_D	N_L	m_1	m_2	Detailcategorie specifieke eisen
6a	Scheur in de kamplaat/dwarsdrager vanuit de teen van de las tussen de kamplaat/dwarsdragerlijf en de dekplaat	100	5	100	3	5	volledig doorgelast (k-naad)
		90	5	100	3	5	hoeklassen

Algemene eisen m.b.t. uitvoering

Lasgeometrie

De las moet vloeiend aanliggen aan het lijf van de dwardrager/kamplaat en dek dekplaat.

Hoeklassen

Lasuitbouw	$40° \leq \alpha \leq 50°$
Spleet	$h_1 \leq 1,0mm$
Keeldoorsnede	$a \geq 5mm$ en $a \geq 0,4t_{kamplaat}$
	(lasafmeting te vergroten met spleet h_1)

Stompe las (k-naad)

Lasuitbouw	$30° \leq \beta \leq 40°$
	$50° \leq \gamma \leq 60°$

Voorbewerking

Dwarsdrager/kamplaat afschuinen tot een lasopeningshoek (α) van 45° tot 50°.

Spanningsanalyse:

Lineaire extrapolatie vanuit A & B naar C. Mesh-afmeting $\leq 0,5t_{kamplaat}$, maar tussen B en C dienen minimaal twee elementen aanwezig te zijn (0,25t groot). Extrapolatie vanuit de elementknopen.

Opmerkingen

Met $t_{kamplaat}$ kan zowel de plaatdikte van het lijf van de dwarsdrager als de kamplaat bedoeld worden.

Detail-nummer	Beschrijving	Detail-categorie	N_D	N_L	m_1	m_2	Detailcategorie specifieke eisen
(6b)	Scheur in de las vanuit de wortel van de las tussen de dekplaat en de kamplaat/dwarsdragerlijf. Enkel voor gebruik met dubbelzijdige en symmetrische hoeklassen.	40	10	100	3	5	

Algemene eisen m.b.t. uitvoering

Lasgeometrie

De las moet vloeiend aanliggen aan het lijf van de dwardrager/kamplaat en dek dekplaat.

Hoeklassen

Lasuitbouw	$40° \leq \alpha \leq 50°$
Vooropening	$h_1 \leq 1{,}0mm$
Keeldoorsnede	$a \geq 5mm$ en $a \geq 0{,}4t_{kamplaat}$ (lasafmeting te vergroten met spleet h_1)

Spanningsanalyse:

De krachten en momenten kunnen direct t.p.v. punt C worden afgelezen, indien er getwijfeld wordt aan de resulaten kan er geëxtrapoleerd worden vanuit punt A en B. Mesh-afmeting afhankelijk van aanwezige spanningsgradiënten (circa 0,5t tot 1t). De lasspanning in de las dient als volgt bepaald te worden:

$$\sigma_w = \sigma_{w,N} + \sigma_{w,M}$$

$$\sigma_{w,N} = \frac{N}{2*a}$$

$$\sigma_{w,M} = \frac{M}{a(a+t)}$$

Opmerkingen

De detailcategorie die hoort bij dit detail is 36*, deze is gelijk aan 40 met een aangepaste vermoeiingscurve zoals hierboven is aangegeven. Met $t_{kamplaat}$ kan zowel de plaatdikte van het lijf van de dwarsdrager als de kamplaat bedoeld worden.

B

Mesh validation

The incorporation of the use of symmetry requires an elastic mesh, which is considered more accurate as this meshing algorithm helps reduce meshes with small angles [52]. However, an additional check is done for detail 1C. The benchmark model is used to compare the elastic mesh with the initial mesh used in the mesh convergence study. The most damaging influence line, wheel A exactly on the trough middle, is compared between the models, see Figure B.1.

Figure B.1: Full model without symmetry vs symmetry model (with elastic mesh)

The lines are the same with the exception at the position of the detail 1C. The model with the elastic mesh gives a stress of -7.11 MPa, and the model with the non-elastic mesh -7.32 MPa, obtaining a difference of about 2.4%. To verify accuracy, a model with really fine mesh is tested with a load at the position of the stress peak. This model is illustrated in Figure B.2

(a) Global mesh

(b) Local mesh refinement
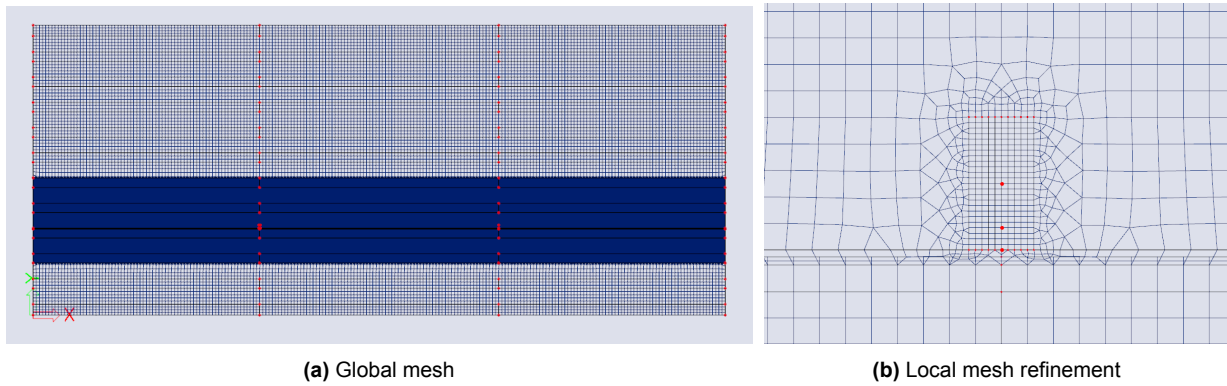
Figure B.2: Global and local mesh for detailed check

This really fine mesh produces a stress in point A of -2.0548 MPa, in point B of -5.4297 and the hot spot stress is then -7.117 MPa, which is considerably lower than the stress of the model with the non-elastic mesh, and slightly higher than the model with the elastic mesh. The assumption is made that this fine mesh is most accurate and close to real values. Therefore, it seems that the model with an elastic mesh is slightly more accurate, although less conservative. It should be noted that this check of one load placement can not be conclusive, but it does increase the certainty of the assumption that the elastic mesh is generally more accurate, especially at stress peaks.

C

Results stiff and flexible design

In this appendix the damage numbers of the designs at the domain ends are displayed. Firstly, the positions are indicated in Figures C.1, C.2 and C.3, after which the damage numbers of the flexible design and the stiff design are given.
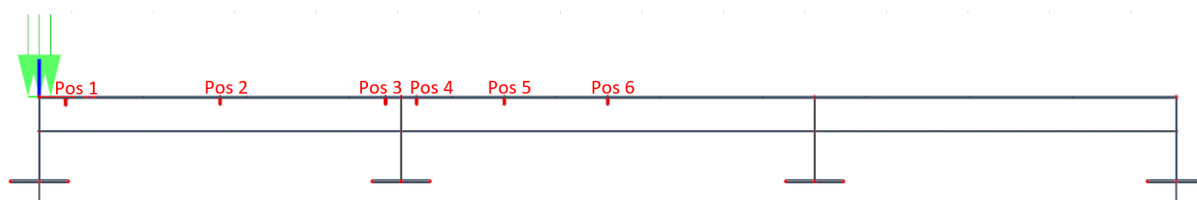
Figure C.1: Longitudinal locations in the deck of detail 1A, 2A and 2B. Transversely, the detail is placed closest to the load.
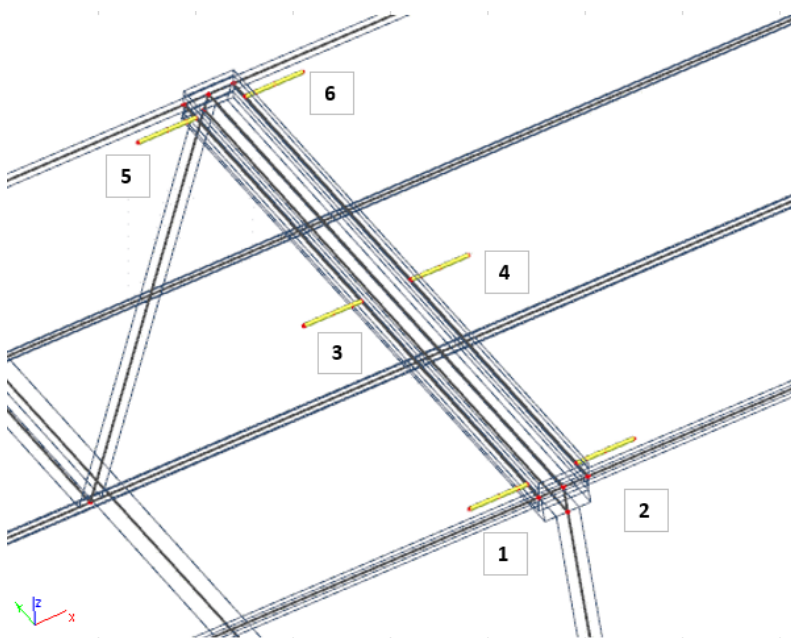
Figure C.2: Positions of detail 5, the details are located at the first crossbeam, and the details are placed closest to the load.
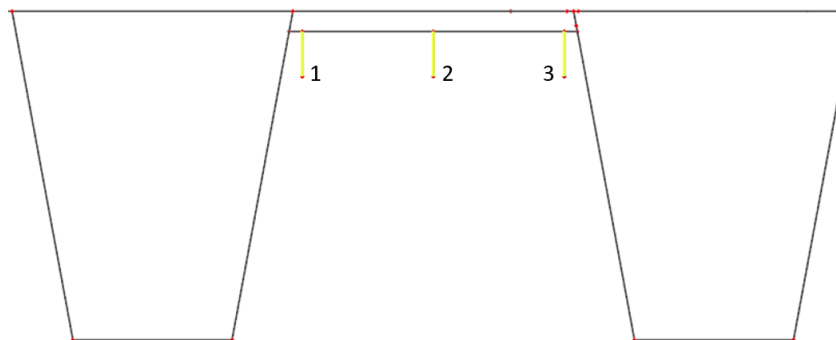
Figure C.3: Positions of detail 6A and 6B, the details are located at the first crossbeam, and the details are placed closest to the load.

C.1. Flexible design

Table C.1: Damage numbers of detail 1A on the flexible design.

Detail 1A		Transversal distribution		
		Between troughs	Above trough leg	Trough middle
Position	1 *	53,5	108,1	68,8
	2	71,6	132,1	76,5
	3	62,0	134,0	96,0
	4	55,6	115,7	81,9
	5	87,4	166,7	105,7
	6	95,7	173,5	101,9

Table C.2: Damage numbers of detail 1C on the flexible design.

Detail 1C	Transversal distribution		
Position	between troughs	above trough leg	trough middle
at crossbeam 2	119,5	344,3	551,6

Table C.3: Damage numbers of detail 2A on the flexible design.

Detail 2A		Transversal distribution		
		Between troughs	Above trough leg	Trough middle
Position	1 *	4.4	4.0	3.4
	2	9.7	7.2	6.0
	3	7.8	6.1	4.6
	4	9.9	6.9	4.7
	5	13.7	9.8	7.7
	6	12.8	9.2	7.8

Table C.4: Damage numbers of detail 2B on the flexible design.

Detail 2B		Transversal distribution		
		between troughs	above trough leg	trough middle
Position	1*	1,6	2,6	4,1
	2	89,2	81,0	114,1
	3	89,2	75,3	76,1
	4	101,0	84,1	83,9
	5	169,5	146,8	172,4
	6	121,5	110,7	148,3

Table C.5: Damage numbers of detail 5 on the flexible design.

Detail 5		Transversal distribution		
		between troughs	above trough leg	trough middle
Position	1	0,00	0,00	0,00
	2	0,00	0,00	0,00
	3	187,0	101,8	32,3
	4	201,7	108,8	32,6
	5	0,03	0,00	0,00
	6	0,01	0,00	0,00

Table C.6: Damage numbers of detail 6A on the flexible design.

Detail 6A		stress type	Transversal distribution		
			between troughs	above trough leg	trough middle
Position	1	s-	0,11	0,39	0,22
		s+	0,03	0,10	0,03
	2	s-	382,68	193,37	38,30
		s+	378,81	189,19	37,05
	3	s-	0,12	0,01	0.0
		s+	0,20	0,02	0.0

Table C.7: Damage numbers of detail 6B on the flexible design. Please note that for detail 6B, the stress on both the left and right sides of the crossbeam web should be considered. However, the parametric model only provides the desired highest stress damage number.

Detail 6B		Transversal distribution		
		between troughs	above trough leg	trough middle
Position	1	9,17	19,88	22,59
	2	149,42	80,80	17,23
	3	14,12	2,04	0,00

C.2. Stiff design

Table C.8: Damage numbers without cutoff limit for detail 1A of the stiff design.

Detail 1A		Transversal distribution		
		between troughs	above trough leg	trough middle
Position	1	6,01E-07	1,19E-07	1,59E-07
	2	2,90E-06	2,57E-06	1,64E-06
	3	6,30E-07	1,32E-07	1,65E-07
	4	6,35E-07	1,28E-07	1,69E-07
	5	2,04E-06	1,13E-06	8,82E-07
	6	2,38E-06	2,01E-06	1,28E-06

Table C.9: Damage numbers without cutoff limit for detail 1C of the stiff design.

Detail 1C	Transversal distribution		
Position	between troughs	above trough leg	trough middle
at crossbeam 2	4,02E-03	6,03E-03	8,27E-03

Table C.10: Damage numbers without cutoff limit for detail 2A of the stiff design.

Detail 2A		Transversal distribution		
		between troughs	above trough leg	trough middle
Position	1	2,80E-05	2,05E-05	1,86E-05
	2	2,59E-04	2,25E-04	1,87E-04
	3	6,09E-05	6,25E-05	4,70E-05
	4	6,90E-05	7,00E-05	5,04E-05
	5	2,93E-04	2,43E-04	1,73E-04
	6	3,36E-04	2,85E-04	2,15E-04

Table C.11: Damage numbers without cutoff limit for detail 2B of the stiff design.

Detail 2B		Transversal distribution		
		between troughs	above trough leg	trough middle
Position	1	1,33E-03	1,67E-03	2,07E-03
	2	2,71E-04	3,55E-04	3,75E-04
	3	3,27E-04	4,38E-04	5,37E-04
	4	4,15E-04	5,55E-04	6,77E-04
	5	5,44E-04	7,41E-04	7,90E-04
	6	3,35E-04	4,50E-04	4,82E-04

Table C.12: Damage numbers without cutoff limit for detail 5 of the stiff design.

Detail 5		Transversal distribution		
		between troughs	above trough leg	trough middle
Position	1	7,19E-05	8,52E-05	1,02E-04
	2	6,41E-05	7,39E-05	8,43E-05
	3	1,62E-05	1,50E-05	1,30E-05
	4	2,63E-05	2,60E-05	2,47E-05
	5	5,94E-06	5,64E-06	3,91E-06
	6	1,57E-05	1,58E-05	1,09E-05

Table C.13: Damage numbers without cutoff limit of detail 6A on the stiff design.

Detail 6A		stress type	Transversal distribution		
			between troughs	above trough leg	trough middle
Position	1	s-	3,49E-03	4,51E-03	5,15E-03
		s+	2,93E-03	3,90E-03	4,45E-03
	2	s-	5,49E-04	4,79E-04	3,09E-04
		s+	4,98E-04	4,31E-04	2,81E-04
	3	s-	2,42E-03	2,26E-03	2,26E-03
		s+	2,50E-03	2,43E-03	2,43E-03

Table C.14: Damage numbers without cutoff limit of detail 6B on the stiff design. Please note that for detail 6B, the stress on both the left and right sides of the crossbeam web should be considered. However, the parametric model only provides the desired highest stress damage number.

Detail 6B		Transversal distribution		
		between troughs	above trough leg	trough middle
Position	1	0,76	1,06	1,32
	2	0,03	0,03	0,02
	3	0,47	0,52	0,67

D

Damage numbers Benchmark model

In this annex the damage numbers of the benchmark model are presented. The locations of the details are in correspondence with Figures C.1, C.2 and C.3.

Table D.1: Damage numbers of detail 1A on the benchmark model.

Detail 1a		Transversal distribution		
		between troughs	above trough leg	trough middle
Position	1	0,17	0,38	0,11
	2	0,40	1,66	0,38
	3	0,15	0,65	0,11
	4	0,11	0,56	0,08
	5	0,34	1,34	0,30
	6	0,37	1,46	0,30

Table D.2: Damage numbers of detail 1C on the benchmark model.

Detail 1C	Transversal distribution		
Position	between troughs	above trough leg	trough middle
At crossbeam 2	0,09	0,38	0,75

Table D.3: Damage numbers of detail 2A on the benchmark model.

Detail 2A		Transversal distribution		
		between troughs	above trough leg	trough middle
Position	1	0,00	0,00	0,00
	2	0,00	0,03	0,03
	3	0,00	0,00	0,00
	4	0,00	0,00	0,00
	5	0,00	0,01	0,01
	6	0,02	0,03	0,02

Table D.4: Damage numbers of detail 2B on the benchmark model.

Detail 2B		Transversal distribution		
		between troughs	above trough leg	trough middle
Position	1	0,00	0,00	0,00
	2	0,00	0,01	0,01
	3	0,00	0,00	0,00
	4	0,00	0,00	0,00
	5	0,00	0,00	0,00
	6	0,00	0,01	0,01

Table D.5: Damage numbers of detail 5 on the benchmark model.

Detail 5		Transversal distribution		
		between troughs	above trough leg	trough middle
Position	1	0,00	0,00	0,00
	2	0,00	0,00	0,00
	3	0,47	0,15	0,02
	4	0,20	0,07	0,00
	5	0,00	0,00	0,00
	6	0,00	0,00	0,00

Table D.6: Damage numbers of detail 6A on the benchmark model.

Detail 6A		stress type	Transversal distribution		
			between troughs	above trough leg	trough middle
Position	1	s-	0,00	0,00	0,00
		s+	0,00	0,00	0,00
	2	s-	0,31	0,00	0,00
		s+	0,44	0,07	0,00
	3	s-	0,00	0,00	0,00
		s+	0,00	0,00	0,00

Table D.7: Damage numbers of detail 6B on the benchmark model.

Detail 6B		stress type	Transversal distribution		
			between troughs	above trough leg	trough middle
Position	1	s-	0,07	2,59	2,01
		s+	0,09	2,78	2,32
	2	s-	0,97	0,32	0,03
		s+	0,80	0,24	0,03
	3	s-	2,15	0,39	0,00
		s+	2,31	0,36	0,00

Relationship S-N curve and deckplate damage curve

In the parameter sensitivity analysis, a remarkable similarity is found between the damage curve of the deckplate and a S-N curve. An effort is taken to try and find relations between these figures. As this could be a fast and efficient way to directly determine damage from stresses.

Initially, a simple fit with three linear lines on a log scale is attempted, as shown in Figure E.1a. For comparison, the S-N curve for detail 1C is provided for deckplate thicknesses greater than 18 mm. Additionally, Table E.1 is included to examine the maximum stresses of the different designs, as these stresses indicate which zone (zone m1 or m2) in the S-N curve they are able to fall into.

**(a)** Damage curve   **(b)** S-N curve
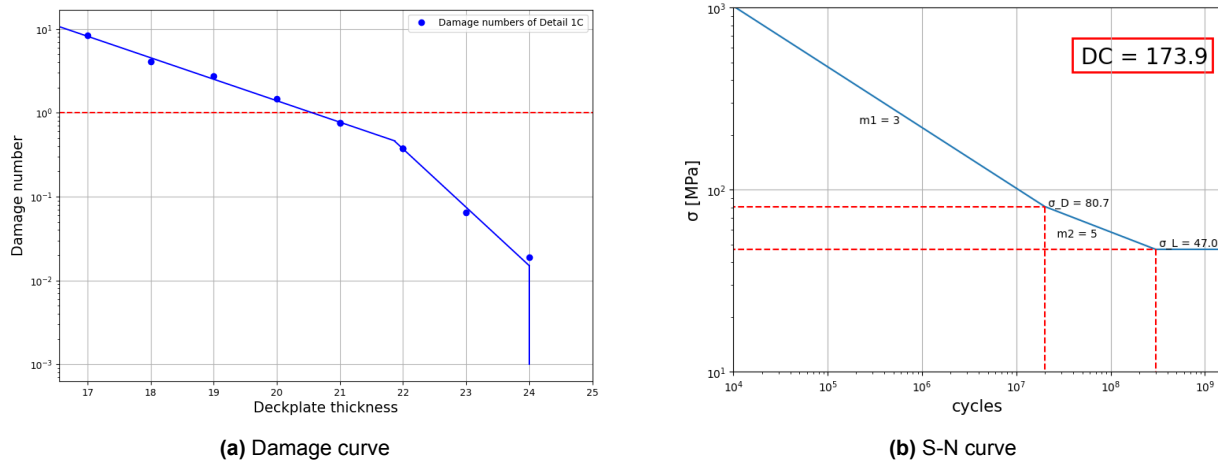
Figure E.1: Damage curve S-N curve corresponding to detail 1C.

Table E.1: Maximum stress ranges per design with different deckplate thicknesses.

Deckplate value [mm]	24	23	22	21	20	19	18
Max stress range [MPa]	50.8	56.4	63.7	71.7	80.8	91.6	100.5

From Table E.1, it can be concluded that although these three linear lines appear to fit, it is probable that the reality is more complex. For designs with a deckplate thickness of 20 mm or greater, the stress magnitudes fall entirely within zone m2 or below the cut-off limit. It is not expected that in the middle of this domain ($t_{dp} = 20 - 24 \ mm$) a sudden change in the slope is observed. A more likely hypothesis is a gradual decrease of slope on log scale, pictured in Figure E.2.
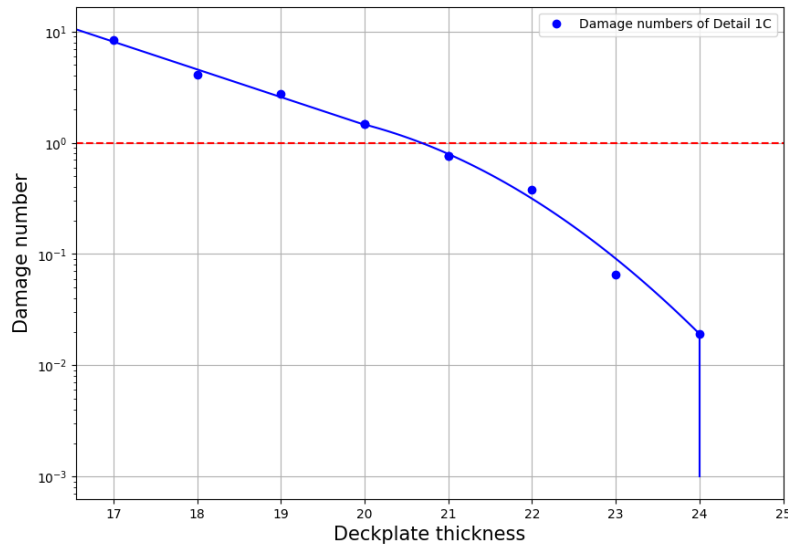
Figure E.2: Damage curve of the deckplate thickness on detail 1C.

A clearer understanding of the fit's accuracy can be achieved by including more data points in the lower domain of the figure. Additional deckplate thicknesses can be examined using theoretical cases where the thickness is measured in half-millimeter increments. This approach is illustrated in Figure E.3.
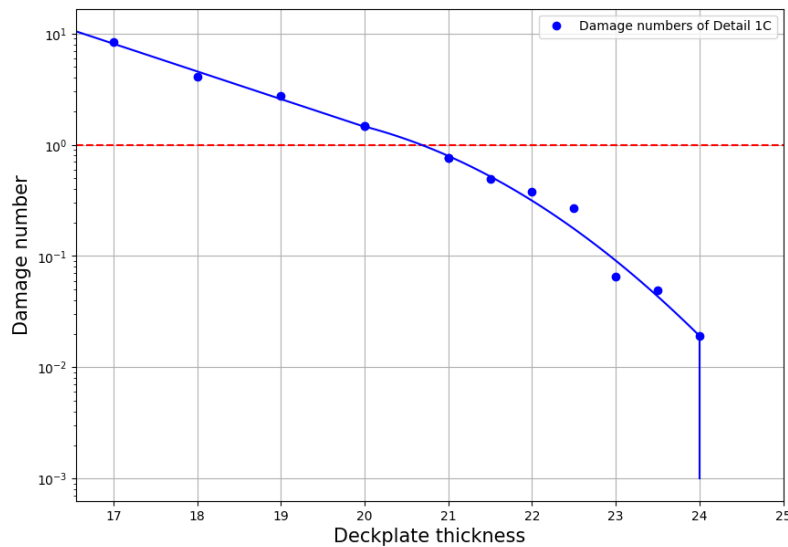
Figure E.3: Expanded damage curve of the deckplate thickness on detail 1C.

The extra points do not provide a definitive answer, they suggest that the both hypothesis can still be accurate as a fit. Although, the validity of the hypothesis involving the three straight lines remains questionable. Further investigation is deemed unnecessary, as the absolute error at these lower points is minimal.

Traffic category influences

This appendix shows the result of the additionally investigated parameters for the traffic type influence on the damage numbers. Influences of the traffic types are shown for damage numbers of the deckplate thickness on detail 1A at midspan, the thickness of the crossbeam for both details and the trough ctc for detail 1A.

F.1. Deckplate thickness
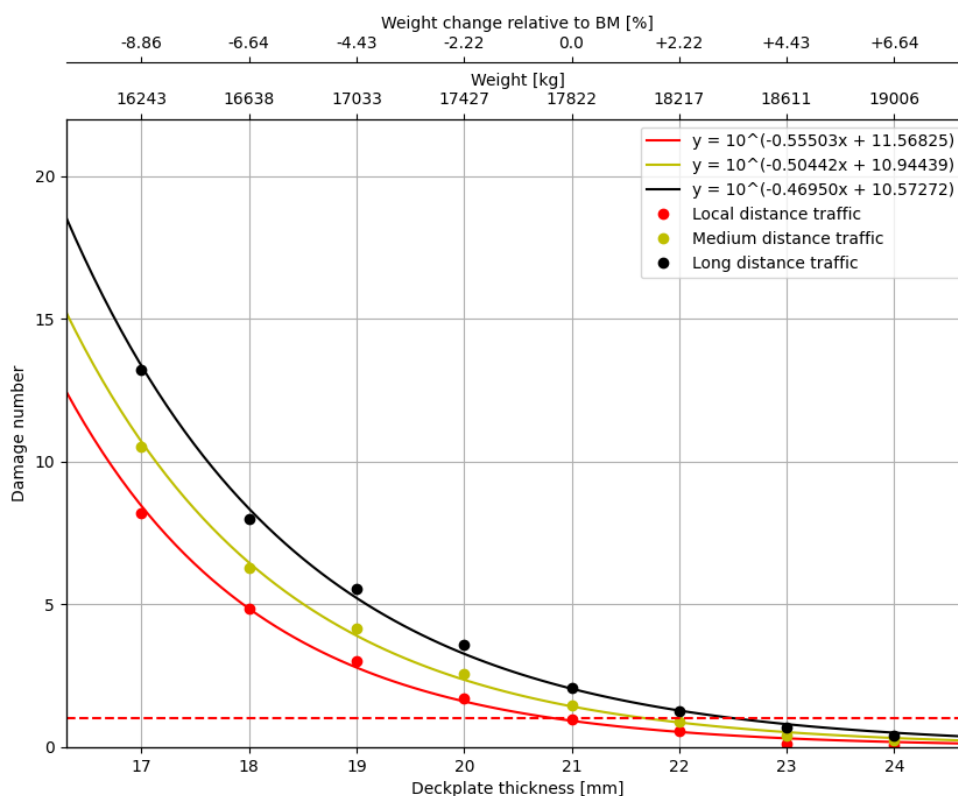
Figure F.1: Influence of traffic categories on bridge response to different deckplate thicknesses for detail 1A at midspan.

Table F.1: Damage numbers and differences of traffic types per deckplate thickness for detail 1A at midspan.

| t_dp | *Damage numbers per traffic type** | | | *Absolute differences* | | | |
	TT1	TT2	TT3	TT3-TT1	TT2-TT1	TT3-TT2	Percentual increase TT3 w.r.t. TT1
17	8,19	10,51	13,23	5,04	2,32	2,72	62%
18	4,84	6,29	7,99	3,15	1,45	1,7	65%
19	3,01	4,17	5,54	2,53	1,16	1,37	84%
20	1,69	2,55	3,58	1,89	0,86	1,03	112%
21	0,96	1,46	2,07	1,11	0,5	0,61	116%
22	0,56	0,87	1,24	0,68	0,31	0,37	121%
23	0,13	0,39	0,67	0,54	0,26	0,28	415%
24	0,07	0,23	0,4	0,33	0,16	0,17	471%

* TT1 = Local distance traffic; TT2 = Medium-long distance traffic; TT3 = Long distance traffic

F.2. trough ctc
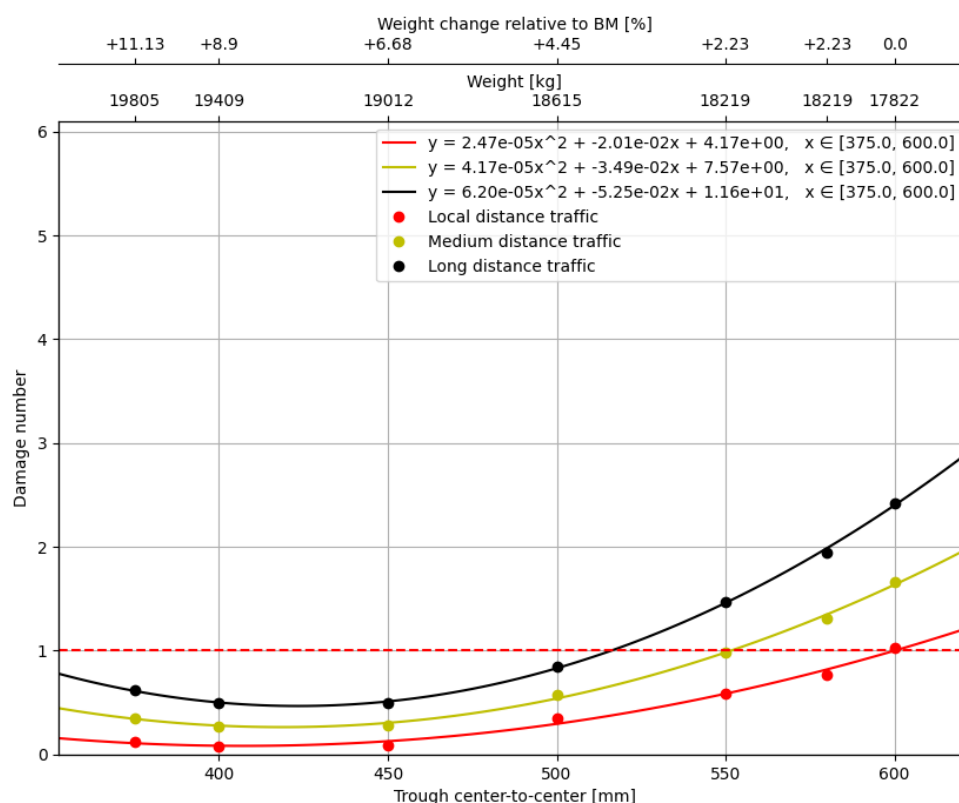
Figure F.2: Influence of traffic categories on bridge response to different trough center-to-center distances for detail 1A inbetween crossbeam 1 and 2.

Table F.2: Damage numbers and differences of traffic types per trough center-to-center distance for detail 1A inbetween crossbeam 1 and 2.

ctc trough	Damage numbers per traffic type*			Absolute differences			Percentual increase TT3 w.r.t. TT1
	TT1	TT2	TT3	TT3-TT1	TT2-TT1	TT3-TT2	
600	1,026	1,658	2,419	1,393	0,632	0,761	136%
580	0,771	1,306	1,95	1,179	0,535	0,644	153%
550	0,583	0,987	1,472	0,889	0,404	0,485	152%
500	0,351	0,576	0,848	0,497	0,225	0,272	142%
450	0,083	0,277	0,49	0,407	0,194	0,213	490%
400	0,082	0,271	0,489	0,407	0,189	0,218	496%
375	0,118	0,352	0,62	0,502	0,234	0,268	425%

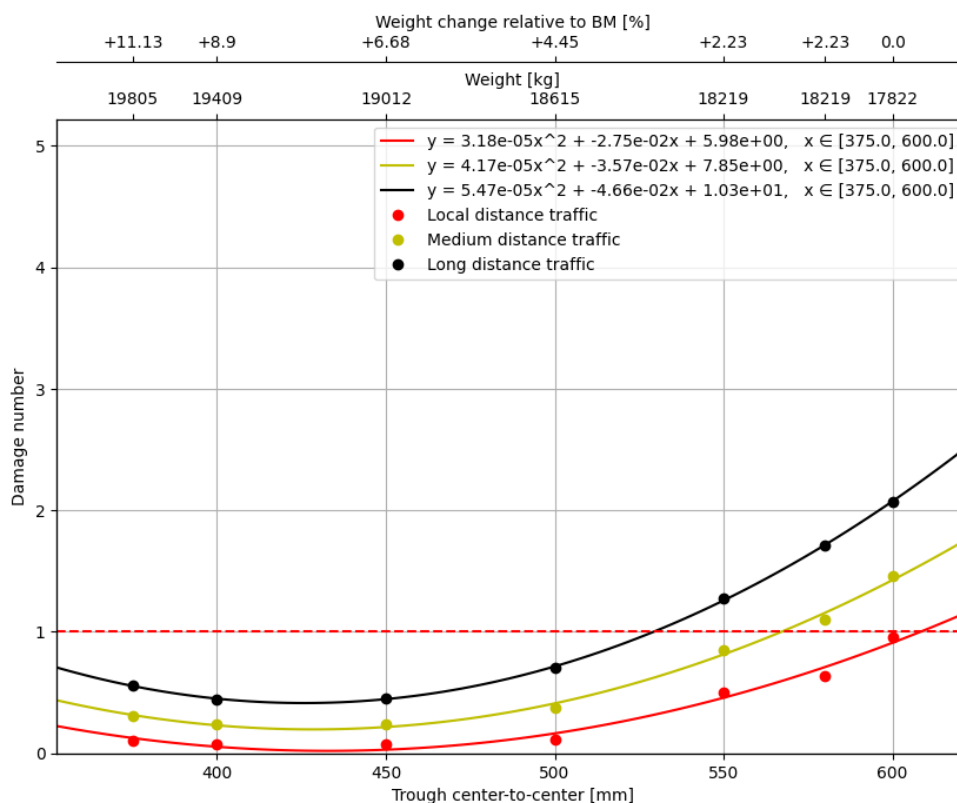* TT1 = Local distance traffic; TT2 = Medium-long distance traffic; TT3 = Long distance traffic

Figure F.3: Influence of traffic categories on bridge response to different trough center-to-center distances for detail 1A at midspan.
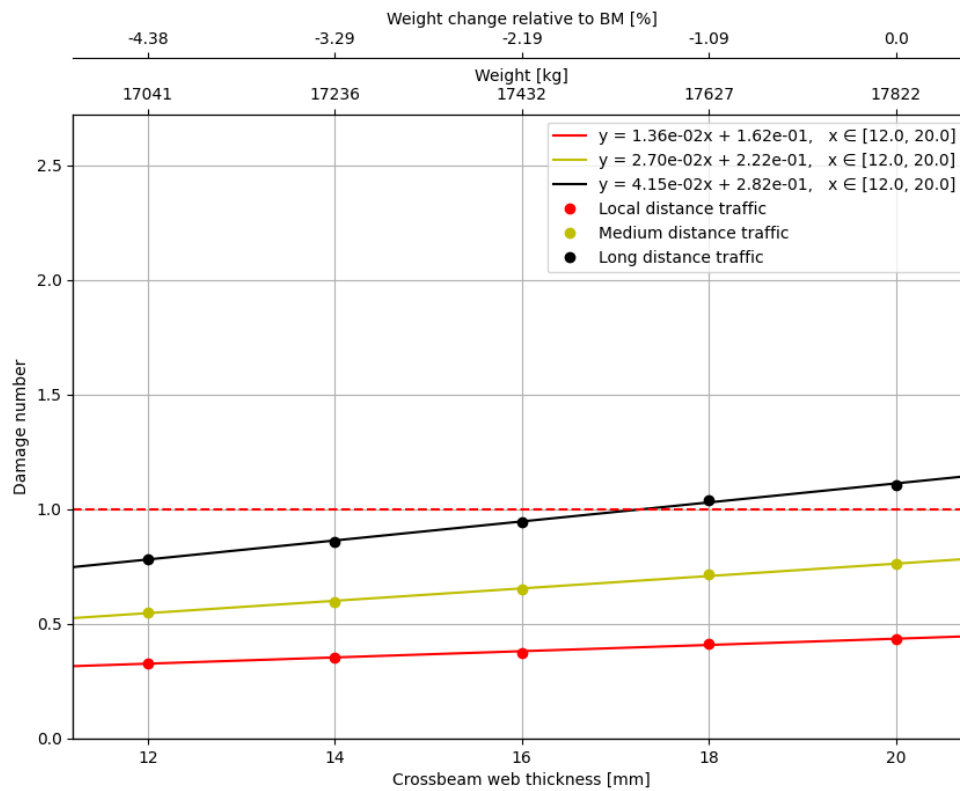
Table F.3: Damage numbers and differences of traffic types per trough center-to-center distance for detail 1A at midspan.

	Damage numbers per traffic type*			Absolute differences			
ctc trough	TT1	TT2	TT3	TT3-TT1	TT2-TT1	TT3-TT2	Percentual increase TT3 w.r.t. TT1
600	0,956	1,458	2,070	1,114	0,502	0,612	117%
580	0,637	1,100	1,713	1,076	0,463	0,613	169%
550	0,497	0,850	1,278	0,781	0,353	0,428	157%
500	0,114	0,379	0,701	0,587	0,265	0,322	515%
450	0,073	0,242	0,451	0,378	0,169	0,209	518%
400	0,071	0,237	0,466	0,395	0,166	0,229	555%
375	0,102	0,304	0,557	0,456	0,203	0,253	448%

* TT1 = Local distance traffic; TT2 = Medium-long distance traffic; TT3 = Long distance traffic

F.3. Crossbeam thickness

For all investigated parameters holds the fact that a lower the damage number means a higher percentual increase of TT3 with respect to TT1. The only exception is the crossbeam thickness, as seen in Table F.4 corresponding to Figure F.4.
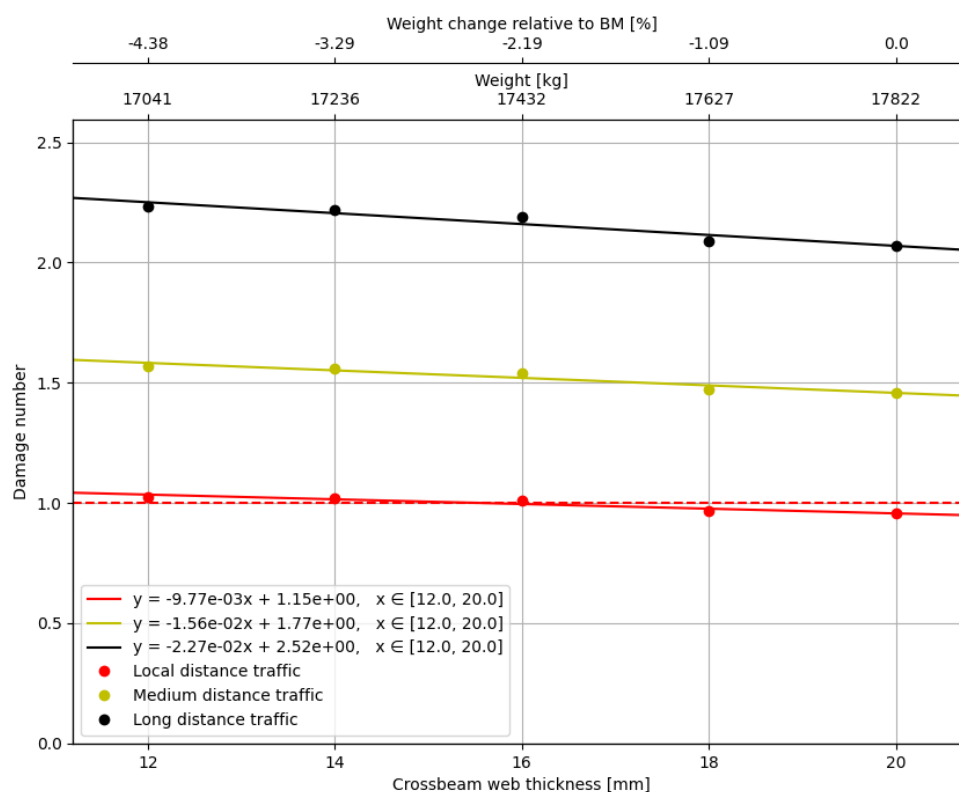

Figure F.4: Influence of traffic categories on bridge response to different crossbeam web thicknesses for detail 1C.

Table F.4: Damage numbers and differences of traffic types per crossbeam web thickness and for detail 1C.

t_cb	Damage numbers per traffic type*			Absolute differences			Percentual increase TT3 w.r.t. TT1
	TT1	TT2	TT3	TT3-TT1	TT2-TT1	TT3-TT2	
12	0,329	0,549	0,782	0,453	0,22	0,233	138%
14	0,351	0,597	0,859	0,508	0,246	0,262	145%
16	0,373	0,649	0,944	0,571	0,276	0,295	153%
18	0,412	0,716	1,041	0,629	0,304	0,325	153%
20	0,435	0,759	1,106	0,671	0,324	0,347	154%

* TT1 = Local distance traffic; TT2 = Medium-long distance traffic; TT3 = Long distance traffic

Figure F.5: Influence of traffic categories on bridge response to different crossbeam web thicknesses for detail 1A at midspan.

Table F.5: Damage numbers and differences of traffic types per crossbeam web thickness and for detail 1A at midspan.

	Damage numbers per traffic type*			Absolute differences			
t_cb	TT1	TT2	TT3	TT3-TT1	TT2-TT1	TT3-TT2	Percentual increase TT3 w.r.t. TT1
12	1,025	1,569	2,232	1,207	0,544	0,663	118%
14	1,022	1,561	2,218	1,196	0,539	0,657	117%
16	1,009	1,541	2,19	1,181	0,532	0,649	117%
18	0,964	1,471	2,089	1,125	0,507	0,618	117%
20	0,956	1,458	2,07	1,114	0,502	0,612	117%

* TT1 = Local distance traffic; TT2 = Medium-long distance traffic; TT3 = Long distance traffic

G

Tables PSA usage

Table G.1: Usage of PSA for determining difference in damage number between the benchmark model and the new design for detail 1C.

parameter	original value [mm]	new value [mm]	Damage new	Damage original	Δ
t_{dp}	21	17	8,215	0,760	7,455
ctc_{cb}	3666	3000	0,760	0,760	0,000
t_{cb}	20	12	0,534	0,760	-0,226
t_{tr}	6	8	0,695	0,760	-0,065
ctc_{tr}	600	600	0,760	0,760	-
h_{tr}	350	400	0,757	0,760	-0,003
$tr_{w,top}$	300	250	0,150	0,760	-0,610
$tr_{w,bot}$	150	180	0,770	0,760	0,010
				Δ_{total}	6,561

Table G.2: Usage of PSA for determining difference in damage number between the benchmark model and the new design for detail 1A at midspan.

parameter	original value [mm]	new value [mm]	Damage new	Damage original	Δ
t_{dp}	21	17	10,68947914	1,458	9,231
ctc_{cb}	3666	3000	1,308	1,458	-0,150
t_{cb}	20	12	1,583	1,458	0,125
t_{tr}	6	8	1,6498	1,458	0,192
ctc_{tr}	600	600	1,458	1,458	-
h_{tr}	350	400	1,462	1,458	0,004
$tr_{w,top}$	300	250	1,4025	1,458	-
$tr_{w,bot}$	150	180	1,44166	1,458	-0,016
				Δ_{total}	9,386

Table G.3: Usage of PSA for determining difference in damage number between the benchmark model and the new design for detail 1A inbetween crossbeam 1 and 2.

parameter	original value [mm]	new value [mm]	Damage new	Damage original	Δ
t_{dp}	21	17	11,494	1,658	9,836
ctc_{cb}	3666	3000	1,733	1,658	0,075
t_{cb}	20	12	1,723	1,658	0,065
t_{tr}	6	8	1,524	1,658	-0,134
ctc_{tr}	600	600	1,658	1,658	-
h_{tr}	350	400	1,6832	1,658	0,025
$tr_{w,top}$	300	250	1,570	1,658	-
$tr_{w,bot}$	150	180	1,660	1,658	0,002
				Δ_{total}	9,868